SERDP

FINAL REPORT

Development and Evaluation of Non-Chromate LHE ZnNi Passivations for DoD Electrical Connectors

Matt O'Keefe
Missouri University of Science & Technology

June 2023

SERDP Project WP-2527

REPORT DOCUMENTATION PAGE

Form Approved
OMB No. 0704-0188

1. REPORT DATE *(DD-MM-YYYY)*	**2. REPORT TYPE**	**3. DATES COVERED** *(From - To)*
30/06/2023	SERDP Final Report	9/27/2018 - 9/26/2023

4. TITLE AND SUBTITLE

Development and Evaluation of Non-Chromate LHE ZnNi Passivations for DoD Electrical Connectors

5a. CONTRACT NUMBER
18-C-0065

5b. GRANT NUMBER

5c. PROGRAM ELEMENT NUMBER

6. AUTHOR(S)
Matt O'Keefe

5d. PROJECT NUMBER
WP-2527

5e. TASK NUMBER

5f. WORK UNIT NUMBER

7. PERFORMING ORGANIZATION NAME(S) AND ADDRESS(ES)
Missouri University of Science & Technology
Materials Science and Engineering
1400 N. Bishop
Rolla, mo 65409

8. PERFORMING ORGANIZATION REPORT NUMBER
WP-2527

9. SPONSORING/MONITORING AGENCY NAME(S) AND ADDRESS(ES)
Office of the Deputy Assistant Secretary of Defense (Energy Resilience & Optimization)
3500 Defense Pentagon, RM 5C646
Washington, DC 20301-3500

10. SPONSOR/MONITOR'S ACRONYM(S)
SERDP

11. SPONSOR/MONITOR'S REPORT NUMBER(S)
WP-2527

12. DISTRIBUTION/AVAILABILITY STATEMENT
DISTRIBUTION STATEMENT A. Approved for public release: distribution unlimited.

13. SUPPLEMENTARY NOTES

14. ABSTRACT
Corrosion protection of metallic components using hexavalent chromium coatings has been widely used for military and commercial application for decades. Hexavalent chromium is a known carcinogen and alternative corrosion inhibitors that do not have negative environmental and health impacts are needed. This project focused on development and evaluation of environmentally friendly trivalent chromium passivation on electroplated zinc nickel to replace hexavalent chromium passivation for electrical connectors.

15. SUBJECT TERMS
CORROSION, REPAIR TECHNOLOGIES, PASSIVATION, PRIMERS AND TOPCOATS, LEAD, surface preparation, electrical connectors, non-chrome, passivation

16. SECURITY CLASSIFICATION OF:			**17. LIMITATION OF ABSTRACT**	**18. NUMBER OF PAGES**	**19a. NAME OF RESPONSIBLE PERSON**
a. REPORT	**b. ABSTRACT**	**c. THIS PAGE**			Matt O'Keefe
UNCLASS	UNCLASS	UNCLASS	UNCLASS	111	**19b. TELEPHONE NUMBER** *(Include area code)* 573-341-6764

Front Matter

Contents

List of Figures

List of Tables

Acronyms

Al: Aluminum
ANSI: American National Standards Institute
AISI: American Iron and Steel Institute
ASTM: American Society for Testing and Materials
BR&T: Boeing Research and Technology
BYU: Brigham Young University
Cd: Cadmium
CPDS/CPDP: Cyclic Potentiodynamic Scanning/Polarization
CrCC/CCC: Chromate conversion coatings
cTLM: Circular Transfer Length Method
DI: Deionized
DoD: Department of Defense
DPC: Diphenylcarbazide
DUT: Device Under Test
EIS: Electrical Impedance Spectroscopy
FIB: Focused Ion Beam
HExCr: Hexavalent Chromium Conversion Coating
HCl: Hydrochloric Acid
I_{corr}: Corrosion Current

LHE: Low Hydrogen Embrittlement
LTLM or TLM: Linear Transfer Length Method
M: Metallic
Mil-DTL: Military Detail Specification
NaCl: Sodium Chloride
Ni: Nickel
OCP: Open Circuit Potential
Pt: Platinum
R_P: Polarization Resistance
RPM: Revolutions per Minute
SAE: Society of Automotive Engineers
SCE: Standard Calomel Electrode
SEM: Scanning Electron Microscopy
SHE: Standard Hydrogen Electrode
SSE: Salt Spray Exposure
TCP: Trivalent Chromium Passivation
TEM: Transmission Electron Microscopy
TLM: Transfer Length Method
XPS: Xray Photoelectron Spectroscopy
XRD: Xray Diffraction
Zn: Zinc
ZnNi: Zinc Nickel

Abstract

Introduction and Objectives: Corrosion protection of metallic components using hexavalent chromium coatings has been widely used for military and commercial application for decades. Hexavalent chromium is a known carcinogen and alternative corrosion inhibitors that do not have negative environmental and health impacts are needed. This project focused on development and evaluation of environmentally friendly trivalent chromium passivation on electroplated zinc nickel to replace hexavalent chromium passivation for electrical connectors.

Technical Approach: Development of deposition processes was done to control the chemistry and morphology of trivalent chromium passivation to optimize corrosion protection of electroplated zinc nickel coatings on steel and aluminum substrates. Data from neutral salt spray exposure, electrical contact measurements, electrochemical testing, and materials characterization analysis of samples was used to adjust deposition conditions for optimal corrosion performance. This data was also used to better understand fundamental corrosion mechanisms and propose a protection scheme for how trivalent chromium passivation mitigates corrosion on electroplated zinc nickel coatings. Once the optimized processing conditions were identified, fully functional electrical connectors were coated, passivated, and tested per electronic industry association specifications and standards.

Results: Novel trivalent chromium passivated zinc nickel coatings on steel and aluminum metallic substrates exposed to hundreds of hours of neutral salt spray exposure had minimal corrosion product and low electrical contact resistance values comparable to hexavalent chromium passivation reference samples. The passivated layers were measured to be less than 100 nanometers in thickness but able to provide active corrosion protection. Chemical composition analysis of the trivalent chromium passivation was found to dependent on the deposition conditions and post-deposition processing. In particular, trace amounts of hexavalent chromium in the passivation could be correlated to the acid level in the deposition bath and heat treatment time and temperature after deposition. The appearance and uniformity, adhesion, torque lubricity, neutral salt spray performance, and shell conductivity of electrical connectors with trivalent chromium passivation on electroplated zinc nickel where comparable in value to hexavalent chromium passivation on zinc nickel and hexavalent chromium passivation on electroplated cadmium connector assemblies. A corrosion protection mechanism based on the oxidation-reduction reaction between trivalent chromium and hexavalent chromium and transport of species to active corrosion sites was proposed.

Benefits: The technology developed during this project demonstrated for the first time that trivalent chromium passivation on electroplated zinc nickel coatings was capable of simultaneously providing corrosion protection and low electrical contact resistance on aluminum electrical connector assemblies. With further investigation and optimization, it is possible to replace the existing connection coating systems that utilize electroplated cadmium and hexavalent chromium passivation with a more environmentally friendly electroplated zinc nickel coating and trivalent chromium passivation.

Executive Summary

Introduction

Electroplated cadmium has been widely used in aerospace applications including electrical connectors due to desirable properties such as galvanic compatibility with commonly used materials, a non-reflective appearance, excellent corrosion protection, and low electrical resistance. Unfortunately, cadmium and cadmium plating operations have many undesirable attributes, especially those related to effluents, toxicity, and carcinogenic nature of the materials that lead to stringent restrictions and regulations. Replacement of cadmium plated coatings with electroplated low hydrogen embrittlement zinc-nickel coatings has been shown to be effective when the zinc-nickel layer is passivated with a conversion coating. Chromate conversion coatings applied to electroplated zinc-nickel improve corrosion resistance. However, chromate conversion coatings also result in the use of, and exposure to, toxic and carcinogenic hexavalent chromium compounds. A variety of corrosion inhibitors have been developed as environmentally friendly alternatives to chromates for a range of applications. Environmentally friendly coatings have the potential to enhance military readiness and reduce costs by providing the necessary corrosion protection and electrical performance without the environmental and health risks associated with chromates.

To address this problem, Missouri University of Science and Technology (Missouri S&T) collaborated with Dipsol of America (Dipsol) and Boeing Research & Technology (BR&T) in St. Louis to develop and evaluate low contact resistance, corrosion resistant passivation layers for Department of Defense (DoD) electrical system components. The team investigated a trivalent chromium passivation (TCP) and a modified cobalt free (Co-Free) version of TCP developed by Dipsal to provide corrosion protection of electroplated low hydrogen embrittlement (LHE) ZnNi. Electrical, electrochemical, corrosion, and materials performance of the passivation layers on test substrates were used to characterize and develop the best performing coatings. BR&T evaluated TCP, Co-Free TCP, and hexavalent chromium passivation on fully assembled, military grade electrical connectors per MIL-DTL-38999 and compared test results to cadmium plated, hexavalent chromium coated connectors.

Objectives

The main objective of the project was to develop trivalent chromium passivation coatings deposited on electroplated ZnNi with comparable corrosion and electrical performance to hexavalent chromium passivation on electroplated cadmium military grade connectors. Understanding and controlling the TCP deposition parameters to optimize performance was done throughout the project. Characterization and analysis of samples to understand how the TCP provides corrosion protection was done to propose a corrosion protection mechanism. Investigations into alternative methods to MIL-DTL-81706B for measuring contact resistance were done.

Technical Approach

Dipsol's IZ-C17+ LHE ZnNi plating process, which has been approved by the U.S. Air Force and Boeing for aerospace and military applications, was used as the LHE ZnNi coating. Missouri S&T and Dipsol worked together to evaluate and optimize the TCP and Co-free TCP passivations on LHE ZnNi test substrates that were previously developed during WP SEED-2527. Initially low carbon steel substrates were used to quickly prepare low-cost samples, and then flat sheet aluminum 6061-T6 with an electroless nickel layer between the aluminum and ZnNi were used to better represent the materials used in electrical connectors. Electrical contact resistance measurements were made per MIL-DTL-81706B using a testing apparatus built specifically for the project. Electrochemical testing including open circuit potential and potentiodynamic polarization to evaluate the response of coatings in a controlled experimental configuration. Neutral salt spray exposure per ASTM B-117 was used as a test of corrosion performance using visual observation and quantitative measurement of the amount of white corrosion product on the surface of samples as a function of exposure time. Scanning electron microscopy, transmission electron microscopy, and x-ray photoelectron spectroscopy analysis were used to gain insight into the appearance, chemical composition, and thickness of the films and coatings. Missouri S&T and Dipsol worked with external vendors to coat and assemble DoD approved connectors that were tested and evaluated by Boeing per military MIL-DTL-38999 specifications which includes appearance and uniformity inspection, environmental exposure, lubricity and adhesion testing, and electrical shell to shell conductivity.

Results and Discussion

Throughout the project ASTM B-117 neutral salt spray testing was used to compare the response of the coating systems to a corrosive environment out to 1000 hours of exposure time. Shown in Figure 1 are optical images of coated substrates after one week (168 hours), two weeks (336 hours), 500 hours, and 1000 hours of ASTM B-117 testing. Bare ZnNi without any passivation had excessive white corrosion product across the surface of samples after one week and did not change through 1000 hours. The ZnNi samples with TCP and hexavalent chromium (HexCr) passivations had little to no visible corrosion after all exposure times. The hexavalent chromium was used as a reference or control specimen throughout the project. Samples that used a cobalt free (Co-Free) TCP passivation had a thin, discontinuous layer of corrosion after one week that increased with time and was very noticeable after 500 hours of exposure.

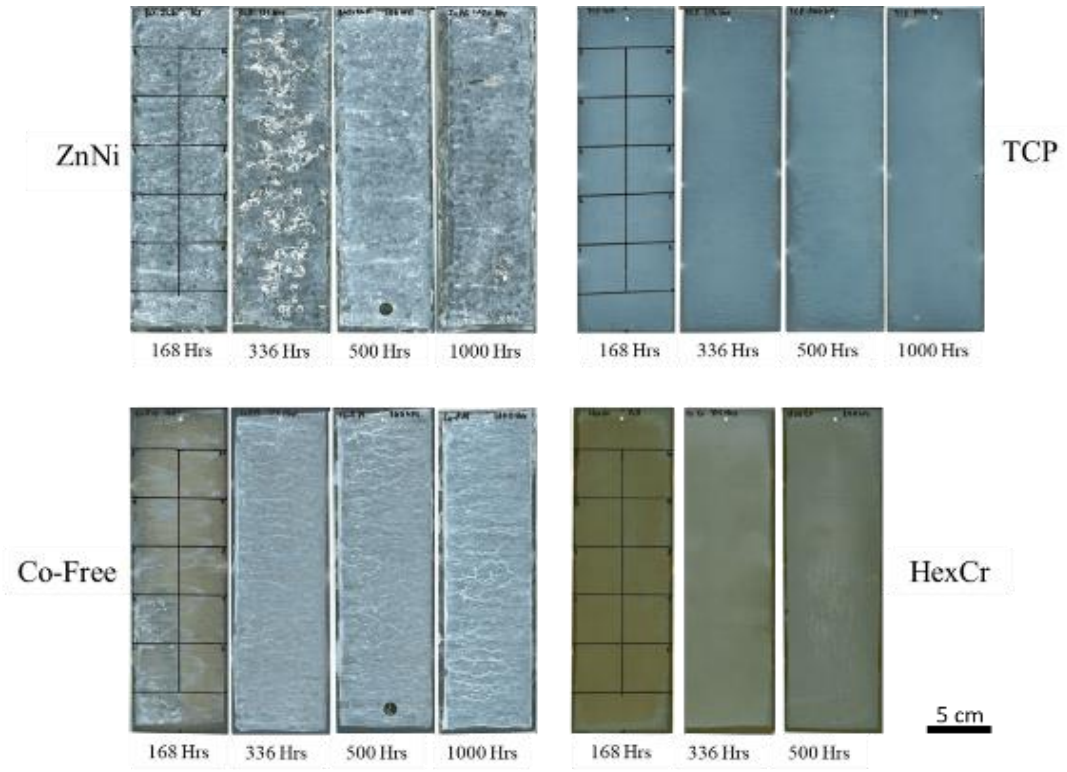

Figure 1 Progression of corrosion with increasing salt spray exposure time for all passivation conditions.

Characterization of samples using transmission electron microscopy (TEM) was done to determine the thickness, morphology, and chemical composition. As depicted in Figure 2 for TCP and Co-Free TCP specimens before (0 hours) and after (1000 hours) of salt spray exposure (SSE) the as-deposited passivations were less than 100 nm thick. It was determined that the light or bright areas within the TCP and Co-Free TCP passivations were pores in the films that formed during the deposition process. After SSE the TCP panels that had no measurable corrosion product and fewer visible pores while the Co-Free TCP had over 5 microns (5000 nm) of corrosion product, consistent with the optical images in Figure 1.

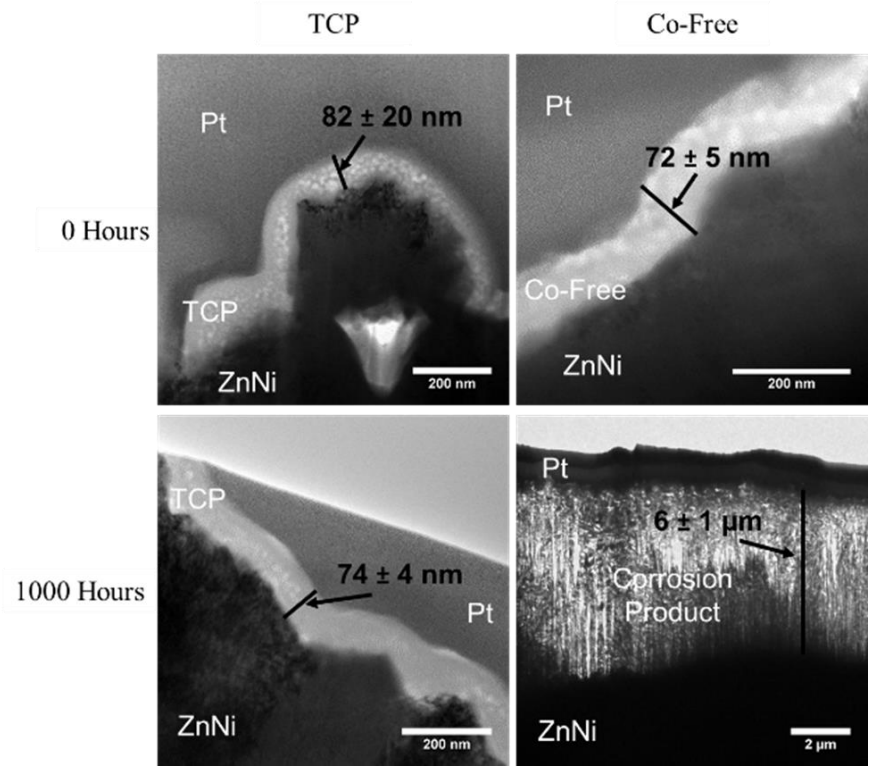

Figure 2 TEM images from TCP and Co-Free TCP lift outs showing the nature of the passivation layers before and after SSE as well as the measured thicknesses at each condition.

Measurement of contact resistance as a function of salt spray exposure time was done using MIL-DTL-81706B methodology. Ten measurements were taken from each sample, corresponding to the ten dark boxes shown on the 168 hour images in the optical images above. Shown in the data plot in Figure 3 are results from contact resistance measurements for bare ZnNi, Co-Free TCP, TCP, and hexavalent chromium samples out to 500 hours of SSE. Included Figure 3 are horizontal red lines that represent the maximum acceptable contact resistance value for as-deposited samples (0 hours SSE) which is 5 mΩ and after 168 hours of SSE, which is 10 mΩ per MIL-DTL-81706B. The results demonstrate that the bare ZnNi had a very high contact resistance after 168 hours of SSE while the Co-Free TCP, TCP, and hexavalent chromium values were below the threshold values. Beyond 336 hours of SSE the Co-Free TCP contact resistance values increased significantly but the HexCr and TCP were well below the maximum permissible value out to 500 hours of ASTM B-117 exposure.

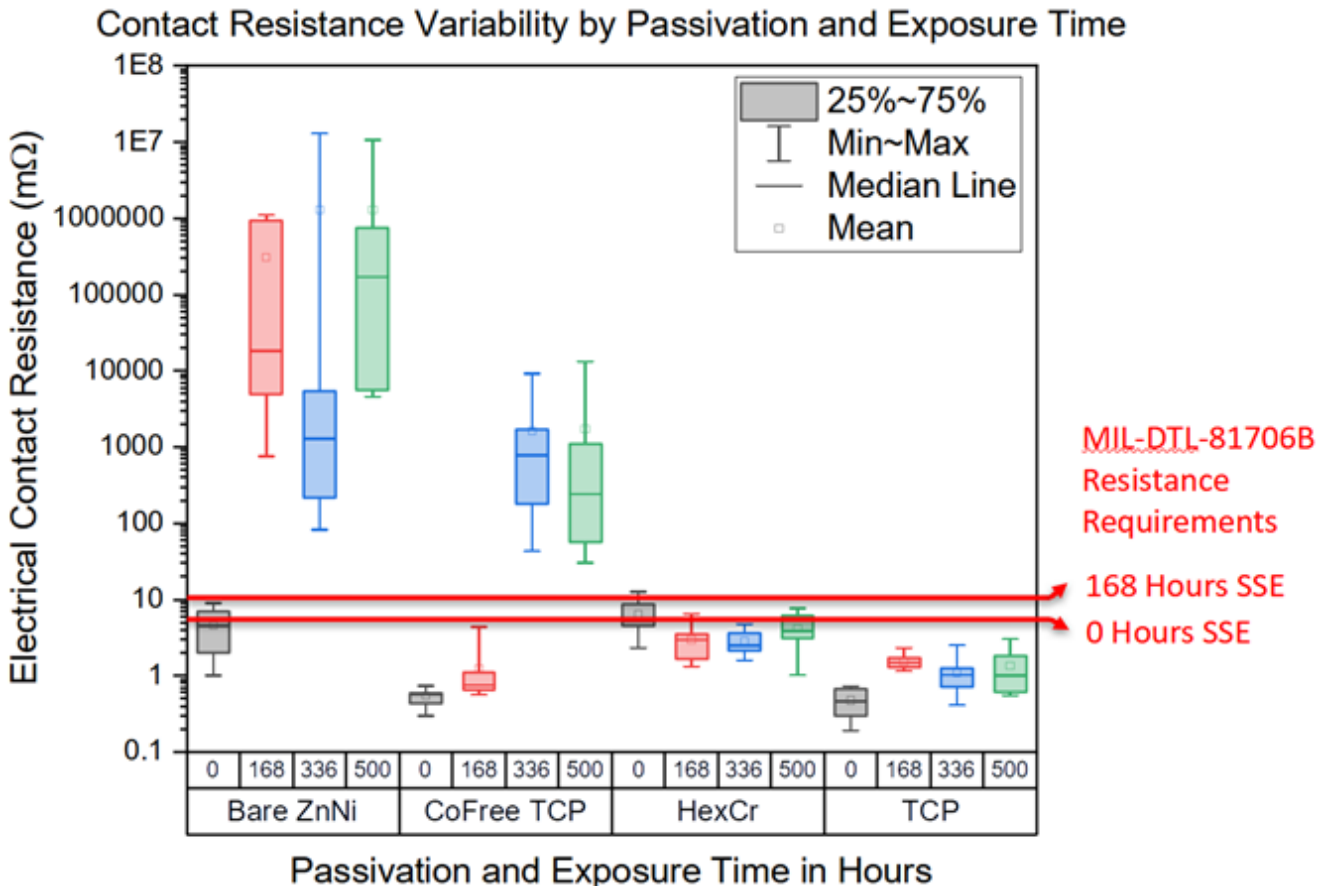

Figure 3 Electrical contact resistance of samples before and after SSE with total measured range and the difference between medians and means visible to demonstrate variability. Red lines represent resistance requirements to approve passivations from MIL-DTL-81706B

The work done to optimize the corrosion resistance and minimize the contract resistance values after ASTM B-117 neutral spray exposure of ZnNi with TCP and Co-Free TCP samples demonstrated that the coatings were capable of passing laboratory test methods on flat panel substrates. Based on those promising results, bare commercial connector and receptacle assemblies were purchased and coated with ZnNi and TCP or Co-Free TCP and subjected to MIL-DTL-38999 test conditions. Connectors and receptacles that had ZnNi with HexCr passivation and MIL-DTL-5015 cadmium and HexCr coatings were also subjected to MIL-DTL-38999 testing as control groups. Shown in Figure 4 are images of the connector assemblies after 452 hours of salt spray exposure. The assemblies with electroplated ZnNi and TCP, Co-Free TCP, or HexCr passivation had a similar matte appearance with uniform discoloration on all surfaces but minimal corrosion product and no visible breakdown of the passivation in specific locations. The MIL-DTL-5015 assemblies did not have any visible corrosion and maintained a shiny surface appearance throughout salt spray exposure. Wired and mated connectors were tested for shell conductivity per EIA 364-83 standard. A total of six assemblies of each coating type were evaluated as three separate groups. As presented in the table on the next page, the ZnNi with TCP and Co-Free TCP had lower millivoltage (lower contact resistance) readings than the ZnNi with HexCr assembly, with the MIL-DTL-5015 samples having the lowest recorded values

ZnNi with TCP at 452 hrs

ZnNi with Co-Free TCP at 452 hrs

ZnNi with HexCr at 452 hrs

MIL-DTL-5015 at 452 hrs

Figure 4 Connector assemblies after 452 hrs of Salt Spray Exposure.

Test Sequence #7 Shell Conductivity				
ZnNi with TCP	Measurement #1 (mV)	Measurement #2 (mV)	Measurement #3 (mV)	
1	6.99	6.97	6.94	Group 1
2	34.25	34.31	34.39	
3	10.15	10.13	10.11	Group 2
4	59.36	58.99	59.11	
5	70.28	70.20	70.32	Group 3
6	22.17	22.14	22.18	

ZnNi with Co-Free TCP	Measurement #1 (mV)	Measurement #2 (mV)	Measurement #3 (mV)	
1	7.01	7.00	7.02	Group 1
2	6.19	6.18	6.18	
3	6.95	6.94	6.96	Group2
4	6.42	6.41	6.45	
5	93.71	93.76	93.74	Group 3
6	36.28	36.30	36.33	

ZnNi with HexCr	Measurement #1 (mV)	Measurement #2 (mV)	Measurement #3 (mV)	
1	36.42	36.41	36.44	Group 1
2	20.74	20.71	20.73	
3	78.11	78.07	78.21	Group2
4	25.89	25.81	25.86	
5	36.42	36.50	36.46	Group 3
6	57.40	57.36	57.48	

MIL-DTL-5015 Electroless Nickel	Measurement #1 (mV)	Measurement #2 (mV)	Measurement #3 (mV)	
1	2.12	2.13	2.13	Group 1
2	2.77	2.77	2.77	
3	2.12	2.12	2.12	Group2
4	3.71	3.71	3.71	
5	4.96	4.96	4.96	Group 3
6	5.21	5.22	2.21	

Throughout the project, test and evaluation of the TCP and Co-Free TCP coatings indicated that corrosion and electrical performance were dependent on the coating deposition conditions and post deposition processing. One of the main differences in coating performance was found to be correlated to whether a post deposition heat treatment was done on samples. In some instances, a post deposition heat treatment at 80°C or 191°C was found to improvement corrosion resistance while in other cases it degraded corrosion performance. Chemical characterization of samples using a 1,5 diphenylcarbazide (DPC) method determined that trace amounts of hexavalent chromium, Cr(VI), were present in TCP and Co-Free TCP samples. As shown in Figure 5, the amount of Cr(VI) in TCP samples was higher than in Co-Free TCP samples before salt spray exposure but the amount of Cr(VI) decreased in TCP specimens with heat treatment. The amount of Cr(VI) decreased with SSE time for both TCP and Co-Free TCP samples. The results indicate that a very low level (micrograms per milliliter) of Cr(VI) was present in the samples, the concentration was dependent on heat treatment, and that the concentration decreased with salt spray exposure time. These results are consistent with the results above as samples with higher concentrations of Cr(VI) had less corrosion, and better electrical performance, than specimens with lower concentrations of Cr(VI).

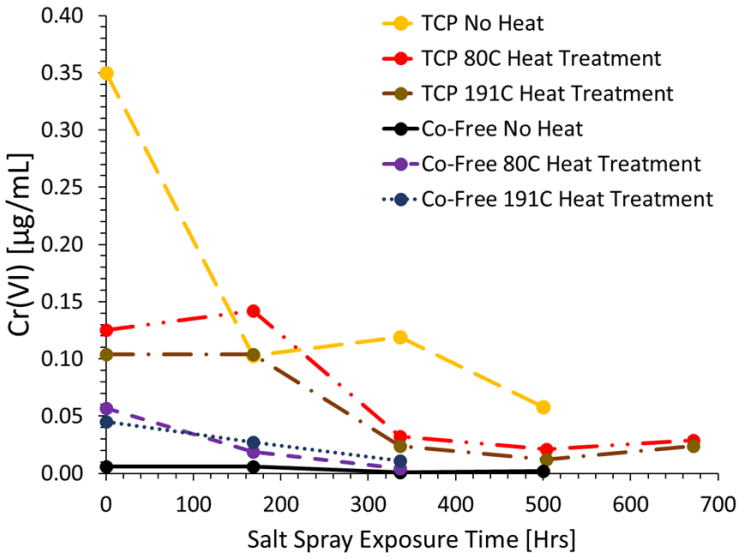

Figure 5 Cr(VI) concentrations after DPC boil test for specimens with and without heat treatment.

Analysis of the data and results of the project was used to propose a corrosion protection mechanism for TCP coatings on electroplated ZnNi exposed to salt spray environments. Depicted in Figure 6 is a schematic representation of the mechanism. When a crack in the TCP coating, containing Cr^{6+} and Cr^{3+}, exposes the underlying substrate (1) and is exposed to a salt spray the Cr^{6+} solubilizes and precipitates as Cr^{3+} corrosion product (2). As corrosion product builds up (3) the availability of Cr^{6+} in the localized area is reduced and a mixture of Cr^{6+} and Cr^{3+} oxides and hydroxides are formed. Once the exposed surface is covered (4), the TCP has a lower amount of Cr^{6+} with residual amounts on the surface related to the precipitated corrosion product.

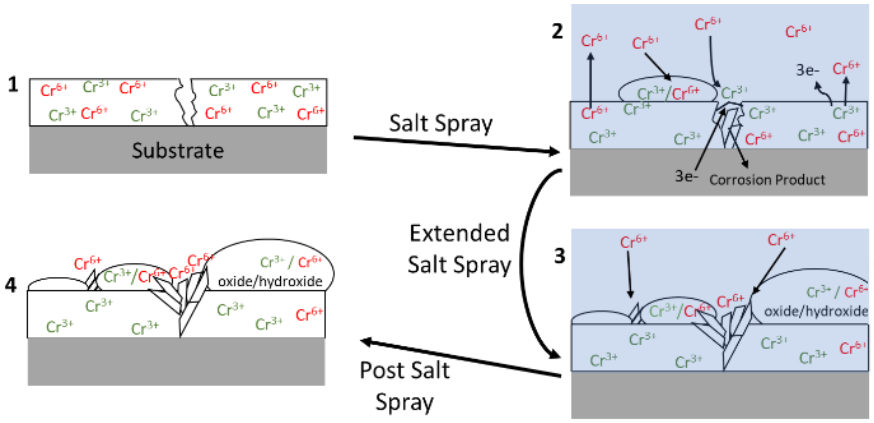

Figure 6 Proposed model of corrosion protection mechanisms.

Implications for Future Research and Benefits

The project demonstrated that trivalent chromium passivation and cobalt free trivalent chromium passivation of electroplated ZnNi were capable of providing corrosion protection and low contact resistance of electrical connector assemblies. During the course of the study, it was determined that trace amounts of hexavalent chromium were present in the trivalent chromium passivation. The amount of the hexavalent chromium present was found to be dependent on the deposition conditions and post deposition heat treatment, both of which can be used to control the amount of hexavalent chromium in the passivation. In addition, standard TCP that contained divalent cobalt performed better that Co-Free TCP for the majority of experimental conditions investigated. Future research to better understand the thermodynamic and kinetic relationship between Cr(VI) and Cr(III) and the presence or absence of Co as a function of processing parameters would provide the basis for controlling and optimizing TCP performance for specific applications. Being able to control the performance of passivation performance using processing conditions would provide the opportunity to customize a TCP coating to a particular end use.

Final Report

Objective

Missouri University of Science and Technology (Missouri S&T) collaborated with Dipsol of America (Dipsol) and Boeing Research & Technology (BR&T) to develop and evaluate low contact resistance passivation layers for Department of Defense (DoD) electrical system components. The team investigated the two most promising non-chromate passivation layers, trivalent chromium passivation (TCP) and a modified cobalt free (Co-Free) version of TCP, developed by Dipsol as part of WP SEED-2527. Electrical, electrochemical, corrosion, and materials performance of the passivation layers on test substrates and fully functional electrical connectors were studied to identify conversion coatings that meet military specifications for electrical resistance. The major outcomes of this project were the identification of environmentally benign passivation layer(s) that can be used on LHE ZnNi plated electrical connectors for military electrical system components along with knowledge of the mechanisms of corrosion protection, degradation and failure.

Background

Substrates and Anti-Corrosion Plating

SAE 1008 Steel.

Steel is produced in different alloyed forms to maximize or minimize a variety of material properties. Historically, the American Iron and Steel Institute (AISI) and Society of Automotive Engineers (now SAE International) developed standards for differentiating between different steel alloys. In 1995, AISI allowed SAE to take over future maintenance of the standards used to produce different steel grades leading to the specifications used today that classify different alloys using a designation of SAE XXXX where the X's are numbers that give information about the alloy [1]. The first number is the primary alloying element, the second denotes a sub-classification of the first number, and the last two represent carbon content in hundredths of a percent [2].

SAE 1008 steel is a low-carbon steel alloy commonly used in extruded, cold upset, and cold pressed parts. It has a chemical composition given in Table 1 Alloy chemical composition to meet standards for SAE 1008 and Al6061that only restricts the amount of carbon, manganese, phosphorus, and sulfur in the steel.

Table 1 Alloy chemical composition to meet standards for SAE 1008 and Al6061

	Composition wt%										
Alloy	**C**	**Mn**	**P**	**S**	**Fe**	**Si**	**Cu**	**Mg**	**Cr**	**Zn**	**Other**
SAE1008	0.1	0.3-0.5	0.04	0.05	rem	-	-	-	-	-	-
Al6061	-	0.15	-	-	0.7	0.4-0.8	0.15-0.4	0.8-1.2	0.04-0.35	0.25	<0.15

This alloy has seen widespread use in the automotive industry to produce structural components for decades. Automotive applications expose metals to natural corrosive environments and so SAE 1008 steel is commonly galvanized with sacrificial zinc or zinc-alloy plating to protect against corrosion.

Aluminum 6061-T6.

Aluminum alloys are classified according to a system set up by the H35 committee of the American National Standards Institute (ANSI) and follows a 4 or 5-digit classification similar to the SAE steel grading system in the case of wrought alloys. For wrought aluminum, the first digit represents the major alloying elements, the second represents variation on a particular alloy, and the last two digits identify the alloy within the series [3]. The alloy designations are typically followed with a temper designation that takes the form of a hyphen followed by a letter indicating the type of tempering, followed by numbers classifying processing within that temper category. The alloys are also limited to have no more elements than 15 wt% with the rest of the weight being aluminum.

6061 is one of the most common of magnesium and silicon alloys of aluminum that serves a general purpose role and has a chemical composition shown in Table 1 Alloy chemical composition to meet standards for SAE 1008 and Al6061. The alloy is easily machined, welded, and precipitation hardened which contributes to its widespread use. The degree of precipitation hardening is affected by the temper and the designation of -T6 represents a piece that was solution heat treated and artificially aged in order to achieve the greatest precipitation hardening. The alloy can have metal coatings applied to protect it from corrosion with several different types available such as cadmium, nickel, and zinc.

Electroless Nickel Plating.

First invented in 1946 by Brenner and Riddell, electroless plating allows deposition of many metals such as Ni, Co, Pd, Au, or Ag without an external electrical source [4]. The deposition is an autocatalytic process wherein a substrate is dipped in a chemical bath with salts of the metal to be plated and a reductant that results in nucleation and growth of the plating on the substrate. This growth is then continued as the deposited metal catalyzes further deposition of the metal which results in a linear growth rate with time after a continuous film has covered the entire surface. This allows for precise control of the film thickness [5].

Nickel was the metal that led to the discovery and invention of electroless plating and was first plated as a Ni-P alloy on steel in a bath that contained hypophosphites. Since that time, many advancements have been made and now electroless deposition of nickel can occur on a variety of substrates including insulators, polymers, and metals with excellent control of a variety of properties such as hardness, density, conductivity, or corrosion resistance [6]. While many applications utilize control of the plating hardness or wear resistance, it can be used on aluminum 6061-T6 alloy to provide a strongly adhered surface that allows for electro-depositing of ZnNi coatings.

Cadmium and γ-ZnNi Coatings.

Electroplated cadmium has many properties that lead to its widespread historical use such as its corrosion resistance (1000 hours until rust in ASTM B117), high electrical conductivity (1.46 x 10^7 S/m), lubricity (~0.5), hardness (~240, Knoop), and ability to be applied as a thin (< 25 μm) layer [7] [8] [9] [10]. In the United States, cadmium was considered an anticipated human

carcinogen since the 1980s and in 2000 the National Institutes of Health (NIH) declared cadmium a known human carcinogen while some studies associate cadmium with kidney damage and diabetes [11] [12] [13] [14]. The toxic and carcinogenic nature of cadmium and its cyanide containing plating process has lead the United States and the European Union to pass regulations limiting the exposure of workers and wildlife to cadmium with a call for alternatives [15] [16] [17].

Several commercially available alternatives to cadmium exist and include gold, tin, ZnCo, ZnFe, SnZn, and ZnNi. Gold plating has excellent corrosion resistance and conductivity, but suffers from a brittle phase that forms when plated on aluminum, high cost, and it is typically deposited with a cyanide containing electroplating bath [18]. Tin plating offers some corrosion resistance (24 hours to rust in 5% salt spray), excellent solderability, and is very cost-effective; however, issues have arisen with tin "whiskers" and the corrosion resistance is not as high as the zinc alloys [19] [20] [21]. ZnCo and ZnFe alloys with 10-20 wt% Co or ~0.75wt% Fe show good corrosion performance, lubricity, and low cost, but inconsistent corrosion performance at temperatures above 250 ºF remains an issue [22] [23] [24] [25] [26] [27]. SnZn coatings with 20-30 wt% Zn have shown comparable corrosion resistance (400 hours to red rust in salt spray) and lubricity to cadmium coatings but have difficulty controlling Zn in plating baths to ensure consistent anti-corrosion performance [28] [29] [30].

Electroplated ZnNi coatings have similar anti-corrosion and tribological properties to cadmium, exceeding cadmium performance in some cases [30]. The primary phase of interest is γ-ZnNi which lies between 14 and 23 wt% Ni on the binary phase diagram shown in Figure 7 [31]. In electrodeposited ZnNi the phases follow a non-equilibrium progression where the γ-phase starts to form at Ni contents as low as 13 wt% and the δ-phase is never observed [32]. Many ZnNi coatings studied were in the range of 5-15 wt% Ni, which explains some variability in corrosion performance including 4 and 96 hours to 6 and 640 hours for white and red rust, respectively [30] [33] [34] [35] [36]. The corrosion resistance maximum at around 13-15 wt% nickel was correlated with cracks in the ZnNi coating with coatings exhibiting small closely spaced cracks offering greater corrosion resistance than wider cracks [37]. ZnNi coatings are typically passivated with a conversion coating after electroplating. The most commonly used passivation is a hexavalent chromium (chromate) layer that significantly improves corrosion protection [38] [39] [40].

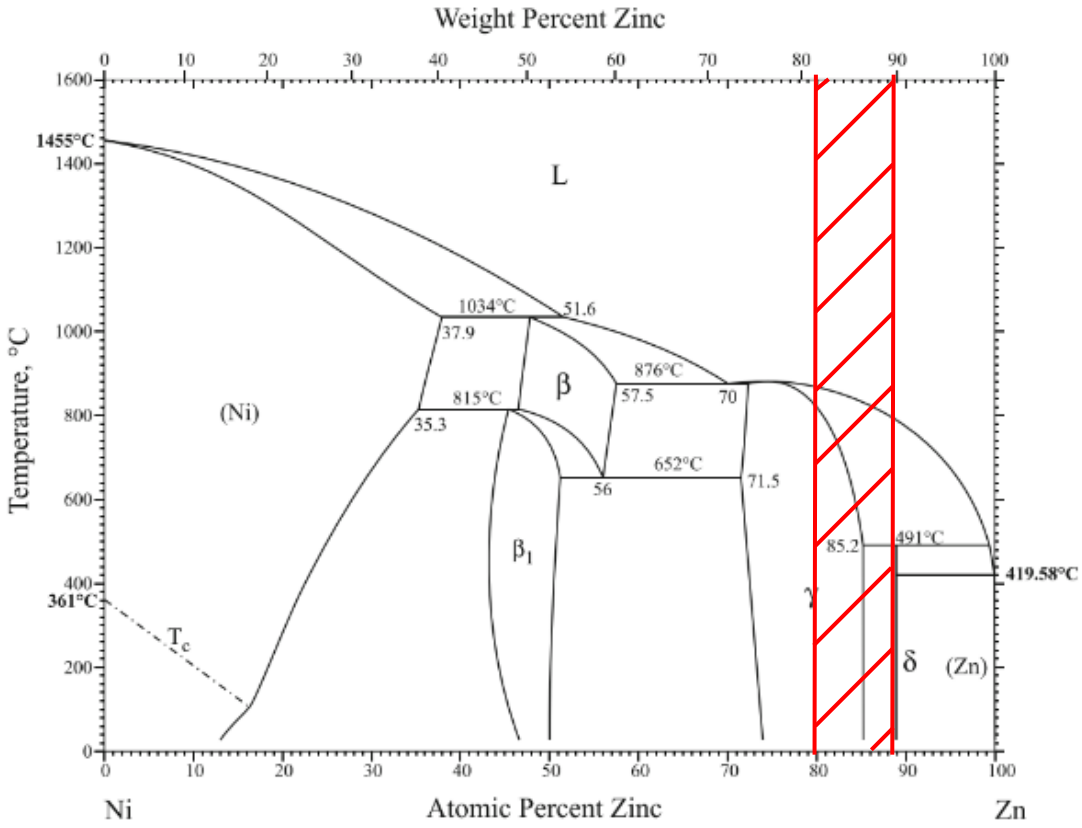

Figure 7 Binary phase diagram of the Nickel-Zinc system from H. Okamoto.31 Red patterned area represents typical commercial ZnNi coating composition (12-20%wt Ni).

Hexavalent Chromate Passivations

Chromate conversion coatings (CCC) have been long used to passivate anti-corrosion coatings of many metallic materials, including cadmium and ZnNi [7] [8] [40] [41] [42]. Formation of a CCC on a given metallic (M) substrate is governed by five chemical reactions shown in equations 1 to 5:

$$M \rightarrow M^{2+} + 2e^- \quad (1)$$

$$2H^+ + 2e^- \rightarrow H_2 \quad (2)$$

$$Cr^{6+} + 3e^- \rightarrow Cr^{3+} \quad (3)$$

$$M^{2+} + 2OH^- \rightarrow M(OH)_2 \quad (4)$$

$$2Cr(OH)_3 + {CrO_4}^{2-} + 2H^+ \rightarrow Cr(OH)_3 \cdot CrOH \cdot CrO_4 + 2H_2O \quad (5)$$

Equations 1 and 2 happen simultaneously with a local increase in pH leading to reduction of Cr(VI) and precipitation of metal hydroxides as shown in equations 3 and 4. Lastly, the Cr(III) and Cr(VI) species precipitate out into a chromate film that consolidates with remaining metal oxide and precipitated metal hydroxide on the substrate surface [42].

CCCs have shown superior corrosion performance on several different substrates and actively protect against damage as from a scratch or scribe [43] [44] [45] [46]. The active protection of non-passivated surfaces is related to reduction of Cr(VI) to Cr(III) at the exposed surfaces [47]. Unfortunately, CCCs are associated with negative health consequences and are being phased out by legal regulations in Europe and the United States [17] [48] [49].

Many non-toxic alternatives to CCCs have been identified including molybdate, zirconium-based, and trivalent chromium compounds although all systems fail to match the anti-corrosion properties of CCCs [42]. Molybdate and zirconium conversion coatings can provide corrosion protection in place of CCCs but are found to be inferior [50] [51] [52] [53]. Trivalent chromium passivation (TCP) systems offer the most promise as a viable alternative as their corrosion performance can match or exceed CCCs on undamaged samples with some degree of active protection [54].

Trivalent Chromate Passivations

Trivalent chromium passivations date back to the 1950s but were not widely adopted until more recent restrictions on CCCs were passed [17] [55]. Deposition of TCP is achieved by skipping reduction of Cr^{6+} to deposit a $Cr(OH)_3$ layer and instead deposit the layer directly [56] [57] [58] [59] [60]. TCPs show some evidence of self-healing capability, but only slightly which is a disadvantage of TCPs compared with CCCs. TCPs do have the advantage that they can retain corrosion protective properties after heating whereas CCCs can lose up to 90% of their corrosion protection after exposure to temperatures >100°C [58].

The variability of TCP coatings can be explained by differences related to bath chemistry, substrate, and bath parameters. For bath chemistry, TCPs are deposited in an acidic solution with a pH $\leq$ 5 with a precursor Cr^{3+} salt, an oxidizer, and usually a transition metal ion such as Co, Ni, or Fe, although these may be a post-treatment [61] [62] [63] [64]. Bath chemistries can also vary with the choice of chromate precursor and acid, or with complexing agents that are sometimes used such as oxalic acid or ammonium bifluoride [60] [65]. These changes result in differences in corrosion performance through changes in the microstructure of the TCP layer, likely via altered bath kinetics [60] [66].

The substrate and bath parameters also affect corrosion resistance by altering the deposition process through oxidation of the metal substrate, evolution of hydrogen at the substrate surface, and co-deposition of Cr/metal oxides and hydroxides [62] [66] [67] [68]. Key bath parameters to control this process include bath pH, temperature, sample immersion time, concentration of Cr^{3+} precursor, concentration of substrate metal ions already present, and presence of a complexing agent [67] [68] [69] [70] [71] [72] [73] [74] [75]. Despite the literature variabilities, some general trends that are observed place TCPs into two general categories: first generation and second generation [59].

First generation passivations are defined by their thickness which is typically <100 nm and tend to have a dense single-layered structure that may or may not be porous [76]. Second generation passivations tend to be in the range of 300-500 nm, potentially up to 1000 nm, and almost always contain a two or three layered structure with a dense uniform surface layer 20-50 nm thick, a bulk porous layer, and an optional dense layer near the substrate interface [59] [66] [77]. These passivations also tend to have better corrosion performance, attributed to the increased thickness.

Heat Treatments.

A few studies have investigated trivalent chromium passivations that have undergone heat treatment post-deposition, and even fewer that have investigated the effects of heat treatments on the passivations themselves. The treatment temperatures tend to range from 90-150°C with times ranging from 30 minutes to several hours but do not significantly degrade the corrosion resistance they provide in contrast to the effect of heat treatment on CCCs [56] [58] [75] [78]. A study by Li and Swain found that aging and heating TCPs provides chemical and physical changes of dehydration and increased hydrophobicity that can benefit corrosion performance to a point, after which further aging and heating is detrimental [78]. A different investigation tied visual changes caused by heat treatments to water filled porosity and dissolved oxygen as performing the heat treatment in a nitrogen atmosphere does not produce the same changes [79]. The ability for TCPs to retain most of their anti-corrosion properties after exposure to elevated temperatures is one advantage TCPs hold over CCCs.

Mechanisms of Corrosion

Corrosion is an electrochemical process wherein a metal substrate will undergo rusting or degradation due to the oxidation or reduction of chemical species at active sites on the surface. Four processes are necessary for corrosion to occur:

1. An anodic reaction (usually oxidation of the metal surface)
2. A cathodic reaction (reduction of dissolved ions)
3. A metallic pathway connecting anodic and cathodic surface sites (for electron conduction from anodic to cathodic sites)
4. An electrolyte (to provide and collect dissolved ions)

Inhibition of corrosion can be achieved by inhibiting any one of these processes. A passivation layer such as TCP works by attempting to inhibit the fourth process by acting as a direct physical barrier between the electrolyte and the surface of the alloy [80].

Corrosion can be uniform or localized wherein the localized corrosion can be one of three categories: pitting, crevice, or stress corrosion cracking. Uniform corrosion represents distributed loss of material from anodic and cathodic sites spontaneously moving across the surface. Pitting and crevice corrosion results from the active sites becoming localized on the surface and focusing material loss only to a fixed area. Stress corrosion cracking is a result of an applied stress speeding up a corrosive reaction. Uniform corrosion is preferred to localized as it is more readily controlled and occurs at a predictable rate [81].

Another type of corrosion related to this project is galvanic corrosion. Galvanic corrosion takes place spontaneously when two different metals with different electromotive potentials are placed into contact in an electrolyte where one metal acts as an anode and the other a cathode. The metal with the more negative potential on the emf series acts as the anode and has a driving force for corrosion measured via Equations 6 and 7.

$$E^{\circ}_{cell} \rightarrow E^{\circ}_{cathode} - E^{\circ}_{anode} \quad (6)$$

$$\Delta G^{\circ}_{cell} \rightarrow -nFE^{\circ}_{cell} \quad (7)$$

The emf series is defined with a metal in an aqueous environment containing its own dissolved ions at unit activity. Hence, the emf series cannot be used to predict the anode or cathode in non-aqueous environments or in aqueous solutions with different dissolved ions. The galvanic series was empirically determined to overcome this limitation. Figure 8 shows the galvanic series as determined for a seawater environment [82].

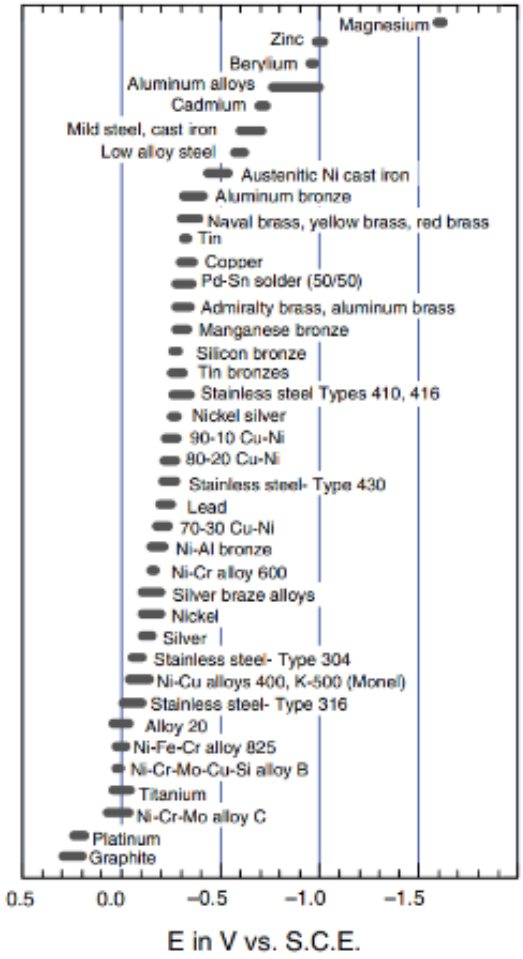

Figure 8 The galvanic series in seawater from LaQue [83]

Galvanic corrosion does allow for cathodic and anodic protection to be used beneficially. Cathodic protection happens by placing a metal into contact with a more anodic metal so that the anodic metal sacrificially corrodes and protects the more cathodic metal [82]. Anodic protection occurs when the metal to be protected acts as the anode in a galvanic couple due to an external power supply that controls the cell potential and keeps the metal in a passive thermodynamic region [84].

Typically, γ-ZnNi coatings contain many crevices that penetrate through the coating to the underlying substrate. These coatings protect the underlying metal by cathodic protection. The CCCs and TCPs passivate a γ-ZnNi coating by preventing electrolyte contact with the surface and underlying substrate. The self-healing mechanisms of CCCs and TCPs protect the underlying

substrate by precipitating Cr^{3+} species onto the cathodic sites where pH is locally lower, slowing the cathodic reaction.

Characterization of Passive Films

Physical Characterization.

Electron microscopy is one of the most prevalent techniques used to physically characterize TCPs. In the case of thick coatings, scanning electron microscopy (SEM) is used to measure the thickness and examine morphology within the layer. For thin coatings, SEM is often used to look for the presence of cracks or pores on the surface as well as to visually compare the roughness of the surface pre- and post-deposition. When paired with energy dispersion spectroscopy (EDS), it has been used to simultaneously examine chemical composition of the passive layer but only on thick coatings [44] [71] [77] [85] [86]. Transmission electron microscopy (TEM) is used more rarely but allows for accurate measurement of thin TCP thickness and verification of the amorphous or crystalline nature of the deposited layer [54] [87] [88] [89]. Even more rarely, atomic force microscopy (AFM) is used to investigate surface roughness and ellipsometry is used to determine layer thickness [90] [91].

Chemical Characterization

Due to the thin nature of the TCP layers, most chemical characterization relies on X-ray photoelectron spectroscopy (XPS) to determine layer composition. Other techniques used include glow discharge optical emission spectroscopy, auger electron spectroscopy, Raman spectroscopy, and inductively coupled plasma optical emission spectroscopy [61] Due to the nature of multiplet splitting in Cr XPS spectra and the fact that TCPs are made up of mixtures of Cr oxides, hydroxides and Zn, multiple chemical characterization methods need to be used to accurately describe the valence state of the Cr present. Unfortunately, only a few studies have confirmed their XPS findings with multiple analytical methods [54] [88] [92]. When investigating specifically the content of Cr(VI), another analytical method based upon 1,5 diphenylcarbazide (DPC) can be used.

Using UV/Vis spectrophotometry a reaction between DPC and Cr(VI) in solution can be quantitatively determined. DPC is oxidized by Cr(VI) to form 1,5 diphenylcarbazone and Cr(III) which then forms a complex with Cr(III) to create a pink color in acidic solutions. This pink color has a peak absorbance at ~540 nm that can be quantitatively measured given a set of known standards has also been measured. The method does suffer from interferences with Fe, Mo, and V, but the absorbance directly from these species is orders of magnitude less sensitive than Cr and thus amounts in the 10-100 µg/mL region can be tolerated without concern. Fe(II) ions create a bigger problem as they can reduce the Cr(VI) thus generating a false negative requiring the use of a buffer such as NaF to ensure accurate measurement [93] [94].

Electrochemical Characterization

Several electrochemical techniques can be used to characterize coated specimens and their corrosion resistance including open circuit potential (OCP), cyclic potentiodynamic polarization (CPDP), and electrochemical impedance spectroscopy (EIS). OCPs are determined by placing the specimen as the anode in a three electrode setup and measuring the potential while waiting for the specimen to equilibrate with an example give in Figure 9. The measured potential represents the point at which no current is flowing in the sample and is the maximum potential difference the cell would see without an applied voltage or current [95]. Comparisons between OCPs in the same

electrolyte allows for determination of which specimens would function as the anode in a galvanic couple or which specimen has a greater driving force for corrosion. In the case of coatings and passivations, it can indicate a reduction in driving force for corrosion or confirm that a coating is/is not acting sacrificially.

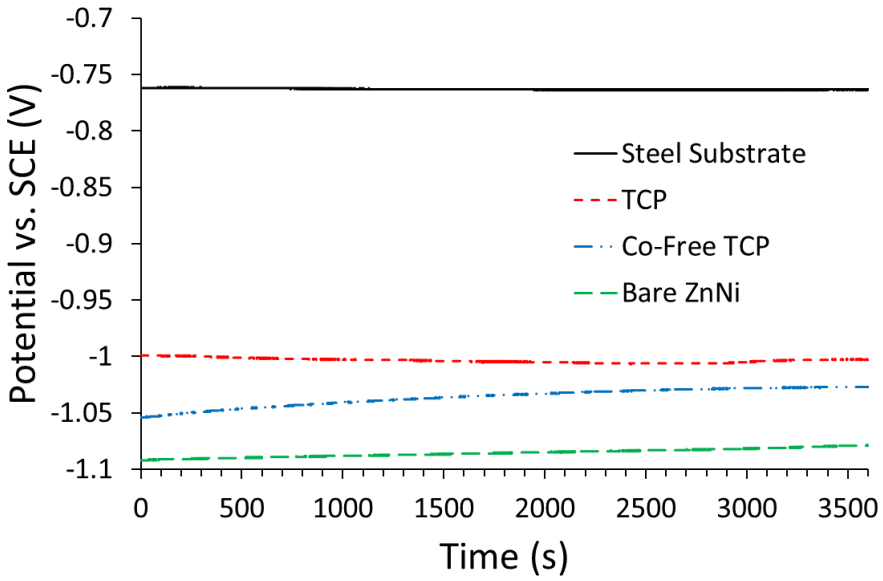

Figure 9 Open circuit potentials of steel samples in 0.6 M NaCl + 0.6 M $NH_4(SO_4)2$

CPDP is done after measuring OCP and begins at a voltage below the OCP. A potential is applied to the cell and sweeps at a slow rate, usually around 0.1667 mV/s, and continues above the OCP to a point where the scan is then repeated in reverse [96]. This serves as a technique to get information from both an anodic and cathodic polarization simultaneously with the understanding that cathodic reactions can affect the subsequent anodic polarization. The CPDP can also show if a region of passivity exists above the OCP and can identify the presence of pitting corrosion.

Figure 10 shows a theoretical curve for a sample demonstrating many possible features visible from a CPDP. A Tafel approximation can be performed at the corrosion potential to estimate the corrosion current, i_{corr}, and the polarization resistance, R_p, which can be compared between specimens to determine if a coating or passivating treatment is reducing the rate of corrosion.

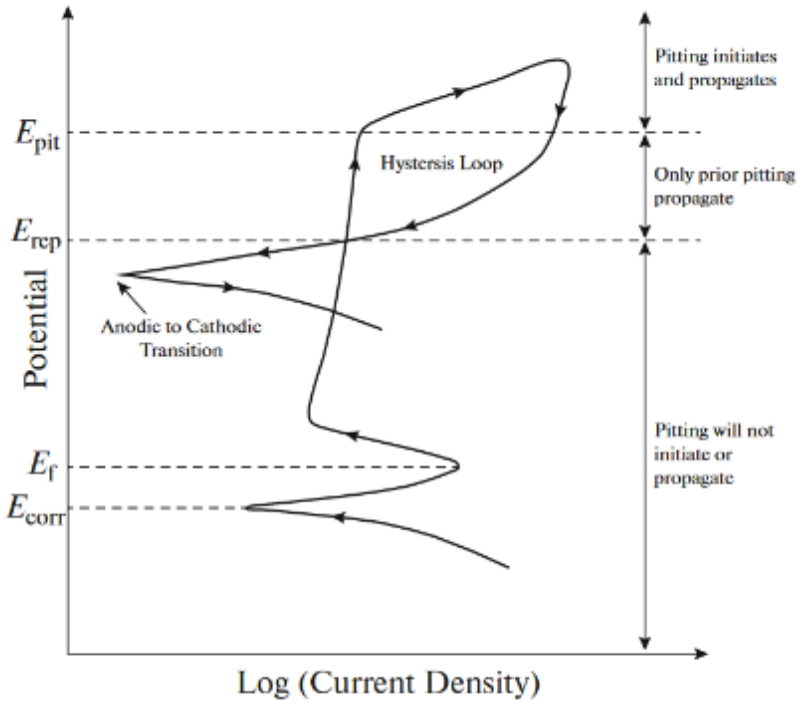

Figure 10 Theoretical CPDP curve showing notable features related to pitting, passivation, and surface breakdown. Image from Ezmailzadeh et al. [97]

Electrochemical impedance spectroscopy is a technique often used in corrosion studies because of the amount of information that can be indirectly obtained. Information can be gathered by visual inspection of changes in the Nyquist and Bode plots to get semi-quantitative comparisons between different specimens. Quantitative information can be obtained through equivalent circuit modeling of the active mechanisms present and then attributed to physical processes via experimentation. Using this quantitative and semi-quantitative data, aspects of the corrosion process and coating morphology can be inferred. EIS data can also detect changes in the surface such as growth of new phases and can be used to compare susceptibility to corrosion of different treatments.

For equivalent circuit modeling to be valid the data must satisfy the Kramers-Kronig relationships for complex quantities which allow real data to be constructed from imaginary data and vice versa. The requirements placed on data are linearity, causality, and stability. Stability is ensured when the perturbation or amplitude of the applied signal does not change as the experiment is run. Linearity is satisfied if the data have a linear response to the applied perturbations. Lastly, causality is satisfied if a response to the perturbation does not occur prior to the perturbation [98].

An equivalent circuit model will always satisfy the Kramers-Kronig relationships as the circuits are mathematical models that are always linear, stable, and causal. For real data, stability and causality can be considered satisfied and it is the requirement of linearity that fails due to non-stationary effects. Non-stationarity is the result of gas evolution, a chemical reaction, or instrumental artifacts that cause time-dependent noise greatest in the low frequency region where sampling times are long. Satisfaction of the Kramers-Kronig relationships is usually verified

analytically by separating impedance data into real and imaginary parts, transforming them, and then recombining to see if the original data is recreated [98]. For corrosion studies, if the original data cannot be recreated, then the data is not valid and either the experiment must be redesigned to slow down corrosion of the studied material, or the lower frequencies studied during EIS must be dropped until stationarity is ensured in the remaining data.

The last consideration when using equivalent circuit modeling of EIS data to investigate a surface is the model fit itself. There are an infinite number of electrical circuits that will provide a valid fit to experimentally gathered EIS data which necessitates knowledge of the surface, coating, or passivation being studied and confirmation of results via different analytical methods. Emphasis must be placed on ensuring the results are physical and real by limiting the number of circuit components to only those that can be justified via chemical or morphological evidence from other characterization methods.

Materials and Methods

TCP Passivation Characterization on γ-ZnNi Coated S1008 Steel

Specimen Preparation

SAE 1008 steel substrates were prepared in two separate batches. One batch had dimensions of 10 cm by 2.5 cm by 0.2 cm and the other 5.1 cm by 2.5 cm by 0.1 cm. Half of the specimens were polished and half were left unpolished. All specimens were prepared for electroplating by five minutes of alkaline cleaning in an aqueous solution containing 90 mL/L of Dipsol 523-SC (alkaline cleaning solution) at 55°C and sixty seconds of surface activation in an aqueous solution containing 40 wt% HCl + 60 g/L of Dipsol 971-SC (acid activator) at ambient temperature. Electroplating was conducted at 300 A/cm2 for twenty-five minutes in the Dipsol IZ-C17+ Zn / Ni deposition bath (proprietary electroplating solution). The resulting ZnNi coating contained approximately 80/20 wt% Zn/Ni and consisted of Ni_5Zn_{21} and $NiZn_3$ γ-phase stoichiometries.

The ZnNi plated panels were then either polished or left as-plated prior to being passivated with TCP or Co-Free TCP. Grinding and polishing was done on a wheel (Buehler Ecomet III) at 500 RPM with each step performed until no scratches from the previous step were visible. Grinding steps used water as the lubricant and went in order from 80 and 120 grit paper with alumina abrasives to 180, 240, 320, 400, 600, 800, and 1200 grit paper with SiC abrasives. Specimens were then polished using 1.0 μm and 0.3 μm alumina suspensions (Buehler MicroPolish) on a polishing cloth (Buehler MicroFloc) with an aqueous lubricant (MetaDi Fluid). Each polishing step was conducted for 30 seconds. Between each grinding or polishing step, specimens were rinsed with soapy water, ultrasonically cleaned in ethanol for 3 mins, and then dried with a heat gun.

Both as-deposited and polished ZnNi-plated specimens were passivated according to the following procedure:

1. 1mL/L HCl acid activation for 15 seconds followed by two 30 second DI water rinses
2. Passivation of the Dipsol IZ-264 TCP (proprietary passivating bath) or the cobalt-free modified IZ-264 TCP (proprietary passivating bath) via chemical bath deposition for 90 seconds

3. 25 second drain followed by 30 second DI water rinse
4. Hot rinsed in DI water for 30 seconds
5. Air dried
6. Heat treated at 191°C for 23 hours in air

Salt Spray Exposure

There were six specimens for every tested condition with two set aside and used for testing at 0 hours of salt spray exposure (SSE), while the remaining four were placed in a salt spray chamber (Cyclic Corrosion Tester, Q-Fog) set up for ASTM B117 [9]. After 500 hours of SSE two of the four specimens were removed and characterized and after 1000 hours of SSE the last two specimens were removed and characterized. After SSE, specimens were rinsed in DI water until no more salt product was removed or 30 seconds, whichever was longest, and then air dried for 24 hours. Dried specimens had contact resistance measured consistent with MIL-DTL-81706B [99] specifications of 200 pounds of force per square inch using copper electrodes with 10 measurements taken per specimen using a source measure unit (2450 Sourcemeter, Keithley 1.00 Amp, Power Line Cycles = 10, 4-wire resistance measurement mode) prior to further characterization.

Imaging

Images after SSE were taken of specimens using a camera or a printer/scanner. Specimens were also imaged using optical microscopy with a digital optical microscope (KH-8700, Hirox). Some specimens were sectioned using a shear cutter and a low speed saw (Isomet 11-1280-160, Buehler) for X-ray photoelectron spectrometry (XPS; Axis 165, Kratos, Al anode, dwell time = 500 ms, spot size = 120 µm, no sputtering used) or scanning and transmission electron microscopies (SEM and TEM, respectively). The amount of corrosion product was measured as the percentage of the panel area that was covered using computerized image analysis (ImageJ; National Institute of Health) to trace the regions where corrosion product was visible and dividing that by the total area of the specimen in pixels from the specimen pictures. Corrosion product from an unpassivated ZnNi specimen after 1000 hours SSE was analyzed via X-ray diffraction (XRD; X'Pert Pro, Panalytical, Cu K_α = 1.540598 Å, fixed slit = 0.38 mm, data angle = 5.015° - 89.975° 2θ, step size = 0.03°). Computerized image analysis was also used to count the cracks per mm by utilizing a method similar to ASTM E112-13 [100] to find the lineal mean intercept of the cracks. Lastly, crack widths were measured using computerized image analysis by taking thirty measurements of randomly selected cracks in SEM images across all images of a sample and averaging.

SEM was done on either a RAITH e-Line PLUS or a Hitachi S-4700 while TEM liftouts were produced using a gallium focused ion beam on an FEI Scios with the following procedure. A representative section of the surface was located and had platinum deposited in a 15 µm by 1.5 µm rectangle with the electron beam at 5 kV and 1.4 nA beam current to a thickness of 200 nm. This was followed by a Pt deposition on the same spot with the ion beam at 30 kV and 0.28 nA to a thickness of 1.5 µm. A cross-section pattern was then used in a 20 µm by 12 µm rectangle to a depth of ~6 µm with the ion beam at 30 kV and 21 nA and then repeated on the other side. Cleaning cross-sections were used to further mill both sides from the edge of the platinum to 1.5 µm into the milled trough at a current of 6.5 nA. A U-shaped cut was made into the cross-section to almost separate it from the substrate and a tungsten probe welded onto one corner of the liftout with platinum. The liftout was then removed and welded onto a Cu TEM grid post and thinned to electron transparency by tilting +/- 2° by using 2.8 nA beam currents for bulk removal followed

by 0.46 nA currents for the final thinning. The last step consisted of a 28 pA cleaning of each side at a 7° tilt for two minutes. TEM images were gathered using a Tecnai F20 scanning TEM (STEM).

Passivation thicknesses were measuring using computerized image analysis on TEM liftout images where 30 lines were drawn perpendicular on a random part of the passivation with the measurements averaged across all lines. When multiple images were available, the 30 lines were split across the available images and averaged the same way.

Electrochemical Characterization

Electrochemical characterization took place in 250 mL of a 0.6 M NaCl (Fisher Scientific, Granular USP/FCC) + 0.6 M $NH_4(SO_4)_2$ (Fisher Scientific, Certified ACS) electrolyte. The electrolyte was placed in a flat cell and used a saturated calomel reference electrode (+0.244 V vs. SHE at 25°C). Electrochemical testing was performed using a potentiostat/galvanostat (Model 273A, Princeton Applied Research) and a frequency response analyzer (SI 1255 HF, Solartron Instruments). Open circuit potentials (OCPs) were measured first for 3600 seconds followed by cyclic potentiodynamic polarizations (CPDP). CPDPs were performed by sweeping from -0.3 V to 0.8 V and back to -0.3 V vs. OCP at a rate of 0.1667 mV/second. Each specimen had electrochemical testing performed three times on three different areas. The OCP and CPDP data were analyzed using CView (3.5h, Scribner Associates) to perform Tafel analysis at the corrosion potential. All values were averaged across the multiple trials done for each sample.

TCP Passivation Characterization on γ-ZnNi Al6061-T6

Specimen Preparation

Test coupons that were 254 mm by 76 mm by 1 mm were sectioned from a sheet of Al6061-T6 as per MIL-DTL-81706B39. The sectioned panels were sent to a commercial vendor for deposition of an electroless nickel layer that was nominally ~5 μm thick. Next, panels were immersed for five minutes in an aqueous solution containing 90 mL/L of an alkaline cleaner (523-SC, Dipsol of America) at 55°C then immersed for 60 s in an aqueous solution containing 40 wt% HCl and 60 g/L of a surface activator (971-SC, Dipsol of America) at ambient temperature. A commercial γ-ZnNi coating (IZ-C17+, Dipsol of America) was deposited by electroplating at 300 A/cm2 for twenty-five minutes. Panels were then either left unpassivated (bare) or passivated with one of three coatings, a trivalent chromium passivation (TCP; IZ-264, Dipsol of America), an experimental cobalt-free version of the TCP (Co-Free; modified IZ-264, Dipsol of America), or a hexavalent chromium conversion coating (HexCr; IZ-258, Dipsol of America). Depositions of passivations began with surface activation by immersion for 15s in an aqueous solution containing 1 mL/L HCl followed by two rinses of 30 s each in deionized (DI) water. Panels were then immersed in the deposition bath for 90 s, drained for 25 s, followed by a 30 s rinse in DI water, a 30 s rinse in 71-82 °C DI water, and drying at ambient temperature in ambient atmosphere. Prior to testing, specimens were rinsed with acetone followed by DI water and allowed to dry for 24 hours. Some panels were scribed with an "X" to a depth of ~10 μm through the middle of the panel using a 1/16" diameter endmill and a computerized numerical control machine (Model 5400, Sherline Products Inc.).

Characterization

Electrical contact resistance was measured using a custom-built apparatus consistent with MIL-DTL-81706B. The apparatus has a 1 in^2 copper top electrode and a 2.4 in^2 copper bottom electrode. Prior to measurements, the copper electrodes were polished with 240 grit SiC paper (50-10015, Allied High Tech Products) for 30 seconds then rinsed with soapy water and ultrasonically cleaned in ethanol (90.4%, Fisher Scientific). The electrodes were then dried with a heat gun and allowed to sit for 24 hours prior to any measurements being taken. The power source for the resistance measurements was a source measure unit (2450 Sourcemeter, Keithley 1.00 Amp, Power Line Cycles = 10, 4-wire resistance measurement mode). Measurements were made at 10 points on the panel surface in the order and locations specified in MIL-DTL-81706B.

Salt spray exposure (SSE) was performed in a chamber (Cyclic Corrosion Tester, Q-Fog) according to ASTM B117 with sodium hydroxide (10.0 N, Alfa Aesar) or hydrochloric acid (36.5%, Fisher Scientific) added to maintain neutral pH [9]. Panels were exposed to salt spray for 0, 168, 336, 500, or 1000 hours. Each passivation had three panels for 0 hours exposure and one scribed panel at all other conditions except for HexCr, which only had two panels at 0 hours and had no panels at 1000 hours because three panels from the original set were not of acceptable quality. After undergoing SSE for the pre-determined amounts of time, panels were removed from the chamber and rinsed in DI water with light abrasion provided by a nitrile glove covered hand for either 30 seconds or until no salt was being removed from the surface, whichever was longer.

Imaging

Specimens were imaged before and after SSE using a printer/scanner and a digital optical microscope (KH-8700, Hirox). Computerized image analysis (ImageJ, 1.52a; National Institute of Health) was used to determine the fraction of the panel area covered by corrosion product on unscribed specimens by tracing the regions where corrosion product was visible and dividing that by the total exposed area of the specimen. For scribed specimens, computerized image analysis traced the corroded areas on the X-shaped scribes and divided the measured area by the total area of the scribe to determine the extent of corrosion in scribed areas. The area density of cracks was determined utilizing a method similar to ASTM E112-13 calculating the lineal mean intercept with computerized image analysis [100]. Electron microscopy specimens approximately 1 cm by 1 cm for electron microscopy were cut from larger panels using a shear cutter and a low speed saw (Isomet 11-1280-160, Buehler). Scanning electron microscopy (SEM) was performed on two different instruments (S-4700, Hitachi or e-Line plus, RAITH). Corrosion product from a Co-Free TCP specimen after 1000 hours SSE was analyzed via X-ray diffraction (XRD; X'Pert Pro, Panalytical, Cu Kα = 1.540598 Å, fixed slit = 0.38 mm).

Liftouts for transmission electron microscopy (TEM) were produced using focused ion beam (FIB) milling (Scios, FEI) with a gallium source. A scanning TEM (STEM; F20, Tecnai) was used to image liftout specimens. Liftouts were produced by choosing a representative section of the surface and depositing platinum in a 15 µm by 1.5 µm rectangle with the electron beam at 5 kV and 1.4 nA beam current to a thickness of 200 nm. The ion beam was then used at 30 kV and 0.28 nA beam current to deposit platinum to a thickness of 1.5 µm. A 20 µm by 12 µm rectangle cross-section pattern was then milled to a depth of ~6 µm with the ion beam at 30 kV and 21 nA and then repeated on the other side. The sample was further milled from the edge of the platinum to 1.5 µm away from the platinum on both sides at a current of 6.5 nA. A U-shaped cut was made to almost separate the cross-section and a tungsten probe welded onto one corner at the top with

platinum. The liftout was removed by finishing the cut and welded onto a Cu TEM grid post and thinned to electron transparency by tilting +/- 2° by using 2.8 nA beam currents for bulk removal followed by 0.46 nA currents for the final thinning. The last step consisted of a 28 pA cleaning of each side at a 7° tilt for two minutes.

Computerized image analysis was used to measure passivation thickness by drawing 30 lines perpendicular to the passivation on randomly selected parts of the images and averaged over all images. Passivation morphology was characterized using computerized image analysis by performing a fast Fourier transform on a section of the image that only contained the passivation layer.

Electrochemical Characterization

A flat cell with a saturated calomel reference electrode (+0.244 V vs. SHE at 25°C) and 250mL of 0.6 M NaCl (Fisher Scientific, Granular USP/FCC) + 0.6 M $NH_4(SO_4)_2$ (Fisher Scientific, Certified ACS) pH 5.3 electrolyte was used for all electrochemical testing. A potentiostat/galvanostat (Model 273A, Princeton Applied Research) and a frequency response analyzer (SI 1255 HF, Solartron Instruments) supplied the electrical signal for all electrochemical testing. Electrochemical tests were performed in order of open circuit potential (OCP) measured for 4000 seconds, followed by five replicates of electrochemical impedance spectroscopy (EIS) from 105 to 10-2 Hz at an amplitude of ±10 mV vs. OCP, and finished with a potentiodynamic polarization (PDP) ranging from -0.3 V to 0.8 V and back to -0.3 V vs. OCP at a rate of 0.1667 mV/second. Each specimen had electrochemical testing performed three times on three different areas to assess repeatability. OCP and PDP data were analyzed using CView (3.5h, Scribner Associates) software to perform Tafel analysis at the corrosion potential and correlating the data with observations of the flat cell made during the PDP. EIS data was analyzed using ZView (3.5h, Scribner Associates) to fit equivalent circuit models and validate data using a Kramers-Kronig fit. Values obtained were averaged across data obtained from each electrochemical test for each analyzed specimen.

Effect of Heat Treatment on Chromate Content and Performance of TCP Passivations

Specimen Preparation

Al6061-T6 sheets were sectioned into test panels that were 254 mm by 76 mm by 1 mm using a shear cutter. The sectioned panels were plated with a layer of electroless nickel ~5 µm thick by a commercial vendor before having electroplated γ-ZnNi (IZ-C17+, Dipsol of America) applied using the procedure summarized in Table 2. The γ-ZnNi was electroplated using a current density of 300 A/cm^2 for twenty-five minutes to produce a layer ~20 µm thick. Next, the panels were passivated with either a commercial trivalent chromium passivation (TCP; IZ-264, Dipsol of America), or a cobalt-free trivalent chromium passivation (Co-Free TCP; IZ-ASCF02, Dipsol of America). Some panels were left unpassivated. Heat treatments chosen for the specimens were 80ºC for 30 minutes or 191ºC for 24 hours done in ambient atmosphere. The heat treatments were chosen to simulate commercially used processes for automotive components (80ºC) and low hydrogen embrittlement bakes for steel (191ºC). The procedure used to prepare panels, deposit passivations, and heat treat coatings is outlined in Table 3. All specimens were cleaned with acetone and rinsed with deionized (DI) water, then allowed to dry for twenty-four hours before testing.

Table 2 Sample cleaning and treatment for electroplating of the γ-ZnNi layer.

Step	Parameter	Material	Temperature	Time
Alkaline Cleaning	90 mL/L	523-SC, Dipsol of America	55°C	300 s
Double Rinse	-	Deionized Water	Ambient	30 s each
Surface Activation	40 wt% 60 g/L	HCl 971-SC, Dipsol of America	Ambient	60 s
Double Rinse	-	Deionized Water	Ambient	30 s each
Electroplating	300 A/cm^2	IZ-C17+, Dipsol of America	25°C	25 mins
Double Rinse	-	Deionized Water	Ambient	30 s each

Table 3 Sample treatment for application and heat treatment of passivating trivalent chromium coatings.

Step	Parameter	Material	Temperature	Time
Acid Activation	1 mL/L	HCl solution	Ambient	15 s
Double Rinse	-	Deionized Water	Ambient	30 s each
Passivation	pH 4.2 pH 4.0	IZ-264, Dipsol of America IZ-ASCF02, Dipsol of America	25°C 25°C	90 s
Drain	-	-	Ambient	25 s
Rinse	-	Deionized Water	Ambient	30 s
Hot Rinse	-	Deionized Water	71-82°C	30 s
Dry	-	-	Ambient	Until Dry
Bake	-	-	80°C 191°C	30 mins 23 hrs

Characterization

Specimens were exposed to neutral salt spray (Cyclic Corrosion Tester, Q-Fog) as described in ASTM B117 [9]. The neutral pH of the 5 wt% aqueous NaCl solution was maintained by additions of either hydrochloric acid (36.5%, Fisher Scientific) or sodium hydroxide (10.0 N, Alfa Aesar). Salt spray exposure (SSE) was performed in one week (168 hours) intervals. After removal from the chamber, test coupons were rinsed with DI water for thirty seconds or until no visible salt remained on the surface, whichever took place first. Specimens were dried with compressed air after rinsing and had a 35 mm by 75 mm section removed for analysis. Visual inspection of test

panels resulted in removal from further SSE if a majority of the panel was covered by corrosion product, otherwise panels were put back into the chamber for another 168 hours of SSE.

The amount of Cr(VI) in the passivations was measured quantitatively using a modified version of the screening boiling test for hexavalent chromium in surfaces listed by the Danish Environmental Protection Agency from IEC 62321. Three types of aqueous solutions were used in the hexavalent chromate analysis. The first was 75 wt% phosphoric acid, the second was 1,5-diphenylcarbazide indicator, and the third was Cr(VI) standards. The solutions were produced as follows:

1. 350 mL of 85 wt% phosphoric acid (Acros Organic) was added to 125 mL of DI water in a 500 mL flask and topped to 500 mL with DI water to produce 75 wt% phosphoric acid solution
2. 1.0g of 1,5-diphenylcarbazide (Certified ACS, Fisher Scientific) was added to 100 mL of acetone (HPLC-UV grade, Pharmco) with 1 drop of acetic acid (99.7%, Sigma Aldrich) and mixed until dissolved to produce the indicator solution
3. 0.113g of potassium dichromate (99%, Acros Organic) was added to 1000 mL of DI water and mixed, then 0.5, 1.0, 1.5, 2.0, or 2.5 mL of that solution were added to 450 mL of DI water and brought to 500 mL with DI water to produce the standards containing 0.04 µg/mL, 0.08 µg/mL, 0.12 µg/mL, 0.16 µg/mL, and 0.2 µg/mL of Cr(VI).

Chromate analysis was performed by placing a coating with 50 ± 5 cm^2 of exposed surface area in a beaker with 50 mL of DI water with a layer of boiling stones. The beaker was covered with a watch glass and brought to a boil for 10 minutes. After boiling the resulting solution was transferred to a sample container and filled to 50 mL with DI water and manually swirled for 15 seconds. One mL of 75 wt% phosphoric acid solution was added to the test solution and swirled for 15 seconds followed by removal of 1 mL of test solution into a 1 cm cuvette as a blank for analysis. Then, 1 mL of 1,5-diphenylcarbazide indicator solution was added to the test solution and swirled manually for 15 seconds followed by removal of 1 mL of test solution into a 1 cm cuvette for analysis. As specimens were sectioned following each SSE exposure time to produce analytical samples, only enough material was available to run each DPC test once per test condition.

UV-VIS spectrophotometry of the solutions was performed using a Thermo Scientific Genesys 10UV that was calibrated using the Cr(VI) standards described above with the calibration curve shown in Figure 11.

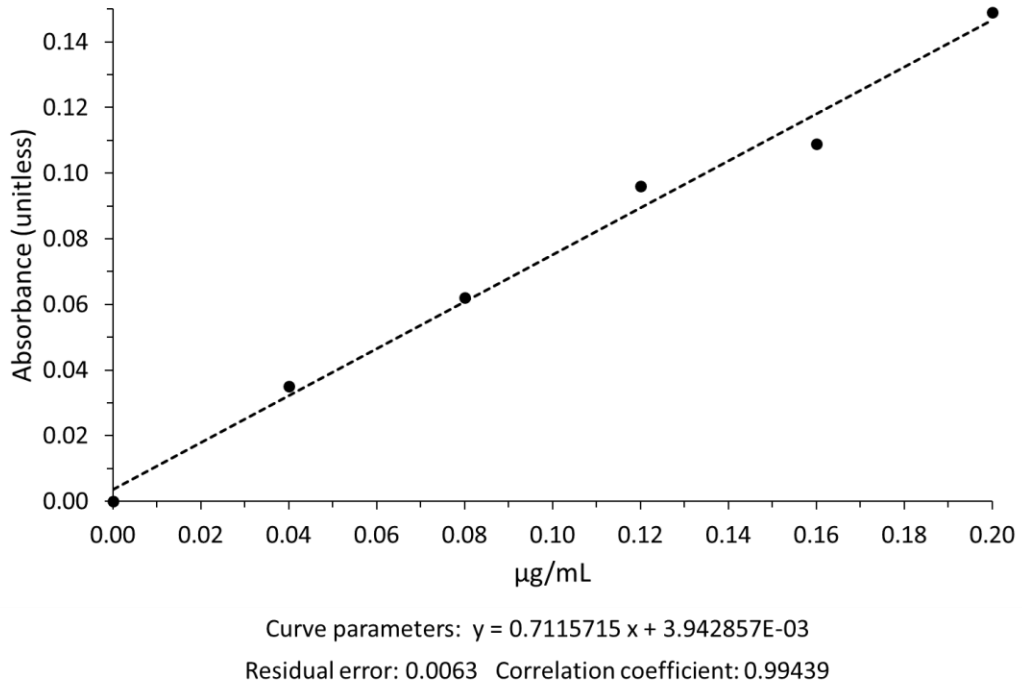

Figure 11 Calibration curve used for determination of Cr(VI) content via UV-Vis spectrophotometry.

All samples were tested immediately after preparation with a time of no longer than 20 minutes between boiling and finished analysis. For analysis, the blank was analyzed first followed by the sample. The concentration of chromate was determined by subtracting the absorbance of the blank from the sample value. Due to the amount of material required for analysis, only one sample was produced from each test specimen.

Validation of this Cr(VI) detection method was performed by taking a section of an TCP panel with no heat treatment that had 0 hours of SSE and repeating the test on the same panel to see if any Cr(VI) would be present after boiling in the first test. Results of this test detected 0.377 µg/mL Cr(VI) on the first 10 minute boil and 0.011 µg/mL on the second boil, an amount below the limit of detection for the analytical method. If the 0.011 µg/mL is assumed to be entirely signal and not noise, then the 10 minute immersion in boiling water should recover ~97% of Cr(VI) in the TCP layers.

Imaging

Corrosion progress and coating morphology were examined before and after SSE by imaging using a printer/scanner and digital optical microscope (KH-8700, Hirox). Computerized image analysis (ImageJ, 1.52a; National Institute of Health) was used to determine the area fraction of exposed surface covered in corrosion product or exhibiting discoloration after rinsing and drying following every interval of SSE. Area fraction was calculated by tracing corroded or discolored regions of each specimen with the polygon tool and dividing by the total exposed area. Any test panel exhibiting corrosion across the entire surface was not further analyzed.

Electrochemical Characterization

All electrochemical testing was performed using 250 mL of 0.6 M NaCl (Fisher Scientific, Granular USP/FCC) + 0.6 M $NH_4(SO_4)_2$ (Fisher Scientific, Certified ACS) electrolyte at a pH of 5.3 in a flat cell with a saturated calomel reference (SCE) electrode (+0.244 V vs. SHE at 25°C). The electrical signal was provided by a potentiostat/galvanostat (Model 273A, Princeton Applied Research) for open circuit potential (OCP) and potentiodynamic polarization (PDP). First, OCPs were measured for 7200 seconds followed by PDPs that swept from -0.3V to 0.8V vs. OCP at a rate of 0.1667 mV/second. Electrochemical tests were performed in triplicate for repeatability. Analysis of OCP and PDP data utilized CView (3.5h, Scribner Associates) software to compare results across test conditions and correlate data to corrosion performance. All electrochemical data reported are values averaged across valid collected data sets for each specimen.

Analysis of Chromate Content and Performance of Heat Treated γ-ZnNi Coated Steel

Specimen Preparation

SAE 1008 coupons measuring 152 mm by 76 mm by 1 mm were used as test specimens. The coupons were either plated with a layer of electroless nickel (EN) ~10 µm thick or left bare and then electroplated with γ-ZnNi (IZ-C17+, Dipsol of America) applied using the series of steps in Table 4. Electroplating of the γ-ZnNi was performed at a current density of 0.03 A/cm^2 for twenty-five minutes to plate a thickness of ~20 µm. Following ZnNi plating the panels were passivated with one of two treatments, a commercial trivalent chromium passivation (TCP; IZ-264, Dipsol of America), or a cobalt-free trivalent chromium passivation (Co-Free TCP; IZ-ASCF02, Dipsol of America). Lastly, one set of EN plated panels for each passivation and the panels with no EN layer were heat treated at 191ºC for 24 hours done in ambient atmosphere. The heat treatment is a commercially used processes for low hydrogen embrittlement bakes on steel. Table 5 outlines the procedure used for cleaning, passivating, and heat treating the relevant panels. An acetone cleaning and deionized water (DI) rinse followed by twenty-four hours of drying was used on all specimens prior to testing. The final batch of specimens was separated into six categories to describe the different experimental conditions and given shorthand identifiers as listed:

1. EN TCP 191ºC – EN-plated, IZ-264 TCP, heat-treated specimens
2. EN Co-free TCP 191ºC – EN-plated, IZ-ASCF02 TCP, heat-treated specimens
3. EN TCP no heat - EN-plated, IZ-264 TCP, no heat treatment
4. EN Co-free TCP no heat - EN-plated, IZ-ASCF02 TCP, no heat treatment
5. TCP 191ºC – IZ-264 TCP, heat-treated specimens
6. Co-free TCP 191ºC – IZ-ASCF02 TCP, heat-treated specimens

Table 4 Sample cleaning and treatment for electroplating of the γ-ZnNi layer.

Step	Parameter	Material	Temperature	Time
Alkaline Cleaning	90 mL/L	523-SC, Dipsol of America	55°C	300 s
Double Rinse	-	Deionized Water	Ambient	30 s each
Surface Activation	40 wt% 60 g/L	HCl 971-SC, Dipsol of America	Ambient	60 s
Double Rinse	-	Deionized Water	Ambient	30 s each
Electroplating	0.03 A/cm^2	IZ-C17+, Dipsol of America	25°C	25 mins
Double Rinse	-	Deionized Water	Ambient	30 s each

Table 5 Sample treatment for application and heat treatment of passivating trivalent chromium coatings.

Step	Parameter	Material	Temperature	Time
Acid Activation	1 mL/L	HCl solution	Ambient	15 s
Double Rinse	-	Deionized Water	Ambient	30 s each
Passivation	pH 4.2 pH 4.0	IZ-264, Dipsol of America IZ-ASCF02, Dipsol of America	25°C 25°C	90 s
Drain	-	-	Ambient	25 s
Rinse	-	Deionized Water	Ambient	30 s
Hot Rinse	-	Deionized Water	71-82°C	30 s
Dry	-	-	Ambient	Until Dry
Bake	-	-	191°C	24 hrs

Characterization

Neutral salt spray (Cyclic Corrosion Tester, Q-Fog) was used to test corrosion performance as described in ASTM B117 [9]. The pH of the 5 wt% aqueous NaCl solution was controlled by pH adjustment through hydrochloric acid (36.5%, Fisher Scientific) or sodium hydroxide (10.0 N, Alfa Aesar) additions. Panels remained in salt spray exposure (SSE) for one week (168 hours) intervals across a total of 4 weeks (672 hours). The test coupons were rinsed with DI water for thirty seconds, or until no visible salt remained on the surface after removal from the chamber. Drying after rinsing was done with compressed air followed by visual inspection and imaging. At each one-week interval, panels were removed from the chamber and labelled with their extent of

SSE to be sectioned for further analysis while the remaining specimens were placed back into the chamber for another week.

Bulk Cr(VI) in the passivations was measured quantitatively by using 1,5-diphenylcarbazide and UV-Vis spectrophotometry on solution obtained by boiling exposed coupon surface in acidic solution to leach the hexavalent chromium. Four types of aqueous solutions were used in the hexavalent chromate analysis. The first was 75 wt% phosphoric acid, the second was 1,5-diphenylcarbazide indicator, the third was Cr(VI) standards, and the fourth was 5 wt% NaF solution. The solutions were produced as follows:

1. 350 mL of 85 wt% phosphoric acid (Acros Organic) was added to 125 mL of DI water in a 500 mL flask and topped to 500 mL with DI water to produce 75 wt% phosphoric acid solution.
2. 1.0g of 1,5-diphenylcarbazide (Certified ACS, Fisher Scientific) was added to 80 mL of acetone (HPLC-UV grade, Pharmco) with 1 drop of acetic acid (99.7%, Sigma Aldrich) then topped to 100 mL with acetone and mixed until dissolved to produce the indicator solution.
3. 0.113g of potassium dichromate (99%, Acros Organic) was added to 900 mL of DI water, topped to 1000 mL with DI water, and mixed, then 0.5, 1.0, 1.5, 2.0, or 2.5 mL of that solution were added to 450 mL of DI water and brought to 500 mL with DI water to produce the standards containing 0.04 µg/mL, 0.08 µg/mL, 0.12 µg/mL, 0.16 µg/mL, and 0.2 µg/mL of Cr(VI).
4. 5.0g of sodium fluoride (Certified ACS, Fisher Scientific) was added to 80 mL of DI water, brought to 100 mL with DI water, and then mixed thoroughly to produce the 5 wt% NaF solution.

Specimen Cr(VI) contents were analyzed by placing a section with 10 ± 1 cm^2 of exposed surface area in a 50 mL beaker with 9 mL of DI water and 1 mL of 5 wt% NaF solutions with a layer of boiling stones. The beaker was covered with a watch glass and brought to a boil for 10 minutes. After boiling the resulting solution was transferred to a sample container and filled to 10 mL with DI water and manually swirled for 15 seconds. Four drops or ~ 0.2 mL of 75 wt% phosphoric acid solution was added to the test solution and swirled for 15 seconds. 1 mL of test solution was then placed into a 1 cm cuvette as a blank for analysis. Then, 4 drops or ~0.2 mL of 1,5-diphenylcarbazide indicator solution was added to the test solution and swirled manually for 15 seconds. A 1 mL sample of test solution was then placed into a 1 cm cuvette for analysis. This process was performed in triplicate for each sample on which data was gathered which covered EN TCP 191ºC, EN Co-free TCP 191ºC, EN TCP no heat, and EN Co-free TCP no heat at SSE times of 0, 168, 336, and 504 hours.

UV-VIS spectrophotometry of the solutions was performed using a Thermo Scientific Genesys 10UV that was calibrated using the Cr(VI) standards described above. All samples were tested immediately after preparation with a time of no longer than 20 minutes between boiling and finished analysis. For analysis, the blank was analyzed first followed by the samples. The concentration of chromate was determined by subtracting the absorbance of the blank from the sample value.

Imaging

Corrosion progress of test specimens were examined after SSE by imaging using a printer/scanner and quantifying the corrosion coverage using computerized image analysis (ImageJ, 1.52a; National Institute of Health). The area fraction of corrosion product was determined by tracing around areas of visual corrosion product in specimen scans and calculated by dividing the traced regions by the total exposed area. The test specimens that had corrosion product across the entire surface were labelled as 100% coverage.

XPS Characterization

Test specimens were sectioned to produce ~1 cm^2 pieces with a shear cutter to be used for XPS analysis**.** Specimens were cleaned with a 30 second DI water rinse and allowed to dry with the test surface upside down in a glass vial laid on its side that only touched the specimen at the corners for 30 minutes. Standard specimens were powdered and were placed into glass vials shortly before testing with no cleaning done prior.

XPS data was gathered using a Thermo Fisher Scientific Nexsa using a monochromatic Al K_α 1487 eV X-ray source (6 mA, 12 kV). A charge compensation system was employed using a mixed flood of electrons and argon ions directed at the sample surface for all specimens to neutralize the surface charge. The carbon 1s spectra from each sample was adjusted to 285.0 eV and used to charge correct every other spectra from the sample. Specimens were first sputtered for 10 seconds at 1500 eV by an argon ion beam before any spectra were taken. Survey spectra (0-1350 eV range) were then gathered with a 400 µm spot size, a 200 eV pass energy, 50 ms dwell time, and 0.5 eV step size over 2 scans. High resolution scans were then gathered on C 1s (280-298 eV), Cr 2p (569-595 eV), and Co 2p (772-812 eV) using a 400 µm spot size, a 12.5 eV pass energy, 100 ms dwell time, and 0.1 eV step size with 4 – 20 scans depending upon signal strength.

Peak fitting of the XPS data was performed using CasaXPS v2.3.23PR1.0 software with a Shirley background used for all peak fits. Line shapes were chosen by starting with a 90% Gaussian/10% Lorentzian on peak fits for the standard samples and then iterated by a 10% change towards more Lorentzian character until the fit with the smallest residual was achieved. Fitting of the Cr 2p and Co 2p spectra followed a complex series of peaks to represent the multiplet splitting of the trivalent chromium and cobalt as well as the divalent cobalt species. Previous research by Biesinger et al. [101] was used as a guide to model this multiplet peak structure with the primary peak allowed to fit at a binding energy ±0.5 eV from Biesinger et al. and subsequent peaks constrained to fixed separations from the primary peak. Full width at half max (FWHM) values were allowed to deviate ±20% on all peaks to allow for sample and machine differences. Once peak fits had been obtained from the standard samples, the results were propagated and refit to each test specimen. Component fits were done using the Marquardt-Levenberg optimization algorithm available within CasaXPS.

Electrical Contact Resistance

Test coupons that were 254 mm by 76 mm by 1 mm were sectioned from a sheet of Al6061-T6 as per MIL-DTL-81706B [99]. Electrical contact resistance was measured using a custom-built apparatus consistent with MIL-DTL-81706B. The apparatus has a 1 in^2 copper top electrode and a 2.4 in^2 copper bottom electrode. Prior to measurements, the copper electrodes were polished with 240 grit SiC paper (50-10015, Allied High Tech Products) for 30 seconds then rinsed with soapy water and ultrasonically cleaned in ethanol (90.4%, Fisher Scientific). The electrodes were

then dried with a heat gun and allowed to sit for 24 hours prior to any measurements being taken. The power source for the resistance measurements was a source measure unit (2450 Sourcemeter, Keithley 1.00 Amp, Power Line Cycles = 10, 4-wire resistance measurement mode). Measurements were made at 10 points on the panel surface in the order and locations specified in MIL-DTL-81706B.

Evaluation of Performance of TCP Passivations on DOD Connectors

Analysis

Testing was performed per the Test Matrix in Table 6.

Table 6 Test Sequence Matrix

Test Sequence #	Test		Group 1	Group 2	Group 3
1	A-Appearance and Uniformity	Air Force Drawing 201027456 ZnNi Specification or Equivalent	X	X	X
2	B1-Shell Conductivity-2.5 mV	EIA 364-83, mated connectors may be wired or unwired	X	X	X
3	C-Coupling Torque Lubricity	EIA 364-13E Method A	X	X	X
4	D-Adhesion	EIA 364-42C Moderate		X	
5	E-Salt Spray	EIA 364-26, Test Condition C, Using ASTM B 117 Salt Spray Cabinet			X
6	C-Coupling Torque Lubricity	EIA 364-13E Method A		X	X
7	B1-Shell Conductivity-2.5 mV	EIA 364-83, mated connectors may be wired or unwired	X	X	
8	B2-Shell Conductivity-5.0 mV	EIA 364-83, mated connectors may be wired or unwired			X
9	A-Appearance and Uniformity	Air Force Drawing 201027456 ZnNi Specification or Equivalent	X	X	X

Group 1 consists of samples 1 and 2 of each plating type

Group 2 consists of samples 3 and 4 of each plating type

Group 3 consists of samples 5 and 6 of each plating type

Calibrated Equipment

Calibrated equipment used in the performance of these test sequences are listed as follows:

- Valhalla, 4300B Micro-Ohm Meter, Control No. 128382
- Snap-On, CTECH1MR100 Digital Torque Wrench, Control No. 6X144031
- Snap-On, TE3FUA Torque Wrench, Control No. 2X886513
- Thermalog, DINFJ32H1NN23, Control No. 6X048777
- Thermalog, DINFJ32H1NN23, Control No. C218379

Results and Discussion

Coating Development

TCP Passivation Characterization on γ-ZnNi Coated S1008 Steel

Visual Inspection After SSE

After SSE, the Co-Free passivations showed less corrosion than the TCPs regardless of whether the substrates were polished, but the difference in corrosion was greater between the unpolished specimens. Figure 12 shows the progression of corrosion build up from 0 to 1000 hours.

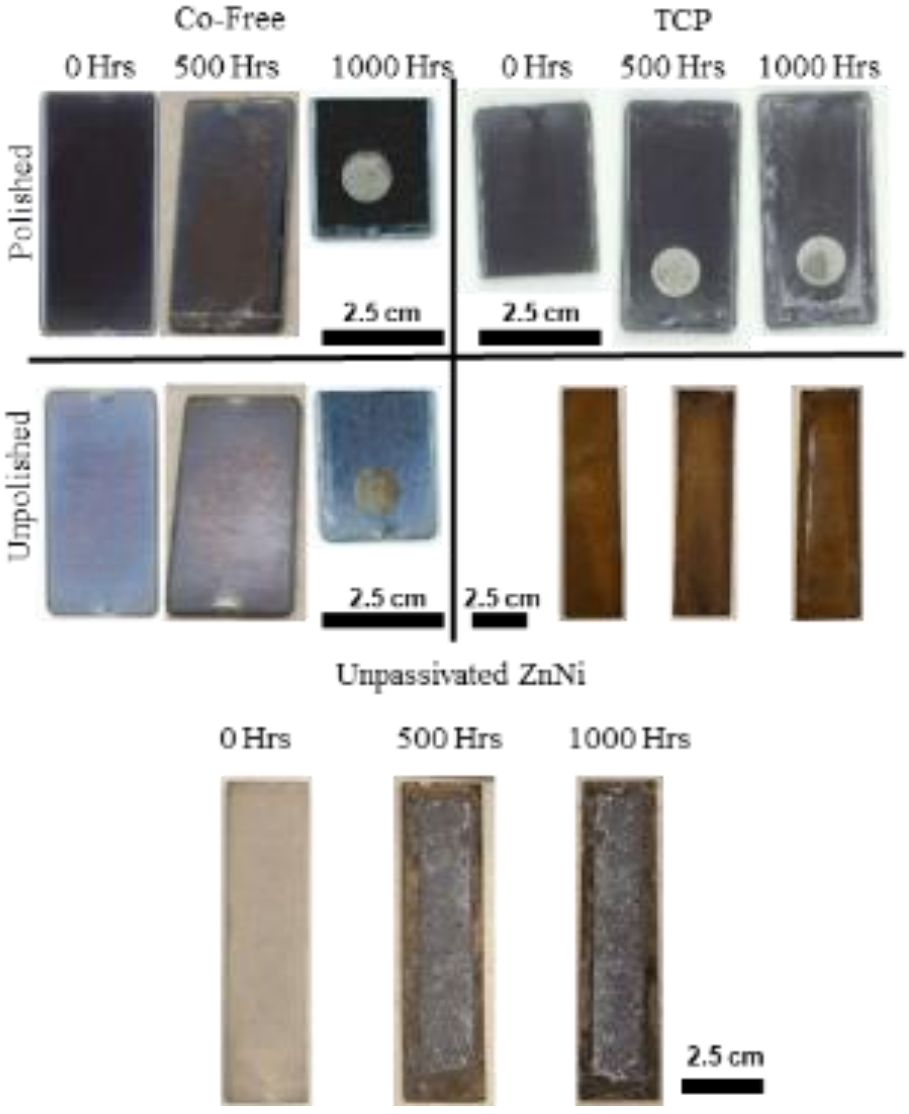

Figure 12 Appearance of different passivated specimens before and after salt spray exposure with unpassivated ZnNi for comparison

The images visually reinforce that the Co-Free passivation performs better than the TCP, which indicates that some aspect of the passivation is beneficial to corrosion performance. The polished TCP showed ~6% corrosion product coverage after 500 h SSE and ~15% corrosion product coverage after 1000 h SSE. For comparison, the Co-Free passivation had ~5% corrosion product coverage at 500 h and ~1% corrosion product coverage at 1000 h. The unpolished specimens followed a similar trend with TCP showing ~4% corrosion produce coverage at 500 h and ~22% at 1000 h, which was more than Co-Free with ~2% at 500 h and ~4% at 1000 h. The high variability in corrosion performance can be attributed to only having two specimens for most conditions with only one specimen for Co-Free 1000 h polished or unpolished, although the results demonstrate the large range of corrosion behavior, which is consistent with other studies.

Optical Microscopy and Crack Measurements

The progression of surface appearance during SSE is shown in Figure 13 (polished substrates) and Figure 14 (unpolished substrates).

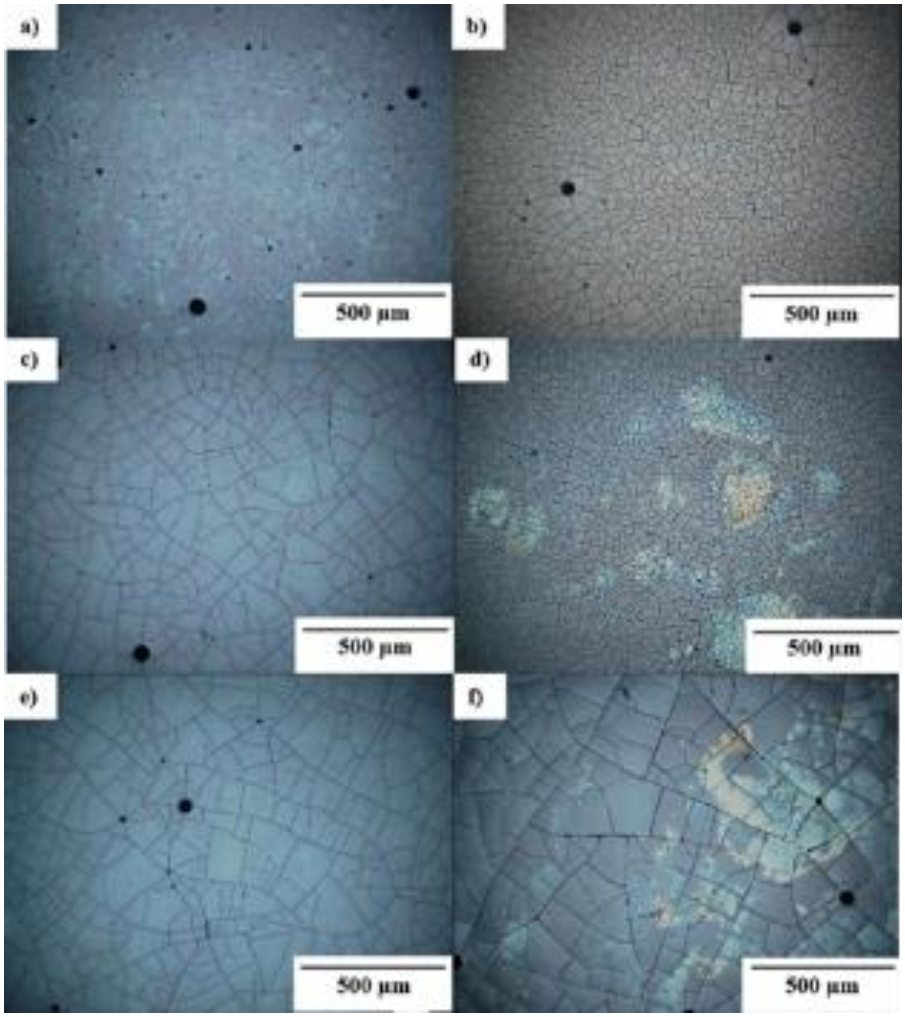

Figure 13 Polished steel samples showing a) TCP at 0 hours SSE, b) cobalt-free TCP (CoF) at 0 hours SSE, c) TCP at 500 hours, d) CoF at 500 hours, e) TCP at 1000 hours, and f) CoF at 1000 hours.

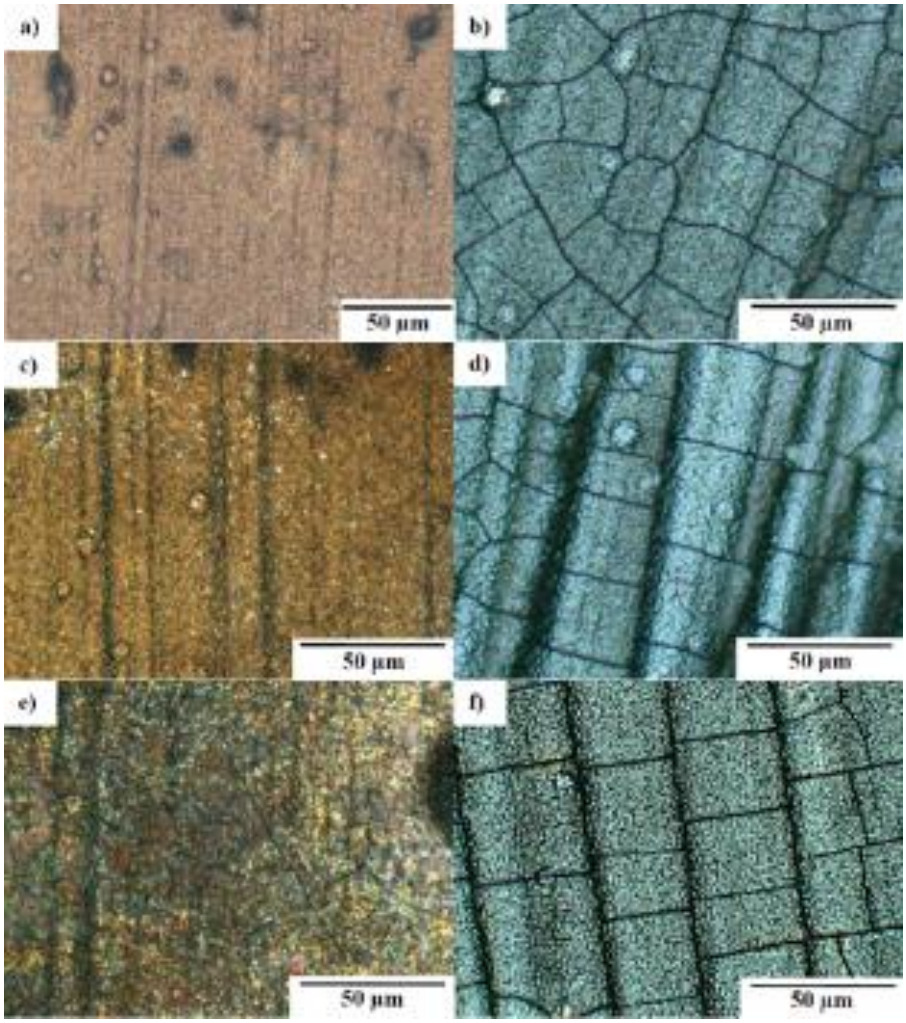

Figure 14 Unpolished steel samples showing a) TCP at 0 hours SSE, b) cobalt-free TCP (CoF) at 0 hours SSE, c) TCP at 500 hours, d) CoF at 500 hours, e) TCP at 1000 hours, and f) CoF at 1000 hours.

Very little corrosion product was observed for either of the passivations on polished specimens, but some staining was observed for the cobalt-free passivation after SSE. Numerous cracks were visible across the surface of both polished passivations with Co-Free passivations having 55 ± 4 cracks/mm after 500 hours SSE and 77 ± 8 cracks/mm after 1000 hours SSE, much more than TCP with 16 ± 4 cracks/mm after 500 hours SSE and 30 ± 3 cracks/mm after 1000 hours SSE. The unpolished cobalt-free passivation had fewer cracks than the polished specimen with 39 ± 15 cracks/mm after 500 hours SSE and 35 ± 10 cracks/mm after 1000 hours SSE, while the unpolished TCP had no visible cracks until 1000 hours of SSE after which it had 34 ± 10 cracks/mm. The specimens followed a trend of increasing cracks with increasing SSE time except for Co-Free passivations on unpolished substrates, which had the opposite behavior, although those specimens had much greater variability leaving open the possibility of sampling error.

Like the results from visible examination, very little corrosion product was observed on all the panel surfaces, except for some localized regions on TCPs on polished and unpolished substrates.

The corrosion product that was visible was clustered around cracks and pores on the surfaces, suggesting that the cracks acted as corrosion initiation sites. Corrosion extent does not correlate with crack width and density but only with the presence of cracks and flaws, likely a result of heterogeneous nucleation requiring less energy for a corrosion site to form. This would also explain why unpolished samples showed more visible corrosion product than polished as an unpolished surface has more grooves and valleys for nuclei to form heterogeneously.

Crack Widths and Corrosion Products

Thicknesses of the passivations were determined using TEM images such as those seen in Figure 15 and Figure 16 where measured values were 69 ± 4 nm for Co-Free TCP on polished substrates and 40 ± 5 nm for TCP on polished substrates.

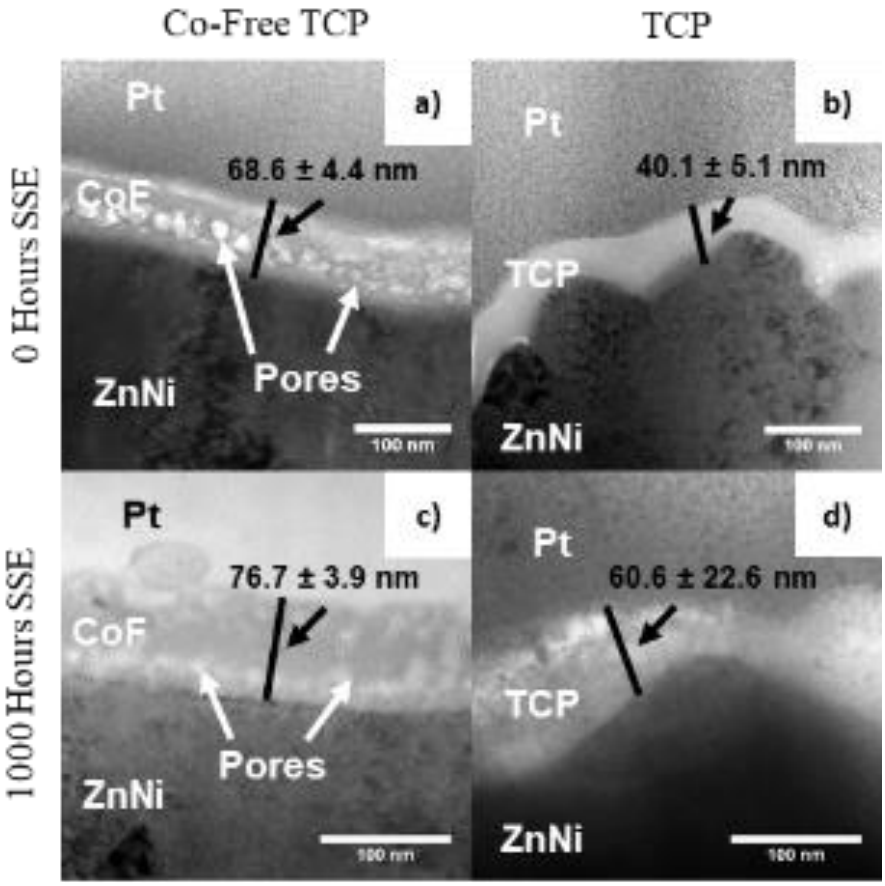

Figure 15 TEM images showing morphology and thicknesses of the unpolished cobalt-free TCP (a and c) and TCP layers (b and d) before and after salt spray exposure.

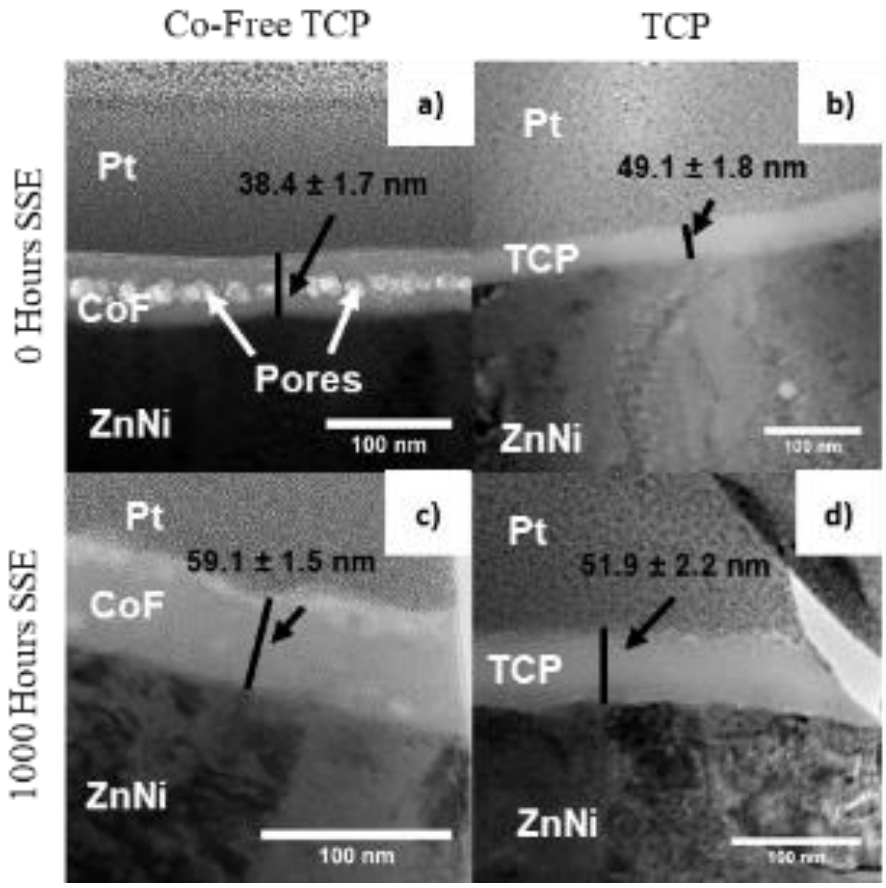

Figure 16 TEM images showing morphology and thickness of polished cobalt-free TCP (a and c) and TCP (b and d) layers before and after salt spray exposure.

Co-Free passivations on unpolished substrates were 38 ± 2 nm thick and TCP passivations on unpolished substrates were 49 ± 2 nm thick. The Co-Free passivations were initially thicker than the TCPs on polished substrates while the reverse was true of the unpolished samples. All passivations were <100 nm thick, which is similar to the "thin" type trivalent chromium based passivation [102] [58] as opposed to the "thick" type seen in some studies [58] [77].

Inspection using SEM (Figure 17 and Figure 18 SEM images showing polished samples for: a) TCP at 0 hours SSE, b) CoF at 0 hours SSE, c) TCP at 1000 hours, and d) CoF at 1000 hours.) shows intergranular crevices visible at high magnifications

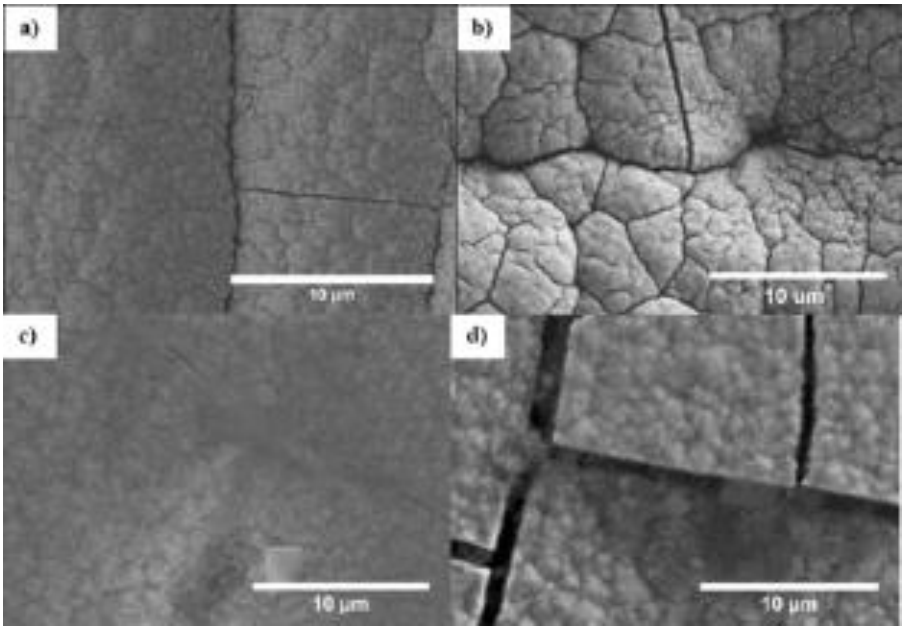

Figure 17 SEM images showing unpolished samples for: a) TCP at 0 hours SSE, b) CoF at 0 hours SSE, c) TCP at 1000 hours, and d) CoF at 1000 hours.

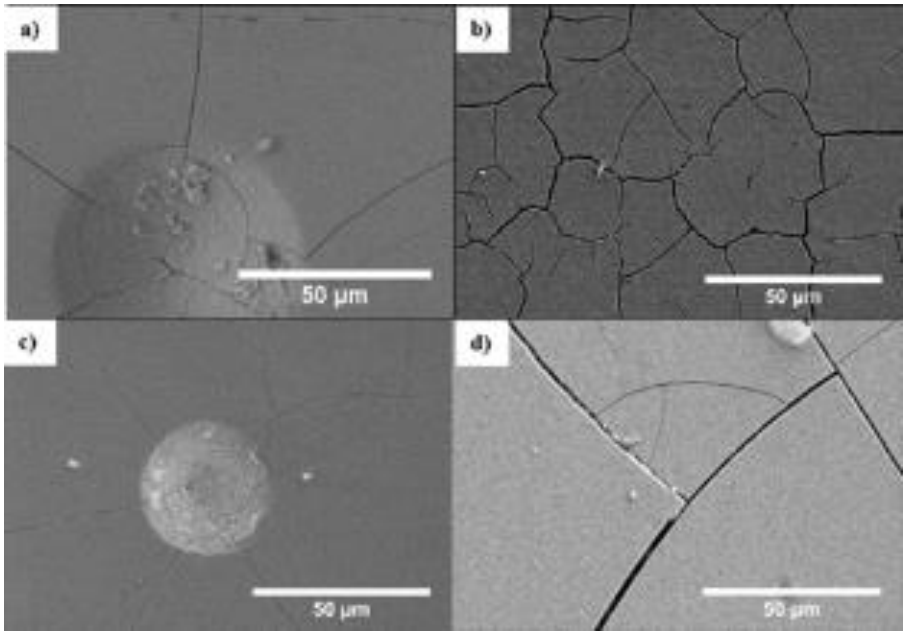

Figure 18 SEM images showing polished samples for: a) TCP at 0 hours SSE, b) CoF at 0 hours SSE, c) TCP at 1000 hours, and d) CoF at 1000 hours.

After 1000 hours of SSE, corrosion products on the Co-Free passivations on unpolished substrates were only visible near or inside of the cracks. In contrast, the TCP on unpolished specimens had a uniform layer of corrosion product across its surface with increasing amounts of corrosion

product located near the small cracks and pores. The passivated polished specimens had only debris visible on the surfaces with a little corrosion product visible within the cracks and pores. Only the unpassivated ZnNi panels had enough corrosion produce for XRD analysis. This analysis (Figure 19) of the corrosion product showed most peaks fit from zinc hydroxide chloride hydrate ($Zn_5(OH)_8Cl_2 \bullet H_2O$) with some zinc carbonate hydroxide hydrate ($Zn_4CO_3(OH)_6 \bullet H_2O$) and some of the underlying ZnNi substrate visible ($NiZn_3$).

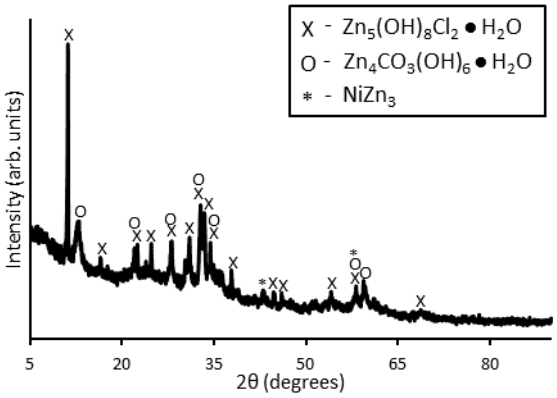

Figure 19 XRD analysis of the 1000 hour SSE ZnNi corrosion product showing zinc hydroxide chloride hydrate (X), zinc carbonate hydroxide hydrate (O), and some underlying ZnNi substrate.

The cracks on the unpolished Co-Free TCP specimens had an average width of 0.8 ± 0.2 µm and were about three times larger than the cracks in the TCP on unpolished specimens that had average widths of 0.2 ± 0.1 µm. Passivations on polished specimens had cracks that were 1.4 ± 0.5 µm wide for Co-Free TCP and 0.3 ± 0.1 µm wide for TCP.

TCP Passivation Characterization on γ-ZnNi Al6061-T6

Appearance

The first aspect of the test specimens examined was the physical appearance after different SSE times. Initially, test panels showed a mostly uniform appearance throughout the interior sections of the panel while edges of the panels took on a darker coloration that corresponded with increased open porosity left behind by gas evolution during electroplating the ZnNi coating. The bare ZnNi panels had a light grey color, TCP panels had a light blue appearance, Co-Free panels had a darker grey/light brown appearance, and the HexCr panels had a dark brown appearance (Figure 20).

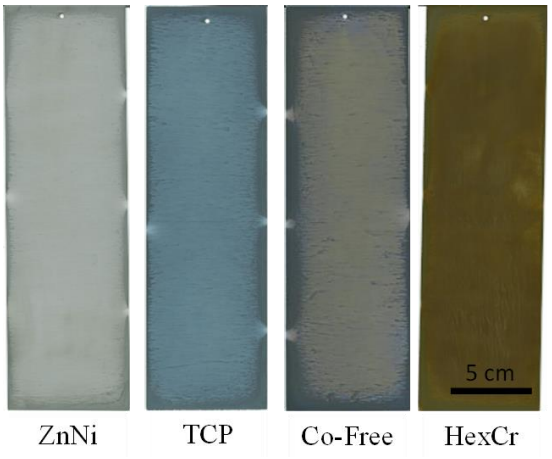

Figure 20 Test specimens as received after acetone cleaning but prior to any testing.

Upon SSE (Figure 21), bare ZnNi specimens were completely covered in white corrosion product, no change in the appearance was noted for TCP after 1000 hours, Co-Free specimens exhibited 39% corrosion coverage at 168 hours and complete uniform corrosion by 336 hours, and the HexCr panels showed a steady change in color towards more gray at every step of SSE but no visible corrosion.

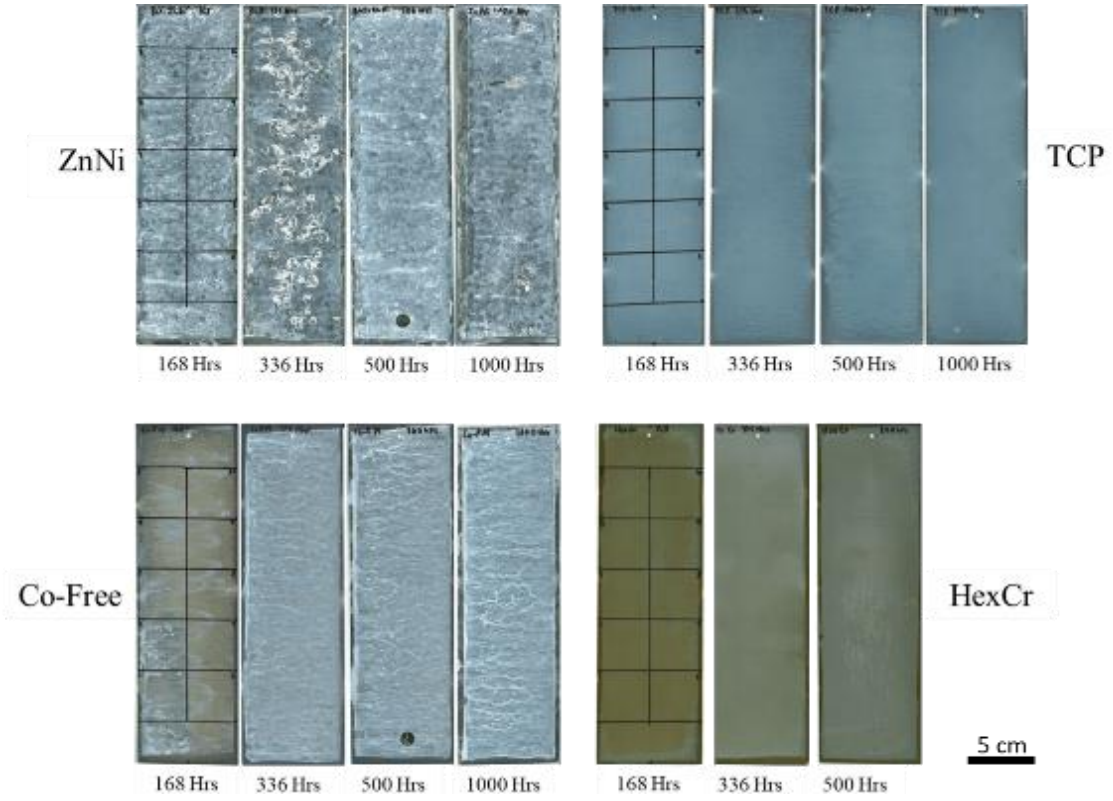

Figure 21 Progression of corrosion with increasing salt spray exposure time for all passivation conditions. Markings on 168 hour SSE panels show where electrical contact resistance measurements were made. Dark circles on bottom of ZnNi and Co-Free 500 hour panel

Examination of Figure 20 and Figure 21 demonstrates the degree to which the HexCr panels change color and the difference in appearance between the corrosion product present on the Co-Free vs. bare ZnNi specimens. For the unscribed condition, TCP and HexCr offer excellent resistance to corrosion while Co-Free begins to corrode at 168 hours and is then uniformly corroded at every condition after 168 hours, although much less corroded than unpassivated ZnNi.

When scribed panels underwent SSE, all panels except HexCr experienced at least some degree of corrosion. Figure 22 shows how scribes affected the corrosion of all passivated panels while Figure 23 shows representative optical micrographs of the scribed sections demonstrating commonly observed features on all passivations.

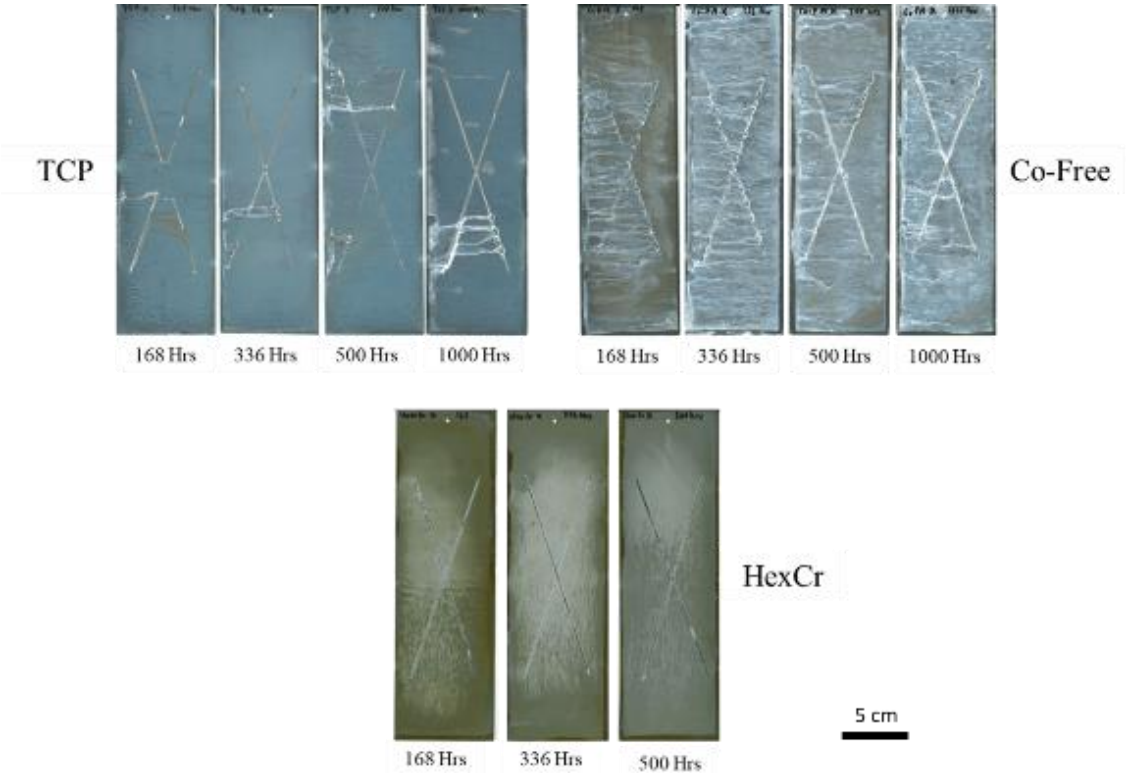

Figure 22 Scribed samples showing corrosion progression of the different passivations at different levels of SSE. Non-metallic spots within scribe of HexCr panels are thin layers of corrosion product that effectively prevent further corrosion.

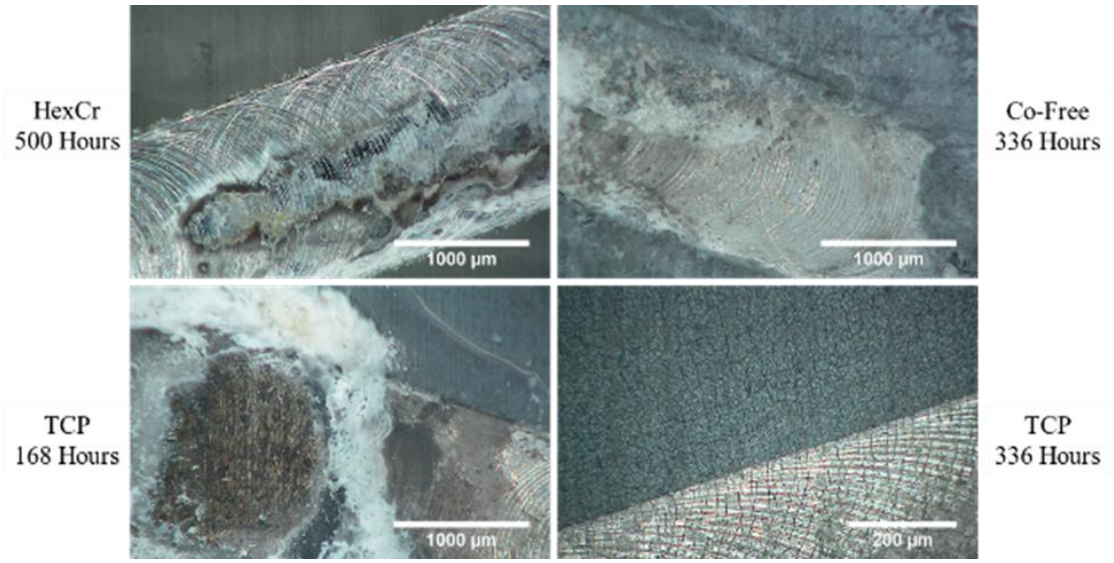

Figure 23 Optical micrographs of specimen scribes to examine active corrosion protection showing shiny metal and corroded patch on HexCr, typical corrosion within a Co-Free scribe, sites of localized and uniform corrosion as well as an uncorroded patch on TCP at 168 hours SSE, as well as the cracks that were observed near some corroded spots on TCP at 336 hours SSE

TCP had moderate and increasing amounts of severe localized corrosion with areas of uniform corrosion within the scribe ranging from surface area coverages of 20% for 168 hours, 43% for 336 hours, 51% for 500 hours, and 84% for 1000 hours of salt spray. TCP showed mixed corrosion results across all SSE conditions with the areas of severe localized corrosion marked by dark brown and white corrosion product visible within the scribe, areas of a thin brown colored corrosion product, and areas where the metal was still shiny and uncorroded. TCP also showed cracks around some of the corroded spots within and outside of the scribe. Co-Free showed complete, 100% surface area corrosion coverage of the scribed area at all levels of SSE with more severe corrosion within the scribe compared with the passivated panel surface. Scribed HexCr panels initially looked free of corrosion, but under microscopic inspection, small areas of corrosion product were scattered throughout the scribe with increasing coverage of 11% corrosion coverage area at 168 hours, 16% at 336 hours, and 24% at 500 hours.

Morphology

Examination via optical microscopy of the specimen surfaces before and after SSE showed that Co-Free passivations initially had some cracks present that could only be seen on ZnNi after corrosion had taken place. Figure 24 shows the initial state of the passivations, which consists primarily of differences in color and cracks in Co-Free that look similar to the cracks near the scribed locations of the TCP panels in Figure 23.

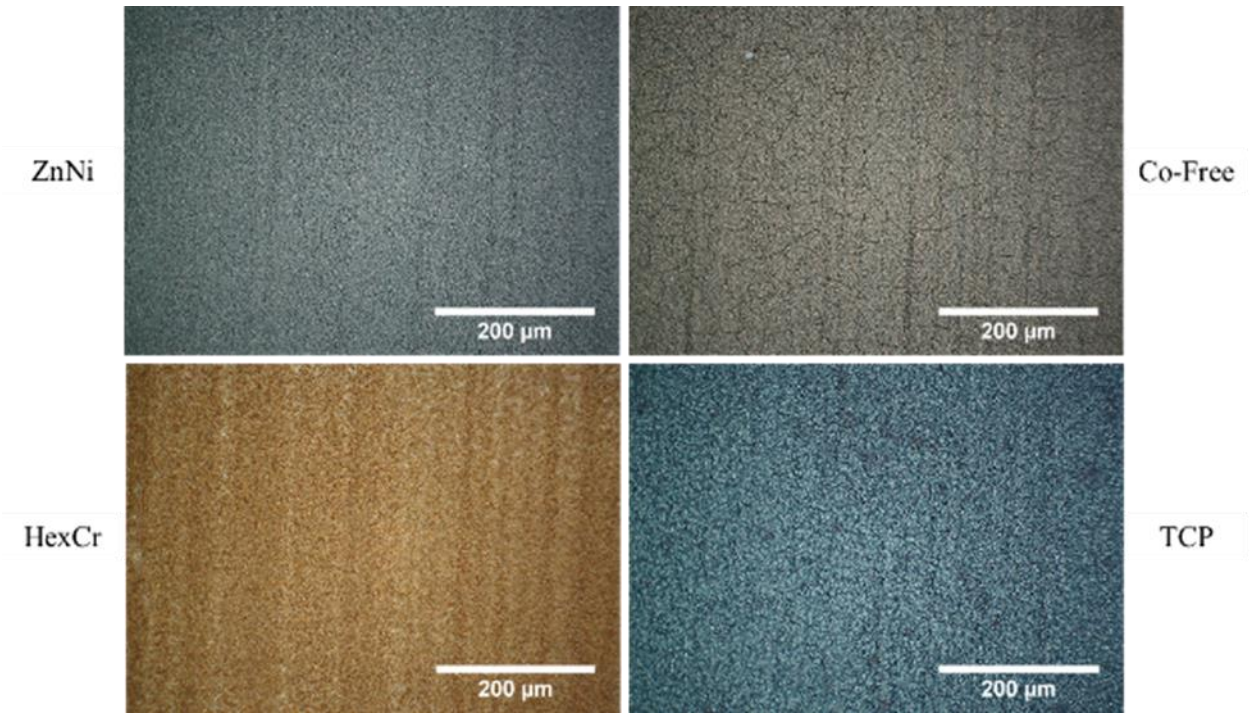

Figure 24 Optical microscopy images of each specimen prior to any SSE. Aside from color changes and the presence of cracks on Co-Free there is little difference between the specimens.

Measurement of the cracks in Co-Free showed the density was about 32 per mm. After SSE, TCP had no discernable changes on the unscribed specimens for all conditions while Co-Free specimens had a thin transparent layer of corrosion product across much of the surface with isolated spots of crystalline platelets after 168 hours (Figure 25).

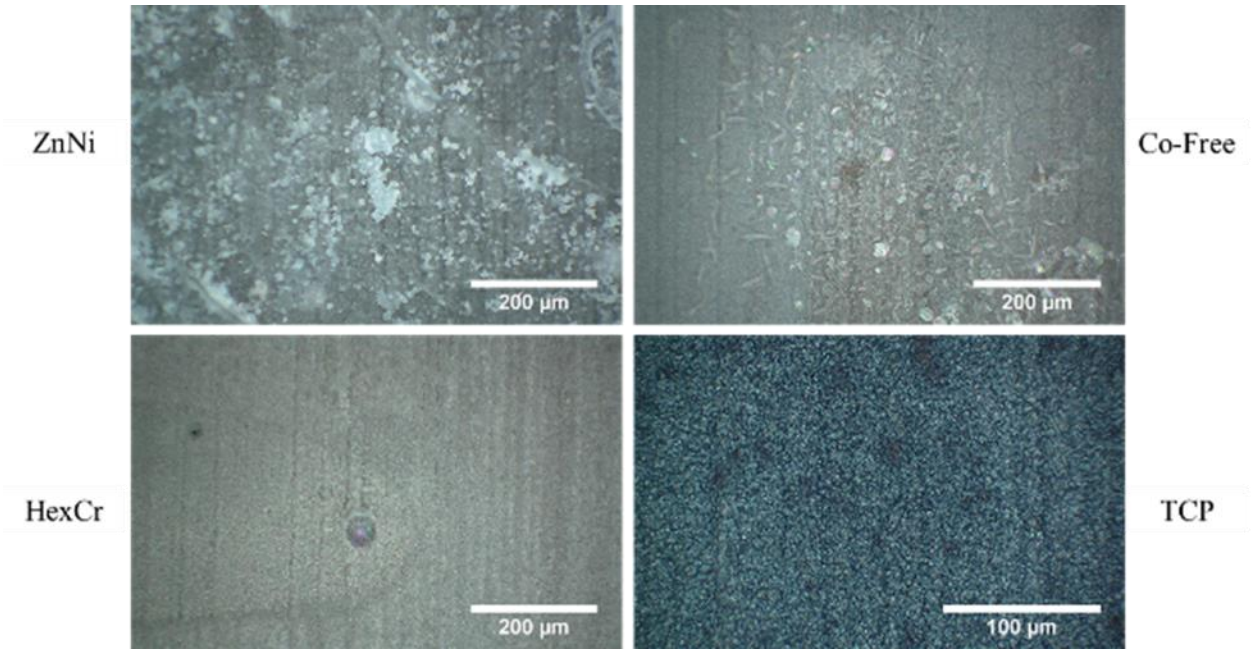

Figure 25 Selected images of specimens after SSE showing no change in TCP, platelet crystals on Co-Free, pore activity on HexCr, and new cracks underneath the corrosion product of bare ZnNi.

Unpassivated ZnNi at all SSE times and Co-Free at times beyond 168 hours were completely covered in a thick layer of corrosion product where some cracks could be seen underneath the corrosion product on the ZnNi specimens. HexCr specimens showed a change in color with some pores and removed portions of the ZnNi coating leaving discolored streaks.

Scanning electron microscopy images showed little difference between ZnNi, TCP, and Co-Free surfaces prior to SSE. The features in the corrosion product on Co-Free after SSE were much larger than the underlying ZnNi features. Figure 26 shows that prior to SSE the ZnNi coating had the roughest/most angular surface features while TCP had the smoothest surface features.

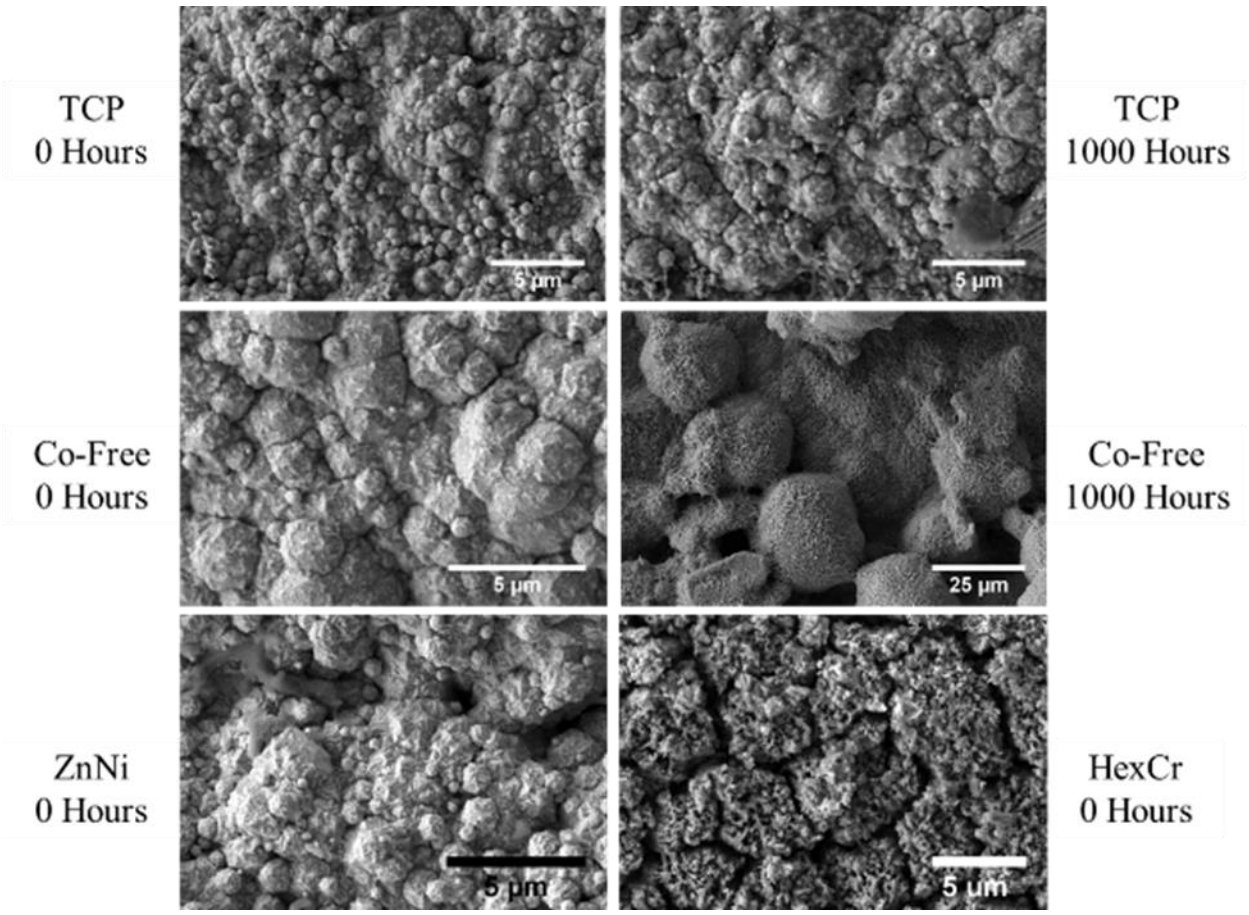

Figure 26 SEM images of the different specimens showing the observed differences between them. The left column compares TCP, Co-Free, and ZnNi prior to SSE while the right column shows the relative lack of change in TCP after 1000 hours SSE compared with Co-Free. HexCr had a surface different from all the other samples, most notably is had many large, deep cracks.

The cracks that were visible on the Co-Free optical micrographs were not easily visible on the SEM images as the cracks generally followed along the intergranular boundaries of the ZnNi coating. HexCr was found to have a rough surface with cracks going visibly down into the passivation layer. After SSE, the TCP specimens showed little difference aside from the presence of sub-micron structures sparsely scattered across the surface believed to be salt that did not wash away during the DI water rinse. The corroded Co-Free surface developed structures about five times larger than the ZnNi nodules that originally comprised the surface which exhibited a large amount of roughness and porosity.

Transmission electron microscopy images of the TCP and Co-Free specimens taken before and after SSE showed that both passivations had similar thickness and porosity prior to SSE. In Figure 27 the average measured thickness for TCP was 82 ± 20 nm before SSE and 74 ± 4 nm after 1000 hours.

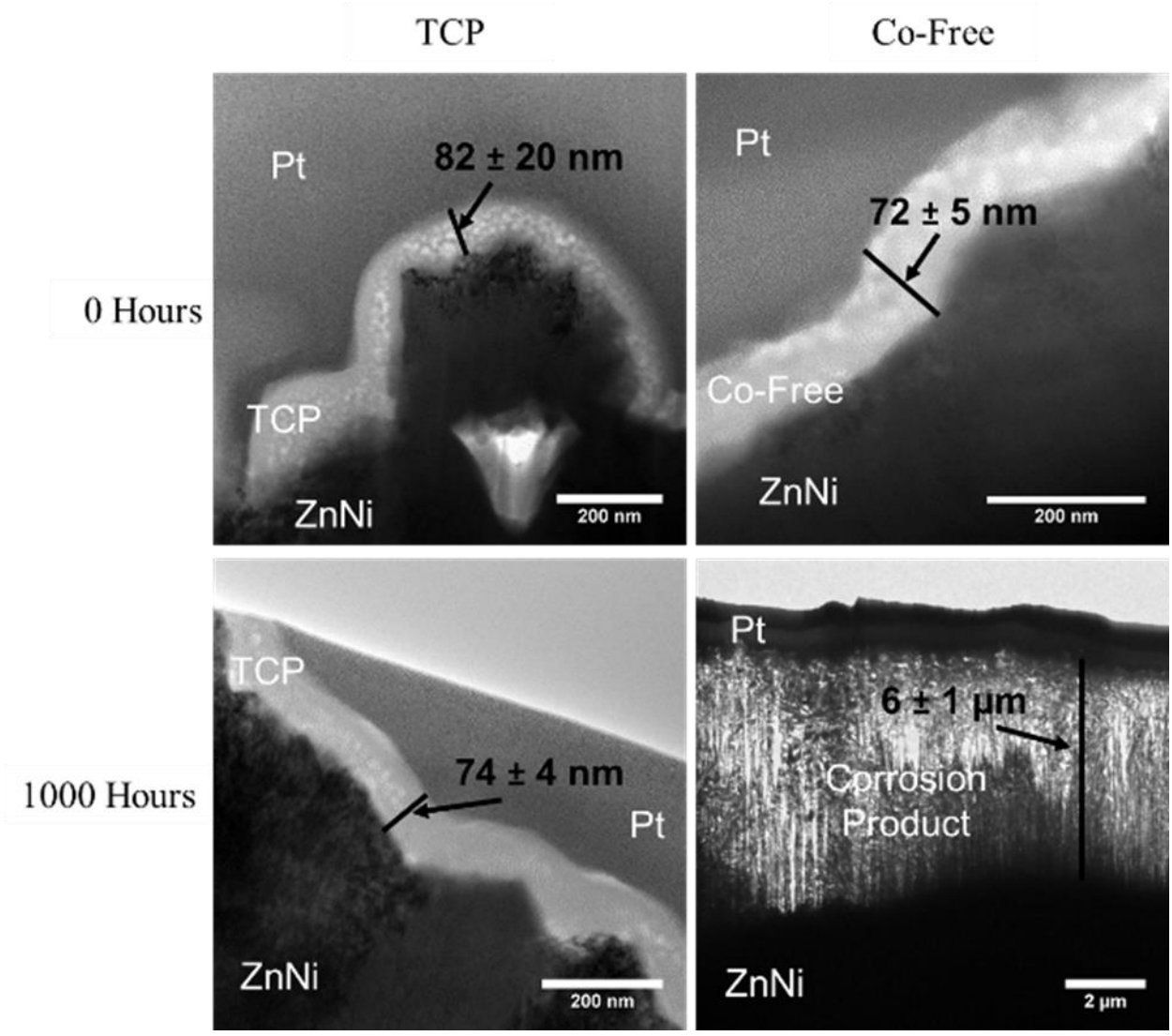

Figure 27 TEM images from TCP and Co-Free liftouts showing the nature of the passivations layers before and after SSE as well as the measured thicknesses at each condition.

Internal porosity, which was also present in the study of the same passivations on 1008 steel substrates [103], can be seen throughout the passivation apparently decreased after 1000 hours SSE. The thickness of Co-Free was 72 ± 5 nm before SSE and was completely replaced by an approximately 6 µm thick layer of corrosion product by 1000 hours SSE that left no trace of the Co-Free passivation. Co-Free showed similar initial internal porosity to the TCP. Both passivations were determined to be amorphous according to a fast Fourier transform of diffraction patterns done on sections completely contained within the passivation layer.

X-ray diffraction was utilized to investigate the corrosion product scraped from a Co-Free TCP after 1000 hours of SSE. Analysis of the spectrum (Figure 28) indicated that the corrosion product consisted of zinc carbonate hydroxide hydrate ($Zn_4CO_3(OH)_6 \bullet H_2O$), zinc chloride hydroxide hydrate ($Zn_5(OH)_8Cl_2 \bullet H_2O$), and a small amount of the underlying ZnNi substrate (Ni_5Zn_{21}).

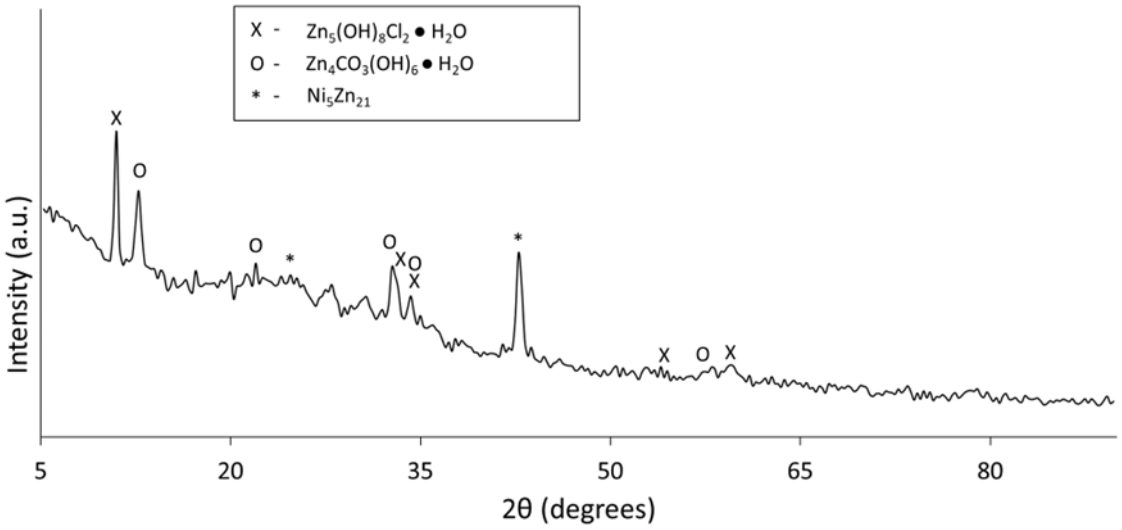

Figure 28 XRD spectrum of corrosion product from a Co-Free TCP sample after 1000 hours of SSE showing the zinc chloride hydroxide hydrate (X), zinc carbonate hydroxide hydrate (O), and a small amount of the underlying ZnNi substrate (*).

These findings were consistent with the corrosion product of unpassivated ZnNi seen in a previous study [103] by the authors.

Contact Resistance

Comparisons of the electrical contact resistance of each specimen before and after SSE showed TCP and HexCr maintained low resistance until 1000 hours SSE while Co-Free maintained low resistance only until 168 hours SSE. Presented in Table 7 and shown in Figure 29, unpassivated ZnNi had an average contact resistance of 0.063 ± 0.035 mΩ prior to SSE but had the greatest electrical contact resistance after 168 hours of SSE at 310 ± 470 Ω.

Table 7 Electrical Contact Resistance Averages and Standard Deviations for all Passivations

		Surface			
SSE Time		Bare ZnNi	TCP	Co-Free	HexCr
0 Hours	Average, mΩ	0.06	0.47	0.54	6.38
	Std. Dev, mΩ	0.04	0.20	0.13	3.26
168 Hours	Average, mΩ	310000	1.50	1.23	2.97
	Std. Dev, mΩ	470000	0.34	1.17	1.55
336 Hours	Average, mΩ	1300000	1.09	1600	2.84
	Std. Dev, mΩ	4100000	0.60	2700	1.01
500 Hours	Average, mΩ	1300000	1.35	1700	4.18
	Std. Dev, mΩ	3300000	0.85	4100	2.07
1000 Hours	Average, mΩ	47000000	1.13	140	-
	Std. Dev, mΩ	50000000	0.30	220	-

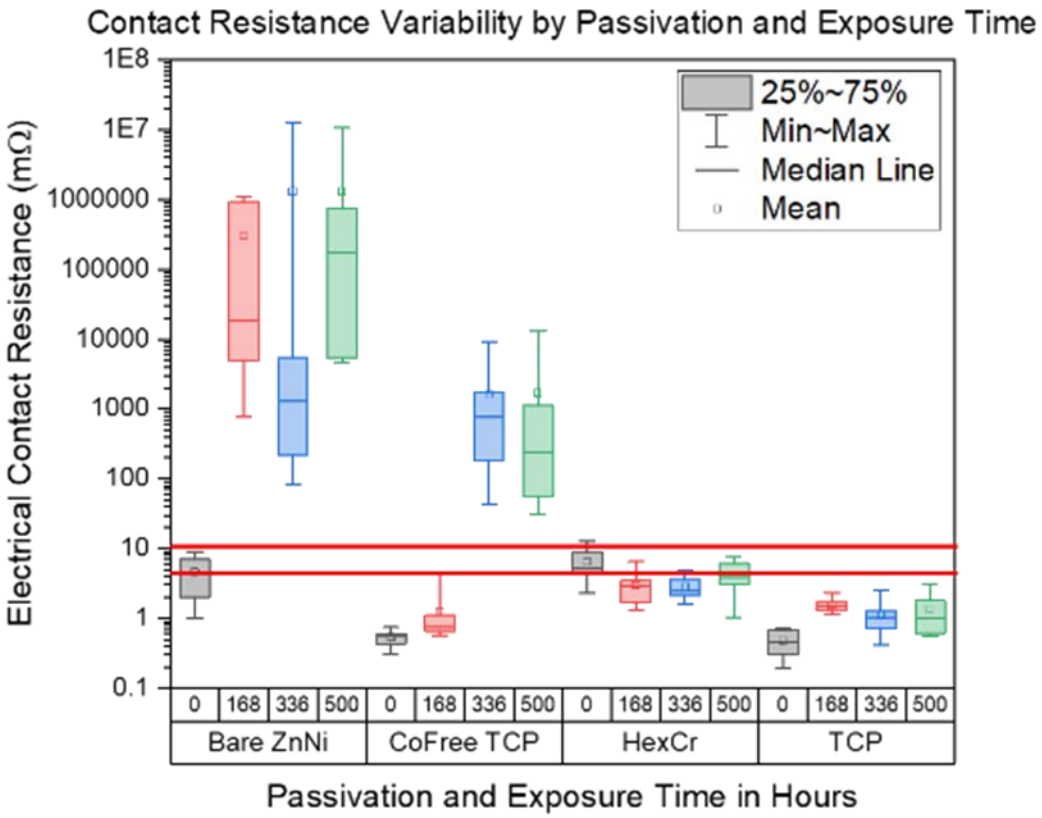

Figure 29 Electrical contact resistance of all samples before and after SSE with total measured range and the difference between medians and means visible to demonstrate variability. Lines marked 0 hours and 168 hours represent resistance requirements to approve passivations from MIL-DTL-81706B.

With a standard deviation nearly 150% larger than the measured average, the contact resistance measurements of heavily corroded samples were unreliable. TCP showed the best contact resistance during corrosion with an initial resistance of 0.5 ± 0.2 mΩ and a final resistance after 1000 hours SSE of 1.1 ± 0.3 mΩ. Co-Free had an initial resistance of 0.5 ± 0.1 mΩ and only had a slight increase in average resistance after 168 hours SSE to 1.2 ± 1.2 mΩ but with a large increase in variability that began to make the measurements unreliable. After 336 hours, average values and standard deviations both increased into the single ohm range representing an increase of three orders of magnitude. HexCr had an average initial resistance of 6.4 ± 3.3 mΩ but decreased after 168 hours of hours SSE to 3.0 ± 1.5 mΩ and after 336 hours of SSE to 2.8 ± 1.0 mΩ, but then increased after 500 hours of SSE to 4.2 ± 2.1 mΩ.

Discussion of differences between SAE1008 and Al6061 results

A previous study by Cho et al. showed that chromium-containing corrosion product depositing in the cracks of trivalent chromium conversion coatings could inhibit corrosion for 50 hours via anodic polarization testing and electrochemical impedance spectroscopy[42]. They found that microcracks in the conversion coating were the sites that held the chromium-containing corrosion

product until the corrosion product grew large enough to cause the cracks to propagate to the substrate and lead to sudden, heavy corrosion. A few differences exist between the study by Cho et al. and the current work as Cho et al. studied TCP that contained cobalt and was 3 to 12 times thicker than the TCP layer reported here. Since the present passivations were so much thinner but the corrosive environment was similar, the same chromium-containing corrosion product should still be formed whether cracks are present or not and would comprise a larger relative volume of the passivation compared with Cho et al.

One of the differences between the Co-Free and TCP passivations was cracks into the ZnNi layer that were present on the Co-Free but not on the TCP. The cracks may seem like an obvious difference that would be responsible for the decreased corrosion resistance of the Co-Free compared to the TCP; however, the previous study on steel substrates found that neither crack density nor crack width correlated with the corrosion performance of these two passivations on ZnNi coated SAE 1008 steel substrates[38]. Furthermore, the chromium-containing corrosion product cited by Cho et al. could be what is initially formed from the Co-Free passivation layer that then fractures and allows growth of zinc carbonate hydroxide hydrate and zinc chloride hydroxide hydrate over the entire surface. This result would explain why the Co-Free samples have corrosion that appears different from the unpassivated ZnNi and does not appear to originate from the cracks. The last observation regarding cracks in the passivations is that HexCr showed many more cracks than Co-Free but also had corrosion performance comparable to or exceeding that of TCP. Since HexCr is known to inhibit corrosion through leaching of Cr(VI) ions from the coating into solution that deposit on sites of active corrosion and halt progression via reduction to Cr(III), the cracks could benefit the corrosion inhibition mechanism by providing a greater surface area for Cr(VI) to dissolve and migrate to corrosion sites[43]. For these reasons, cracks alone are not responsible for the difference in corrosion performance.

The exchange current density and polarization resistance of Co-Free and TCP were different before and after SSE. Both passivations start with similar exchange current densities, but as the SSE time increased, the exchange current density of the TCP decreased more than Co-Free, suggesting that any changes to the surface or formation of corrosion product reduces current flow more in cobalt containing TCP passivation than in the Co-Free passivation. While both passivations have a decrease in polarization resistance after SSE, TCP always had a higher polarization resistance and less visible corrosion than Co-Free. This indicates that the presence of cobalt in the passivation results in a process that leads to a more corrosion resistant film.

Bare ZnNi had the lowest exchange current density and highest polarization resistance of all specimens initially. After SSE, when a large amount of corrosion product was visible, bare ZnNi had the highest current density and lowest polarization resistance of all the specimens, reinforcing that passivation of the electroplated ZnNi coating prevents visible corrosion of the surface. HexCr started with a lower exchange current density and higher polarization resistance among the passivations and showed little change with SSE. Since the lowest current density and highest polarization resistance of unpassivated ZnNi lead to the formation of large amounts of corrosion product, the HexCr, TCP, and Co-Free passivations have exchange reaction(s) that happen at a greater rate than ZnNi corrosion but does not produce visible corrosion product.

The work of Hesamedini and Bund examined the oxidation of Cr(III) to Cr(VI) in TCPs related to fluid filled internal porosity within the passivation layer [79]. They reported that water filled porosity within the TCPs on Zn-coated steel heated in an oxygen containing environment can result

in oxidation of chromium species to the Cr(VI) valence state. They concluded that the amount of oxidation was independent of the presence of cobalt but depended upon the amount of porosity in a TCP, with more pores promoting more oxidation through consumption of water. More Cr(VI) in a TCP allows it to exhibit similar active corrosion protection as usually seen in HexCr, such as observed in Guo and Frankel, and could explain the limited corrosion in the TCP scribed specimens after SSE in this study [54]. The scribed sample results where the Co-Free failed to protect the scribe and the TCP partially protected the scribe implies active corrosion protection and that some of the exchange current density measured in TCP could be from Cr(III) to Cr(VI) oxidation while the Co-Free exchange current density is caused by formation of corrosion product. These results suggest that Cr(III) to Cr(VI) oxidation depends upon cobalt contained in the passivation and not the porosity present in the passivation while Hesamedini and Bund argue the opposite. However, when the Co-Free and TCP passivation were applied to ZnNi coated steel substrates in the previous investigation, similar results to those from Hesamedini and Bund were obtained. This suggests that oxidation of Cr(III) to Cr(VI) can be affected by an interaction with the underlying substrate.

Three differences were observed among the specimens prepared for the previous study of ZnNi coated SAE 1008 steel substrates and the present study: 1) substrate; 2) the presence of a ~5 µm layer of electroless nickel between the ZnNi and substrate; and 3) heat treatment. Because the aluminum substrate is beneath an electroless nickel layer, the substrate is not be expected to have a direct effect on corrosion of the ZnNi coating surface, although it is possible that the electroless nickel could interact with the corrosive solution at areas where porosity or cracks in the ZnNi would allow the solution to reach the electroless nickel layer. Since no localized corrosion was observed at cracks on Co-Free and with nickel being more noble than zinc, exposure of nickel is not expected to promote reaction of the ZnNi coating during corrosion. Another consideration is that the low hydrogen embrittlement heat treatment that was performed on the steel specimens in the previous study, but not the aluminum specimens in the present study, could play a role through the oxidation mechanism reported by Hesamedini and Bund. More research is needed to confirm this hypothesis. Given the data gathered in the present study, the presence of cobalt influences the corrosion performance of the TCPs by being a beneficial component in the oxidation of Cr(III) to Cr(VI). Since the work of Hesamedini and Bund as well as the study done by the authors both used steel substrates and found TCP corrosion resistance to be independent of Co in the coating, it is apparent that oxidation of Cr(III) to Cr(VI) should depend upon an intermediate species that can be provided by steel substrates or cobalt, and as such TCPs on non-ferrous substrates have corrosion performance improved by cobalt additions.

To answer the question of whether TCPs can be viable alternatives to commercial HexCr for corrosion protection depends upon the requirements of MIL-DTL-8170639. A viable alternative must have an electrical contact resistance of <5 mΩ after passivation and <10 mΩ after 168 hours of SSE. Both the Co-Free and TCP were found to have electrical contact resistances lower than HexCr up to 168 hours of SSE and as such are considered viable alternatives although the extended SSE times and scribed samples tests show that the cobalt-containing TCP offers the best protection.

Analysis of Chromate Content and Performance of Heat Treated γ-ZnNi Coated Steel

APPEARANCE

The initial appearance of the test coupons varied among all experimental conditions with the greatest differences due to the heat treatment. Figure 30 shows representative test coupons before

testing or SSE. The bare ZnNi specimens had a dull grey color with shiny reflective interior regions surrounded by matte edges. Specimens with a TCP coating had a darker purple-blue appearance after the 80°C heat treatment. Increasing the heat treatment to 191°C resulted in a strong brown color with some purple regions throughout. Specimens with a Co-free TCP coating showed little change in appearance between heat treatments and held a light-blue color with some purple regions.

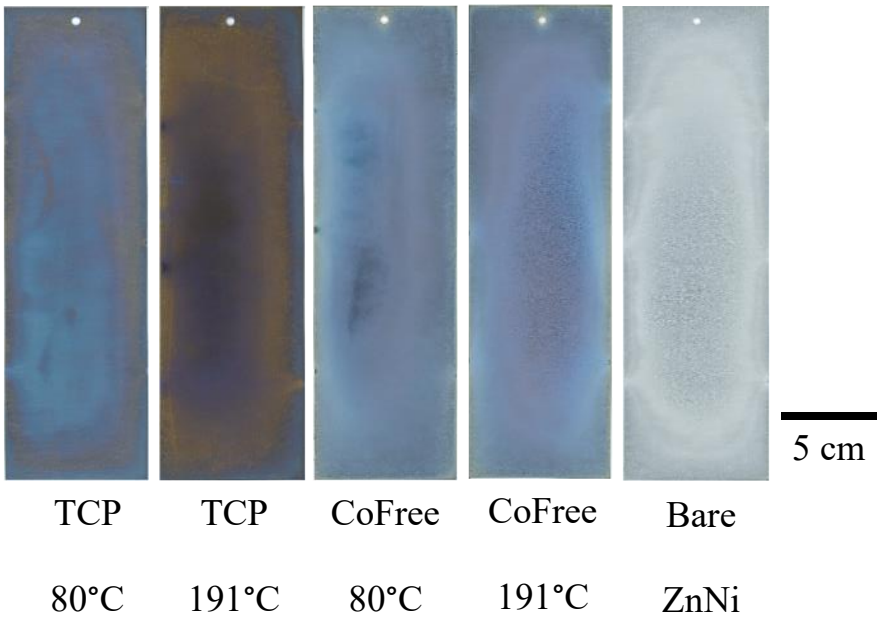

Figure 30 Visual appearance of test specimens showing the differences between heat treated passivating coatings

After 168 hours of SSE, some corrosion was observed on all specimens. The unpassivated ZnNi panels were fully covered in corrosion product. The Co-free TCP heat treated at 80°C had 41 ± 7% area covered in corrosion product while the Co-free TCP at 191°C had 26 ± 10% area covered in corrosion product. The TCP specimens heat treated at 80°C exhibited 10 ± 1% of the area covered in discoloration. The TCP heat treated at 191°C had a similar amount of discoloration at 8 ± 1%.

After 336 hours of SSE, all specimens showed more signs of corrosion (Figure 31).

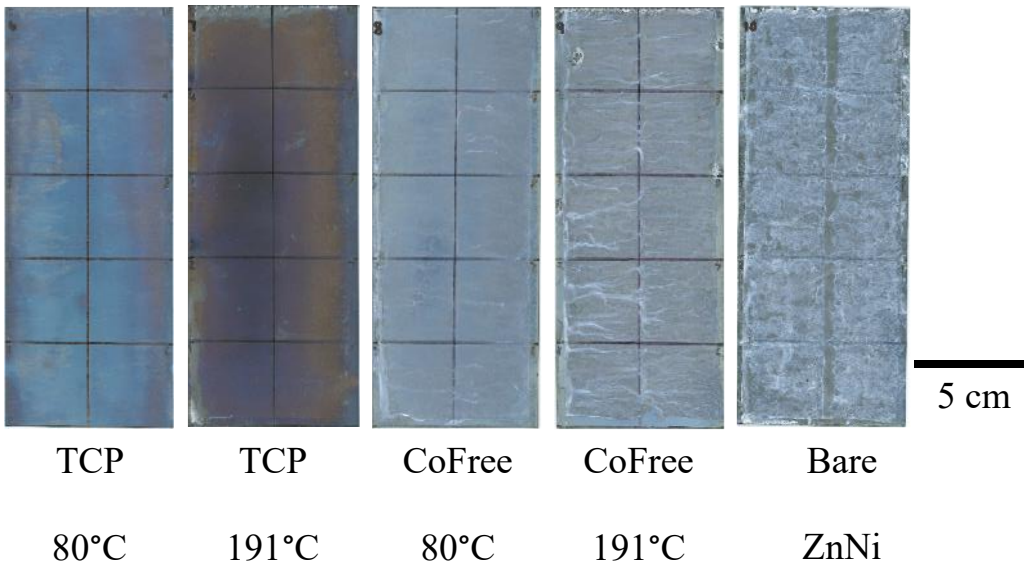

Figure 31 Test specimens after 336 hours of SSE. The marked areas were guides to section the samples for later analysis

For the passivated specimens, the Co-free TCP specimens heat treated at 191°C had less corrosion than the Co-free TCP specimens heat treated at 80°C with 42 ± 5% corrosion coverage compared with 55 ± 6%. The TCP specimens heat treated at 80°C showed more visible corrosion than at 168 hours SSE with 27 ± 6%. TCP specimens heat treated at 191°C exhibited 9 ± 1% corrosion coverage.

The TCP specimens retained a similar appearance after 336 hours of SSE. The TCP specimens heat treated at 80°C showed multiple streaks of color change while the TCP specimens heat treated at 191°C showed multiple scattered areas of color change. In contrast to TCP specimens, all of the Co-free TCP specimens had visible corrosion product on the surfaces. As a result, the Co-free TCP specimens did not undergo additional SSE after 336 hours.

The TCP specimens were returned to the salt spray chamber and exposed for a total of 672 hours of SSE. The panels were not completely covered in corrosion product and were returned to the salt spray chamber for 1000 hours of total salt spray exposure. The TCP specimen heat treated at 80°C was removed for being nearly completely covered in discoloration. The TCP specimens heat treated at 191°C lasted until 1359 hours of SSE before developing visible corrosion product across their entire exposed surface.

Morphology

Optical micrographs taken prior to SSE are shown in Figure 32.

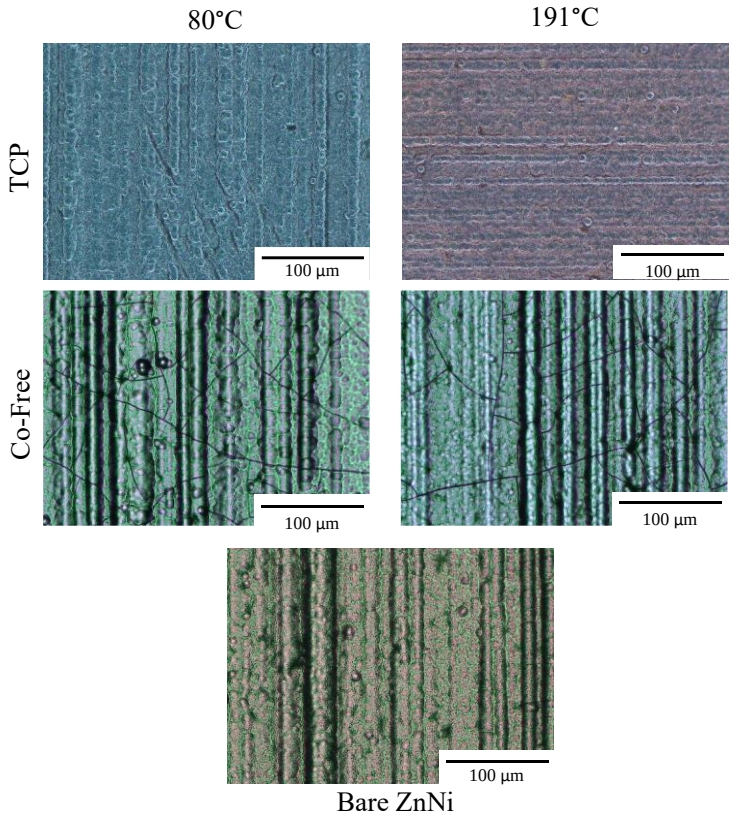

Figure 32 Optical micrographs of specimens taken at 1000X magnification prior to SSE

The sample morphology at this scale was dominated by ZnNi features that grew from roll marks of the underlying Al 6061 substrate during electroplating. The most notable difference was that the Co-free TCP specimens had cracks through the ZnNi coating. In contrast, the TCP specimens and bare ZnNi specimens had no visible cracks. After SSE, specimens other than bare ZnNi showed localized areas of both pristine and corroded surfaces.

Figure 33 shows micrographs of specimen regions that appear to have either corrosion product or visible color change after visual inspection after 336 hour SSE.

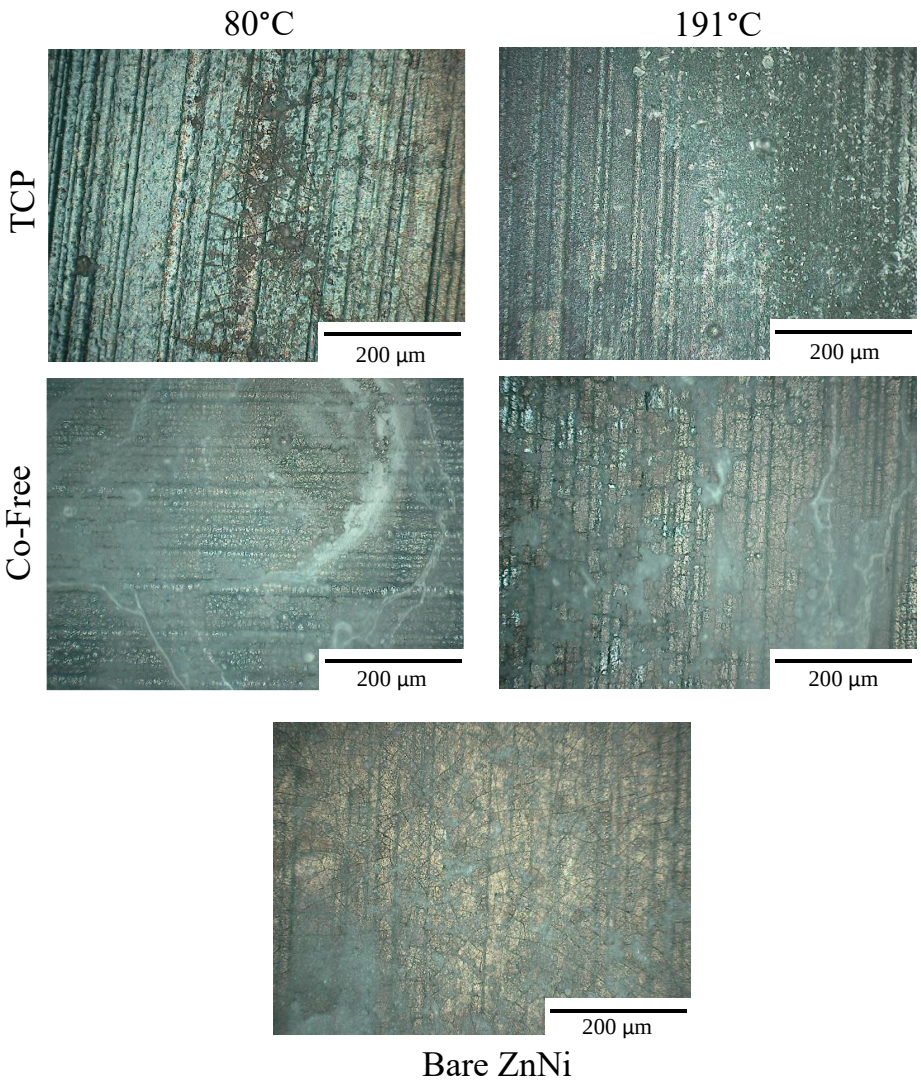

Figure 33 Optical micrographs of visibly corroded areas of specimens taken at 500X magnification after 336 hours SSE

Corroded bare ZnNi surfaces developed numerous cracks underneath the corrosion product. The heavily corroded regions of the Co-free TCP specimen heat treated at 191°C exhibited a similar appearance. Areas with cracks present sometimes had visible corrosion product nearby as seen in most images, but pristine regions with cracks also existed on the specimens. Some instances of color change or corrosion product had no obvious flaw nearby such as the images shown for Co-free TCP specimens heat treated at 80°C that are shown in Figure 33.

Cr(VI) Measurement

Chromate testing was performed for the TCP and Co-free TCP coatings at SSE exposure times ranging from 0 hours (as-heat treated passivations) until the point at which the panels were fully corroded to track the Cr(VI) content in the specimens. Figure 34 shows the combined results and revealed that the TCP specimens contained more Cr(VI) in the passivation layer at all times

compared to the Co-free TCP specimens. The Cr(VI) content decreased as SSE time increased for both types of passivation, and both heat treatments.

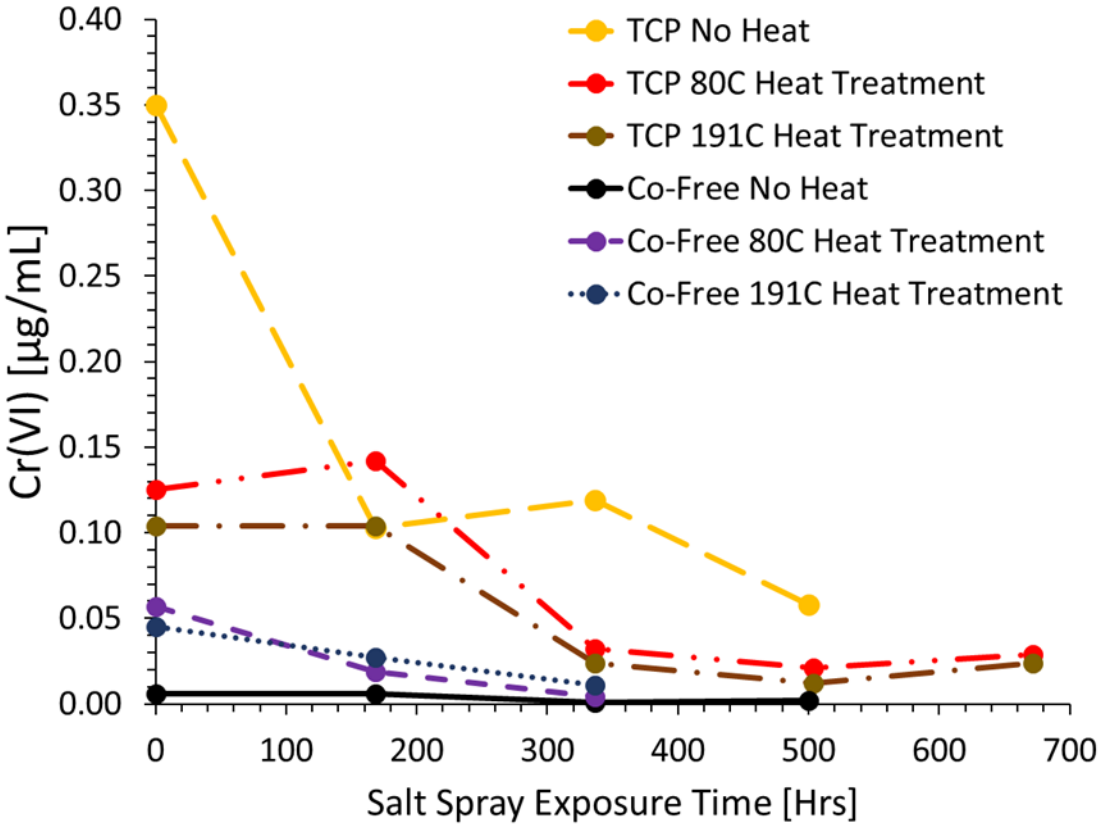

Figure 34 Cr(VI) concentrations after DPC boil test for specimens with and without heat treatment

Chromate analysis was also performed on passivations that were deposited on γ-ZnNi coated Al6061-T6 that had not undergone heat treatment. These panels were part of a previous study of corrosion behavior [103]. The purpose of this analysis was to determine if heat treatment affected the Cr(VI) content. The levels of Cr(VI) detected (Figure 34) show that TCP specimens with no heat treatment had higher initial levels of Cr(VI) and higher Cr(VI) content was maintained throughout SSE. Heat treatment resulted in a decrease in Cr(VI) content. In contrast, Co-free TCP specimens showed an opposite trend with heat treatment as the specimen without heat treatment had Cr(VI) contents close to the margin of error for the boil test (< 0.005 µg/mL) revealing that heat treating the Co-free TCP resulted in an increase in Cr(VI) content.

Analysis of Chromate Content and Performance of Heat Treated γ-ZnNi Coated Steel

Image Analysis of Corroded Panels

The amount of corrosion measured on test panels increased across all experimental conditions with increasing salt spray exposure (SSE) time, visible in Figure 35 and Figure 36.

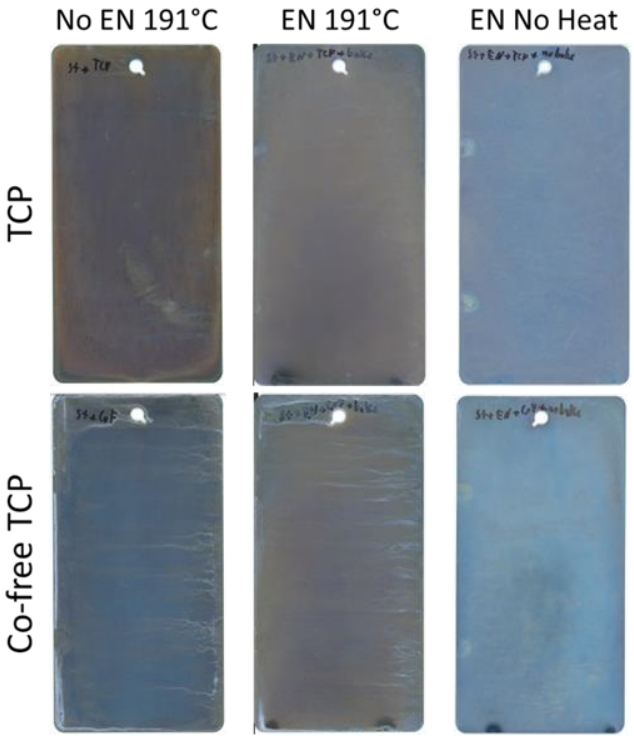

Figure 35 Corrosion product coverage on TCP and Co-free TCP panels after 168 hours of salt spray exposure

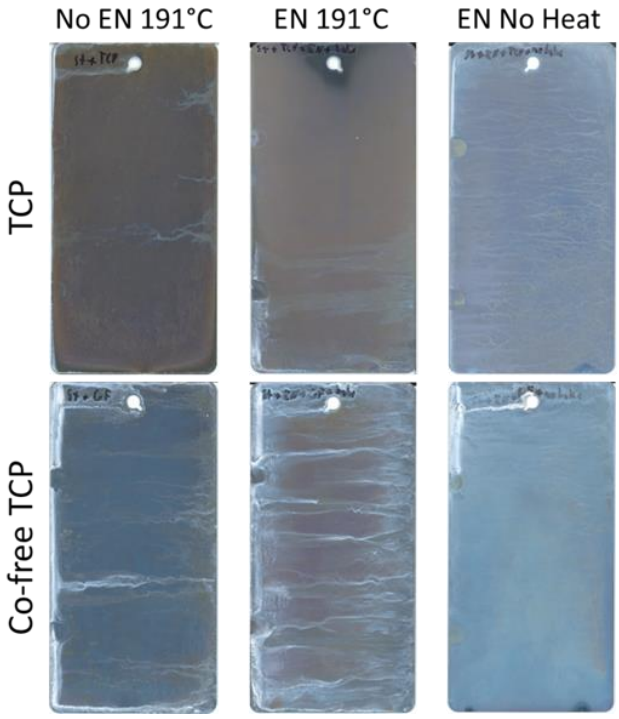

Figure 36 Corrosion product coverage on TCP and Co-free TCP panels after 672 hours of salt spray exposure

The values in Table 8 show that Co-free TCP specimens exhibited a greater increase in corrosion coverage with increasing SSE times than either set of heat-treated TCP panels.

Table 8 Extent of corrosion coverage in percentage of surface exhibiting visible corrosion product for Co-free TCP and TCP panels after varying SSE times

		SSE Exposure Time							
		168 Hrs		**336 Hrs**		**504 Hrs**		**672 Hrs**	
Co-free TCP	**191C**	4.6	± 3.2	19.2	± 3.0	20.5	± 4.7	46.5	± 5.8
	EN 191C	13.5	± 3.3	17.9	± 2.7	49.1	± 6.7	100	-
	EN no heat	6.8	± 1.5	5.1	± 1.7	15.8	± 3.3	26.3	± 11.4
TCP	**191C**	4.4	± 2.7	9.4	± 1.1	10.4	± 1.3	9.4	± 4.3
	EN 191C	3.5	± 1.7	7.1	± 1.8	9.0	± 3.7	23.8	± 22.5
	EN no heat	6.0	± 0.4	24.1	± 7.2	54.8	± 5.0	100	-

The EN Co-free TCP no heat exhibited the least corrosion product after SSE showing only a moderate increase from 6.8 ± 1.5% at 168 hours SSE, to 26.3 ± 11.4% after 672 hours SSE. The Co-free TCP 191°C panels showed a greater increase in corrosion coverage, ranging from 4.6 ± 3.2% after 168 hours SSE, to 46.5 ± 5.8% after 672 hours SSE. The EN Co-free TCP 191°C exhibited the greatest corrosion product coverage from 13.5 ± 3.3% at 168 hours SSE to being completely covered in corrosion product after 672 hours SSE.

The TCP panels followed a different trend than the Co-free TCP panels. The EN TCP no heat panels exhibited the greatest corrosion product coverage and the heat-treated TCP panels exhibited the least corrosion product. The EN TCP no heat panels exhibited 6.0 ± 0.4% corrosion coverage at 168 hours SSE and were completely covered in corrosion product after 672 hours SSE. The TCP 191°C showed the least corrosion product with 4.4 ± 2.7% after 168 hours SSE and increasing slightly to 9.4 ± 4.3% after 672 hours SSE. The EN TCP 191°C exhibited similar amounts of corrosion product to TCP 191°C with 3.5 ± 1.7% at 168 hours SSE but exhibited a large increase in coverage and variability to 23.8 ± 22.5% after 672 hours SSE.

XPS CHEMICAL ANALYSIS

The first XPS tests were done on specimens of $K_2(CrO_4)_2$, Co_3O_4, and Cr_2O_3 to gather peak fits for species of Cr metal, CrO_3, Cr_2O_3, CoOOH, Co_3O_4, CoO, Co metal, $Cr(OH)_3$, and $Co(OH)_2$ to use as standards for analysis of test specimens when analyzing chemical shifts. Figure 37 shows the peak fits used for components on Cr 2p and Co 2p peaks in each standard specimen and later propagated to experimental specimens.

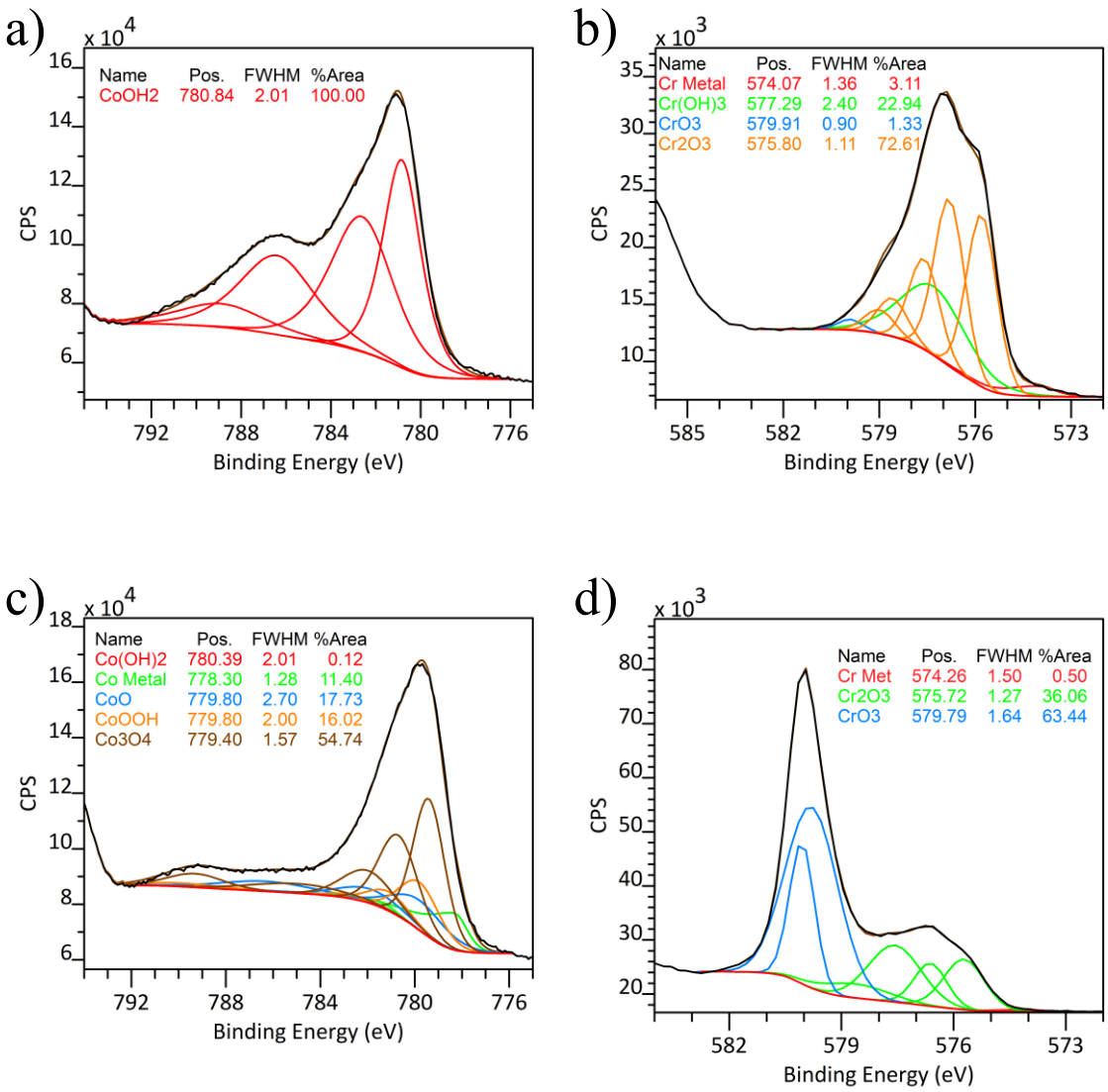

Figure 37 Peak fits used for chromium and cobalt components on known standard specimens: a) $CoOH_2$, b) Cr_2O_3, c) Co_3O_4, d) $K_2(CrO_4)_2$

Table 9 and Table 10 show the elemental quantification results of all experimental specimens for the Co-free TCP and TCP specimens. General trends are seen in both data sets with Zn and C content generally increasing and Cr generally decreasing with SSE time in both sets. Differences between the two data sets include the presence of Ca and Co in the TCP, the presence of Zr, and, in a few cases, F in the Co-free TCP. Levels of N and Cl were observed in both sets but Cl was primarily observed in the Co-free TCP coatings.

Table 9 Elemental quantification from XPS survey spectra for Co-free TCP specimens. Element numbers are reported in atomic %.

Co-Free TCP	SSE Time(hrs)	O	C	N	Cr	Cl	Zr	Zn	F
191C	**0**	64	11	1	17	1	3	3	0
	168	53	23	2	14	1	2	5	0
	336	45	26	1	8	0	1	20	0
	504	40	34	3	8	1	2	12	0
	672	39	38	2	9	1	2	9	0
EN 191C	**0**	54	18	1	19	1	4	4	0
	168	48	20	0	9	0	0	23	0
	336	46	24	0	8	1	0	21	0
	504	42	27	2	9	0	0	20	0
	672	45	25	1	8	0	0	21	0
EN no heat	**0**	47	22	2	16	1	3	6	3
	168	39	30	2	12	1	1	16	0
	336	35	47	1	6	1	1	9	0
	504	43	28	1	8	0	0	20	0
	672	37	37	4	8	1	1	12	0

Table 10 Elemental quantification from XPS survey spectra for TCP specimens. Element numbers are reported in atomic %.

TCP	SSE Time(hrs)	O	C	N	Cr	Cl	Zn	Ca	Co
191C	**0**	55	18	0	15	2	5	3	2
	168	49	16	1	19	0	13	1	1
	336	38	41	2	9	0	8	0	0
	504	36	44	4	8	0	7	1	0
	672	39	39	3	9	1	8	0	1
EN 191C	**0**	52	14	1	19	3	6	2	3
	168	47	20	1	18	0	13	0	1
	336	42	32	1	9	0	14	1	1
	504	38	40	4	9	0	9	0	0
	672	45	27	2	9	0	17	0	0
EN no heat	**0**	46	26	2	14	0	9	1	2
	168	39	20	1	12	0	26	1	1
	336	43	31	1	8	0	16	1	0
	504	43	29	2	8	0	18	0	0
	672	43	28	2	8	0	19	0	0

Peak fitting results of the Cr 2p spectra in the experimental specimens are displayed in Table 11 and Table 12, while Table 13 contains the peak fit results for Co 2p only in the TCP specimens.

Table 11 Chromium species analysis from peak fitting Cr 2p spectra in Co-free TCP specimens. Species numbers reported as % of fit area.

Co-Free TCP	SSE Time(hrs)	Diff. Charge	$Cr(OH)_3$	CrO_3	Cr_2O_3
191C	**0**	0	69	2	29
	168	0	85	3	12
	336	4	77	2	17
	504	3	91	2	4
	672	2	74	2	22
EN 191C	**0**	0	91	2	7
	168	10	66	4	20
	336	21	62	5	13
	504	7	69	2	22
	672	14	51	2	33
EN no heat	**0**	1	97	2	0
	168	4	88	1	7
	336	7	78	2	13
	504	9	89	2	0
	672	6	92	2	0

Table 12 Chromium species analysis from peak fitting Cr 2p spectra in TCP specimens. Species numbers reported as % of fit area.

TCP	SSE Time(hrs)	Diff. Charge	$Cr(OH)_3$	CrO_3	Cr_2O_3
191C	**0**	0	84	1	15
	168	1	73	0	26
	336	1	75	1	23
	504	3	77	0	20
	672	1	88	1	10
EN 191C	**0**	1	48	1	50
	168	2	55	0	53
	336	6	65	1	28
	504	1	96	0	3
	672	2	98	0	0
EN no heat	**0**	1	76	0	23
	168	11	38	0	51
	336	14	75	4	7
	504	16	68	3	14
	672	17	54	3	26

Table 13 Cobalt species analysis from peak fitting Co 2p in TCP specimens. Species numbers reported as % of fit area.

TCP	SSE Time(hrs)	$Co(OH)_2$	CoO	CoOOH	Co_3O_4
191C	**0**	88	12	0	0
	168	67	33	0	0
	336	58	42	0	0
	504	63	34	3	0
	672	40	60	0	0
EN 191C	**0**	38	62	0	0
	168	76	24	0	0
	336	63	37	0	0
	504	62	33	0	5
	672	41	51	8	0
EN no heat	**0**	76	24	0	0
	168	70	30	0	0
	336	n/a	n/a	n/a	n/a
	504	n/a	n/a	n/a	n/a
	672	n/a	n/a	n/a	n/a

Co-free TCP specimen peak fit results of Cr 2p exhibited primarily $Cr(OH)_3$ species at all levels of heat treatment and SSE time. The EN Co-free TCP no heat exhibited less Cr_2O_3 than the other two conditions, but all specimens had peak fits improved by adding a small amount of CrO_3 to the fit, which implies that a low level of Cr^{6+} was present in all of the coatings. The EN Co-free TCP 191°C specimen displayed a higher percentage of Cr metal species; however, the discussion will explain that this is likely differential charging of the specimens and the amount was included in the data tables to display how much error of the peak fit area could be contributed to this factor.

The TCP specimen peak fit results for Cr 2p show a similar general trend with $Cr(OH)_3$ being the predominant species detected in the analysis. The TCP specimens also exhibited a relatively greater amount of Cr_2O_3 species than the Co-free TCP specimens. The primary difference between the two data sets comes from the amount of CrO_3 detected in the TCP specimens as the amount was generally lower and the fit was not always improved by adding CrO_3 to the peak fit. Lastly, the EN TCP no heat specimens displayed a greater amount of differential charging than the heat-treated specimens, which is indicative of a greater amount of corrosion product.

The Co 2p peak fitting results from the TCP specimens showed that most detected cobalt species were in the hydroxide and divalent oxide forms. For the heat-treated TCP specimens, the 504 and 672 hour SSE times exhibited small amounts of trivalent cobalt species, either CoOOH or Co_3O_4 and excluding the 672 hour SSE time TCP 191°C data point. For the EN TCP no heat specimens, there was not enough signal to detect the presence of cobalt from 336 to 672 hours of SSE time.

DPC Chromium Analysis

Chromate Measurement of Cr(VI) in test specimens via leaching with 1,5-diphenylcarbazide with increasing SSE time is shown in Figure 38. Co-free TCP 191°C showed the lowest measured Cr(VI) at all times with 0.9 ± 0.6 ng/cm^2 at 0 hours SSE and decreasing slightly to 0.5 ± 0.2 ng/cm^2 at 504 hours SSE. Both TCP conditions and the Co-free TCP no heat condition followed similar trends from 0 to 336 hours SSE with detected amounts ranging from 5.4-7.1 ng/cm^2 at 0 hours to 1.3-2.7 ng/cm^2 at 336 hours SSE. After 504 hours of SSE the TCP no heat showed a large increase in detected Cr(VI) to 13.1 ± 0.6 ng/cm^2. The TCP 191°C exhibited a greater amount of Cr(VI) at 504 hours SSE with 2.7 ± 0.7 ng/cm^2 compared to 1.3 ± 0.4 ng/cm^2 in the Co-free TCP no heat condition after the same SSE time.

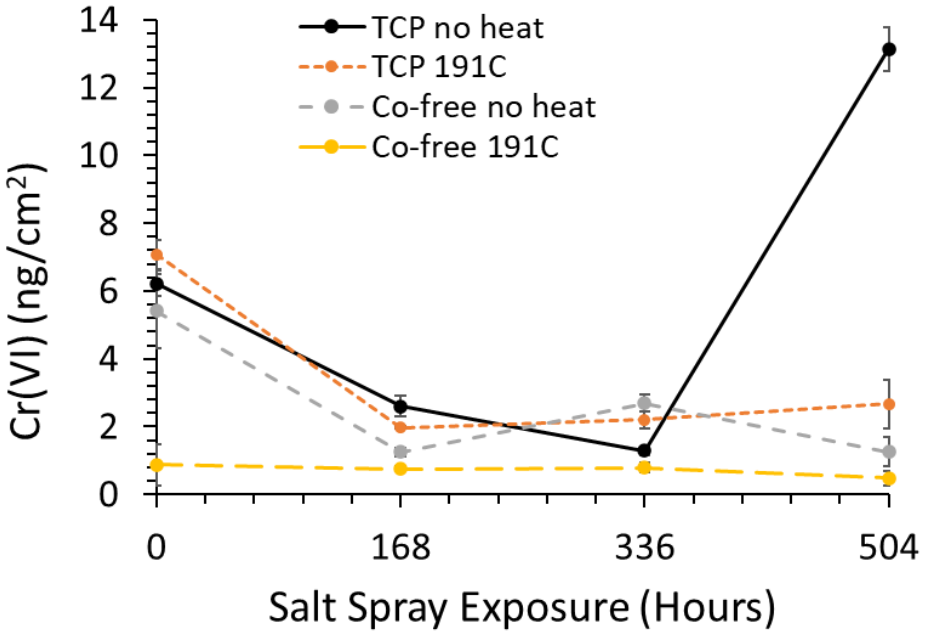

Figure 38 Measured Cr(VI) content in all test conditions from DPC analysis

Proposed Corrosion Protection Mechanism

Figure 39 shows the proposed model for corrosion protection of TCP's.

1. There is an initial amount of Cr^{6+} present in the passivation layer.
2. In the presence of electrolyte, Cr^{6+} goes into solution and precipitates at corrosion sites.
    a. Some Cr^{3+} oxidizes to Cr^{6+}
    b. Some Cr^{6+} precipitates as oxide/hydroxide
3. Corrosion product grows and prevents e- transfer for Cr^{6+} reduction, precipitated species are now mixed Cr^{6+} and Cr^{3+}
4. Remaining Cr^{6+} in solution collects on surface of corrosion product with drying, less corrosion product = lower surface concentration of Cr^{6+}

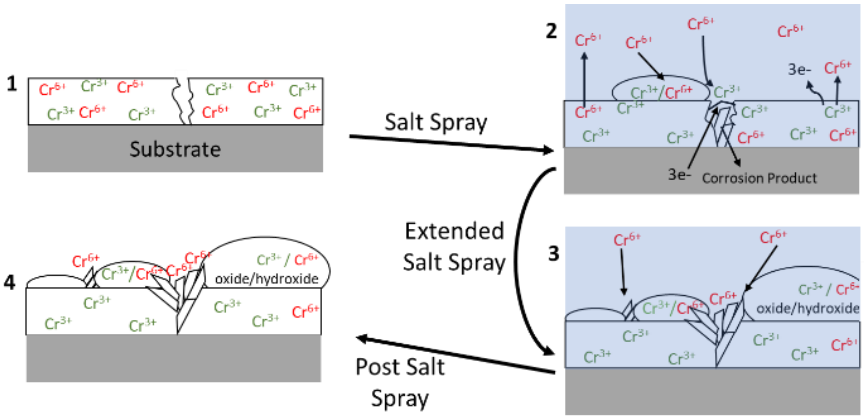

Figure 39 Proposed Model of Corrosion Protection Mechanisms

Connector Testing

Connectors and receptacles were divided into groups as shown in Table 14.

Table 14 Test Sequence 2 Shell Conductivity Results

Test Sequence #2 Shell Conductivity				
ZnNi with TCP	Measurement #1 (mV)	Measurement #2 (mV)	Measurement #3 (mV)	
1	6.55	6.54	6.55	Group 1
2	5.36	5.36	5.35	
3	5.25	5.26	5.25	Group2
4	6.22	6.21	6.22	
5	5.62	5.61	5.62	Group 3
6	6.02	5.02	5.01	

Co Free TCP	Measurement #1 (mV)	Measurement #2 (mV)	Measurement #3 (mV)	
1	7.16	7.15	7.16	Group 1
2	6.83	6.82	6.81	
3	7.99	7.97	7.99	Group2
4	8.65	8.64	8.65	
5	6.47	6.47	6.46	Group 3
6	9.30	9.31	9.30	

ZnNi with Hex Cr CC	Measurement #1 (mV)	Measurement #2 (mV)	Measurement #3 (mV)	
1	9.02	9.01	9.00	Group 1
2	6.63	6.61	6.63	
3	6.76	6.75	6.75	Group2
4	7.14	7.13	7.14	
5	7.58	7.57	7.57	Group 3
6	12.68	12.67	12.68	

MIL-DTL-5015 Electroless Nickel	Measurement #1 (mV)	Measurement #2 (mV)	Measurement #3 (mV)	
1	3.04	3.53	3.04	Group 1
2	3.53	3.53	3.54	
3	5.25	3.03	3.05	Group2
4	6.22	4.35	4.36	
5	5.62	4.24	4.25	Group 3
6	6.02	3.30	3.30	

Representative photographs of as received connectors and receptacles are shown in Figure 40.

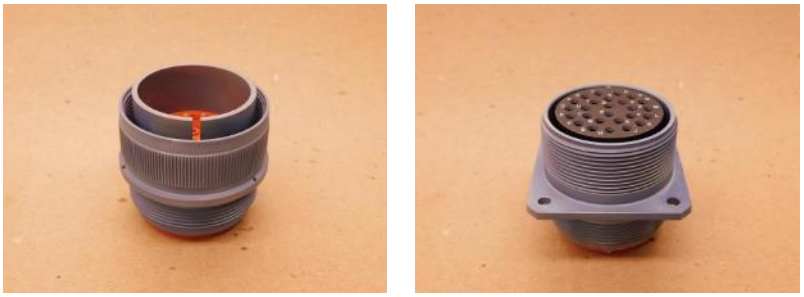

ZnNi with TCP Connector and Receptacle

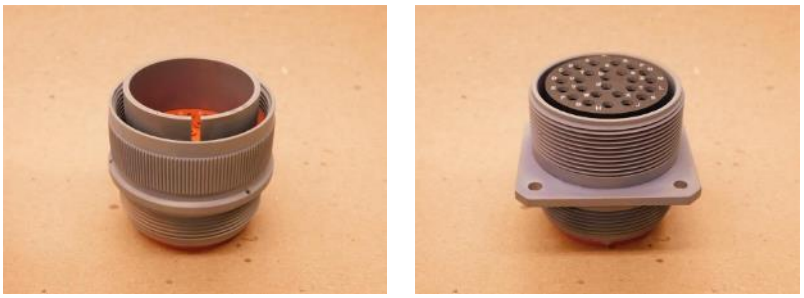

CoFree TCP Connector and Receptacle

ZnNi with CrCC Connector and Receptacle

MIL-DTL-5015 Electroless Nickel Connector and Receptacle

Figure 40 Representative photos of as received connectors

Following initial photographs, the connectors and receptacles were fully populated with pins and sockets attached to 12” lengths of wire to be representative of a typical installation. Images of the

control group (Group 1) are shown in Figure 41. Group 1 samples were subjected to only shell conductivity and mating torque testing as per the Test Matrix.

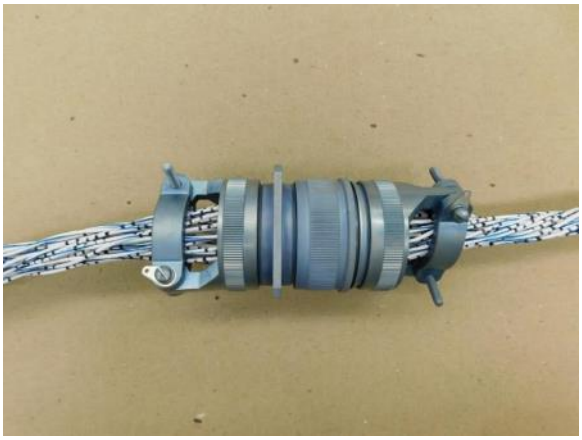

ZnNi with TCP Assembled

CoFree TCP Assembled

ZnNi with CrCC Assembled

MIL-DTL-5015 Electroless Nickel Assembled

Figure 41 Representative Assembled Connectors

Shell Conductivity

Testing was performed on all mated pairs per EIA365-83. A Valhalla Scientific 4300B Micro-Ohm Meter was used to measure the voltage drop across the mated connectors. Four point alligator clips were used to connect to the solder tabs attached to the back shell clamps on the mated connector pairs. Images of this test fixture with a sample mounted are shown in Figure 42. Three measurements were taken for each mated pair as shown in *Table 15*.

Figure 42 Mated Pair Test Fixture

Table 15 Test Sequence 3 Coupling Torque Results

Test Sequence #3 Coupling Torque Lubricity

ZnNi with TCP	Torque (in. lb)	
1	15	Group 1
2	16	
3	14	Group 2
4	17	
5	18	Group 3
6	17	

Co Free TCP	Torque (in. lb)	
1	15	Group 1
2	14	
3	16	Group 2
4	15	
5	17	Group 3
6	16	

ZnNi with Hex Cr CC	Torque (in. lb)	
1	15	Group 1
2	18	
3	14	Group 2
4	16	
5	17	Group 3
6	15	

MIL-DTL-5015 Electroless Nickel	Torque (in. lb)	
1	9	Group 1
2	13	
3	11	Group 2
4	14	
5	12	Group 3
6	10	

Coupling Torque

This measurement was made on all samples used in the testing. The receptacle of each mating pair was held in a smooth jaw vice to facilitate assembly. The vice jaws were covered in tape to eliminate any damage to the plating. A custom fixture was fabricated to grip the connector shell and a torque wrench was used to measure the mating torque. The fixture is shown in Figure 43.

Figure 43 Coupling Torque Test Fixture

The results of the measurements are shown in Table 16.

Table 16 Test Sequence 6 Coupling Torque Results

Test Sequence #6 Coupling Torque Lubricity

ZnNi with TCP	Torque (in. lb)	
1	16	Group 1
2	14	
3	16	Group 2
4	15	
5	17	Group 3
6	19	

Co Free TCP	Torque (in. lb)	
1	16	Group 1
2	15	
3	15	Group 2
4	14	
5	27	Group 3
6	24	

ZnNi with Hex Cr CC	Torque (in. lb)	
1	12	Group 1
2	16	
3	14	Group 2
4	15	
5	18	Group 3
6	17	

MIL-DTL-5015 Electroless Nickel	Torque (in. lb)	
1	8	Group 1
2	10	
3	12	Group 2
4	12	
5	13	Group 3
6	13	

Adhesion

Adhesion testing was performed on all Group 2 mated samples per EIA 364-42C. A text figure was fabricated to allow the samples to be dropped from the required heights per the EIA document as shown in Figure 44.

Figure 44 Impact Test Fixture

All of the samples were subjected to the Moderate test sequence which requires 8 drops at 4 feet and 8 drops at 8 feet. After each drop the connector was rotated 1/8" by the use of a bolt on the end of the 5.5ft square bar to allow each drop to originate from a different index position. Representative post test images of the connectors are shown in Figure 45. Damage from the impact testing can be seen in the photos but no evidence of plating delamination was found.

ZnNi with TCP Pre-Impact

Post-Impact

CoFree TCP Pre-Impact

Post-Impact

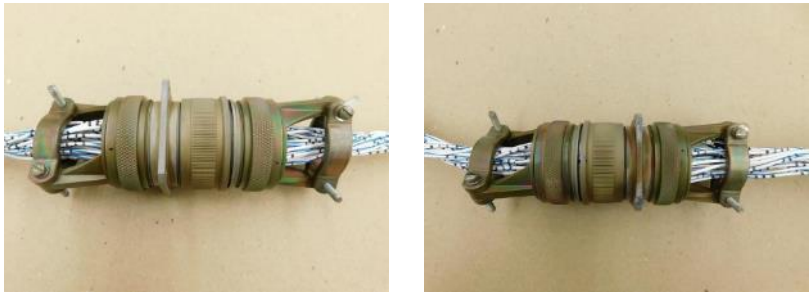

ZnNi with CrCC Pre-Impact Post-Impact

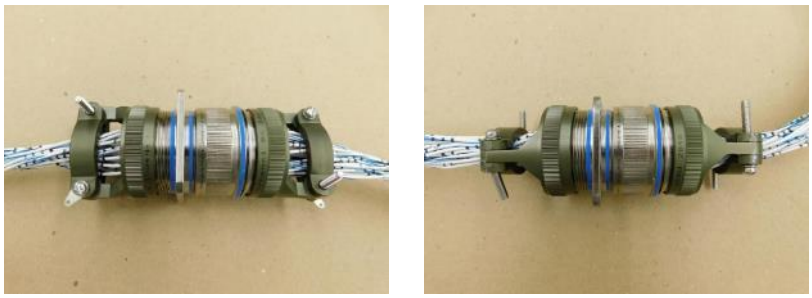

MIL-DTL-5015 Pre-Impact Post-Impact

Figure 45 Representative Images of Impact Testing

Salt Spray

Group 3 samples were exposed to the Salt Spray environment per EIA-364-26 test condition C. Prior to testing all samples were wiped down with IPA to remove any contaminants that could alter the results. Samples were placed in the salt spray chamber on racks as shown in Figure 46.

Figure 46 Salt Spray Setup

After 452 hours of exposure, the samples were removed from the samples were removed from the chamber and de-mated. Images of the test samples at the 452 hour mark are shown in Figure 47.

ZnNi with TCP at 452 hrs

CoFree TCP at 452 hrs

ZnNi with CrCC at 452 hrs

MIL-DTL-5015 at 452 hrs

Figure 47 Assemblies after 452 hrs of Salt Spray Exposure

The samples were then placed back into the salt spray chamber for an additional 48 hours. Following salt spray, images were taken of each sample as shown in Figure 48.

ZnNi with TCP

ZnNi with CrCC

MIL-DTL-5015

Figure 48 Assemblies after additional 48 hrs of Salt Spray

Following the salt spray testing an optical inspection of the connectors and receptacles was conducted. The examination found that the Zinc Nickel with the Hex CrCC connectors and receptacles exhibited spotting/discoloration of the coating.

The examination also found the shell of MIL-DTL-5015 connector number 5 had a section of the nickel plating that lifted during the testing. The back shell of MIL-DTL-5015 connector 5 receptacle also had damage to a small circular area. Both of these locations are shown in Figure 49.

Figure 49 Damage to MIL-DTL-5015

Coupling Lubricity

Testing was performed on all samples in the same manner as sequence 3 and the results are shown in Table 17.

Table 17 Test Sequence 6 Coupling Lubricity Results

ZnNi with TCP	Torque (in. lbs)	
1	16	Group 1
2	14	
3	16	Group 2
4	15	
5	17	Group 3
6	19	

Co-Free TCP	Torque (in. lbs)	
1	16	Group 1
2	15	
3	15	Group 2
4	14	
5	27	Group 3
6	24	

ZnNi with Hex Cr CC	Torque (in. lbs)	
1	12	Group 1
2	16	
3	14	Group 2
4	15	
5	18	Group 3
6	17	

MIL-DTL-5015	Torque (in. lbs)	
1	8	Group 1
2	10	
3	12	Group 2
4	12	
5	13	Group 3
6	13	

Shell Conductivity

Shell conductivity testing was performed on all mated samples in the same manner as Sequence 2 and the results are shown in Table 18.

Table 18 Test Sequence 7 Shell Conductivity Results

Test Sequence #7 Shell Conductivity				
ZnNi with TCP	Measurement #1 (mV)	Measurement #2 (mV)	Measurement #3 (mV)	
1	6.99	6.97	6.94	Group 1
2	34.25	34.31	34.39	
3	10.15	10.13	10.11	Group2
4	59.36	58.99	59.11	
5	70.28	70.20	70.32	Group 3
6	22.17	22.14	22.18	
Co Free TCP	Measurement #1 (mV)	Measurement #2 (mV)	Measurement #3 (mV)	
1	7.01	7.00	7.02	Group 1
2	6.19	6.18	6.18	
3	6.95	6.94	6.96	Group2
4	6.42	6.41	6.45	
5	93.71	93.76	93.74	Group 3
6	36.28	36.30	36.33	
ZnNi with Hex Cr CC	Measurement #1 (mV)	Measurement #2 (mV)	Measurement #3 (mV)	
1	36.42	36.41	36.44	Group 1
2	20.74	20.71	20.73	
3	78.11	78.07	78.21	Group2
4	25.89	25.81	25.86	
5	36.42	36.50	36.46	Group 3
6	57.40	57.36	57.48	
MIL-DTL-5015 Electroless Nickel	Measurement #1 (mV)	Measurement #2 (mV)	Measurement #3 (mV)	
1	2.12	2.13	2.13	Group 1
2	2.77	2.77	2.77	
3	2.12	2.12	2.12	Group2
4	3.71	3.71	3.71	
5	4.96	4.96	4.96	Group 3
6	5.21	5.22	2.21	

Additional solder tabs were added to the salt spray samples to allow a better connection to the connectors. The solder tabs that were initially installed on the connector samples exhibited corrosion and were not used for measurements in sequences 7 and 8.

Alternative Contact Resistance Metrologies

Introduction

The goal of this project was investigating alternatives to the contact resistance measurement methodology documented in MIL DTL 81706B. This outlines a method of pressing a metal panel between two copper electrodes of defined area and geometry at 200 ± 2 psi. A four-terminal measurement of the resistance of the panel is then made to eliminate the apparatus and electrode resistance from the measurement. This methodology has been used for decades and has advantages of simplicity and robustness in that it can be used to measure contact resistance even on highly corroded panels. However, it is also known to have issues with repeatability and reproducibility and cannot be used to measure contact resistance directly on non-planar surfaces such as military connectors. Considering these issues, the goal was to develop an alternative methodology with the following characteristics.

- Repeatability and reproducibility better than 81706B
- Simplicity of use comparable to 81706B
    - Possibly using the same basic apparatus
- Possibly offering more information than 81706B
- Possibly being usable on curved surfaces

This report covers the investigation of various alternatives, particularly the selected method of cTLM: circular Transfer Length Model.

Possible Alternatives

Four Line Microprobe

Four terminal electrical conductivity and contact resistance measurement goes back to Lord Kelvin [104]. In this method the current carrying and voltage sensing electrodes are electrically separated from one another to eliminate lead and contact resistance from low-resistance measurements. If desired, it also enables calculation of lead and contact resistance.

Researchers at Brigham Young University developed a four-line microprobe for measuring conductivity and contact resistance of thin-film battery electrodes [105]. The initial design of this probe was manufactured on a glass substrate and was tested with some success on the SERDP SEED project. This design was updated by BYU to use a flexible polymer substrate enabling a higher pressure to be used with the probe and for potential use on curved DUTs (Figure 50).

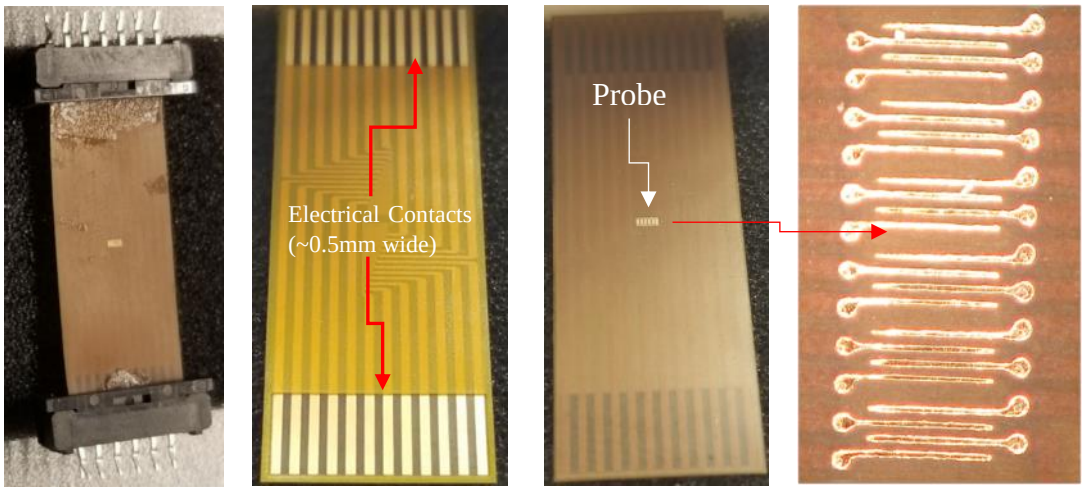

Figure 50 Original BYU Microprobe and 2nd Generation Flexible Microprobe

Theory

The mathematical model of the 4-line microprobe and test results were reported in two papers. A summary of the papers follows.

- Mathematical Model of Four-Line Probe to Determine Conductivity Properties of Thin-Film Battery Electrodes [106]
- Micro-Four-Line Probe to Measure Electronic Conductivity and Contact Resistance of Thin-Film Battery Electrodes [105]

The probes were designed with a line spacing of 70um to be compatible with the typical film thickness of lithium-ion battery electrodes (30-100um). This use of lines and spacing size on the same order as the film thickness means that normal simplifying assumptions of 4-point probes do not apply. Rather than use finite element modeling to generate solutions, the authors developed a 2D model with simpler boundary conditions to be used for validation of designs and a 3D model with complex boundary conditions to be used for actual data collection.

Actual testing involves two testing modes: a tangential mode which is similar to a normal 4-point probe measurement; and an orthogonal mode where current is passed through the test sample into the current collector of the battery. Changing from one mode to another can be done with simple relays and the data is fed in real time into the 3D model to calculate resistivity, contact resistance, etc.

Results

Internally, use of the BYU probe was problematic. Only rarely was contact with the DUT achieved and results were not repeatable. Additionally, although the probe had been re-designed and made on a polymeric flexible substrate the probe lines were still vulnerable to damage from the substrate. The result was that probe line integrity rarely lasted longer than 5-10 attempted measurements. Because of this, six samples were sent to BYU for measurement and analysis.

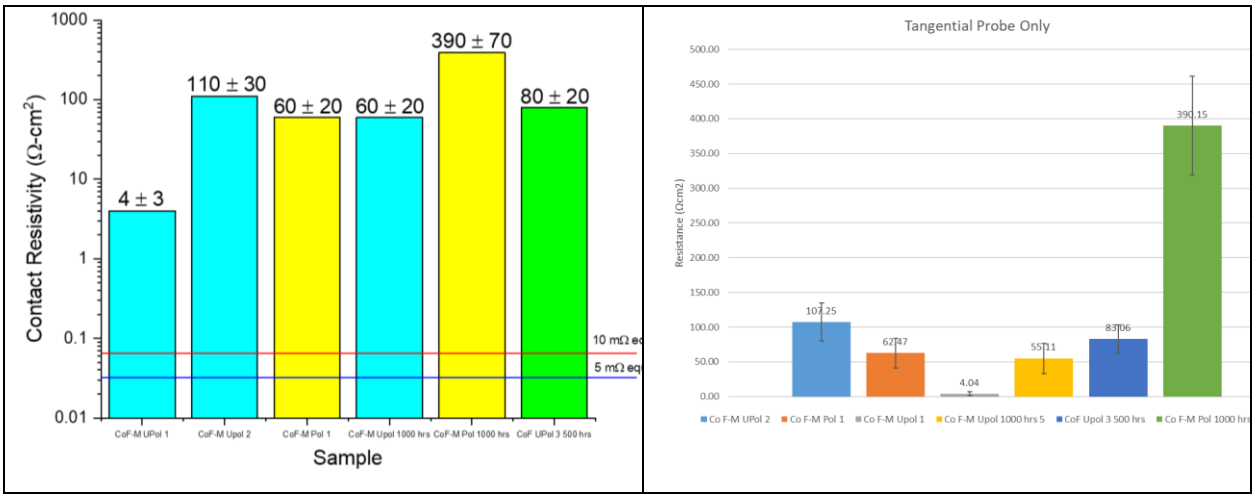

Figure 51 BYU 4-line Microprobe Results

BYU also had considerable difficulty in measuring the samples. Assuring good electrical contact of the probe to the samples and probe degradation after contact were issues. To ensure good electrical contact the samples were sputter coated with carbon prior to measurement with the 4-line microprobe and the resulting measurements are shown in Figure 51. The resulting contact resistance measurements were several orders of magnitude higher than those achieved with the standard 81706B methodology. At this point, there was some discussion with BYU on how to improve the suitability and robustness of the microprobe design for contact resistance measurement of our samples, but BYU eventually ceased responding to communications.

Linear TLM

The transfer length method (TLM or linear TLM [107]) consists of using more than three contacts that have unequal spacing between them (Figure 52). Measured resistance values are plotted with the distance between contacts as the x-axis. The sheet resistance can be calculated from the slope of the line, contact resistance is calculated from the y-intercept, and the transfer length is calculated from the x-intercept.

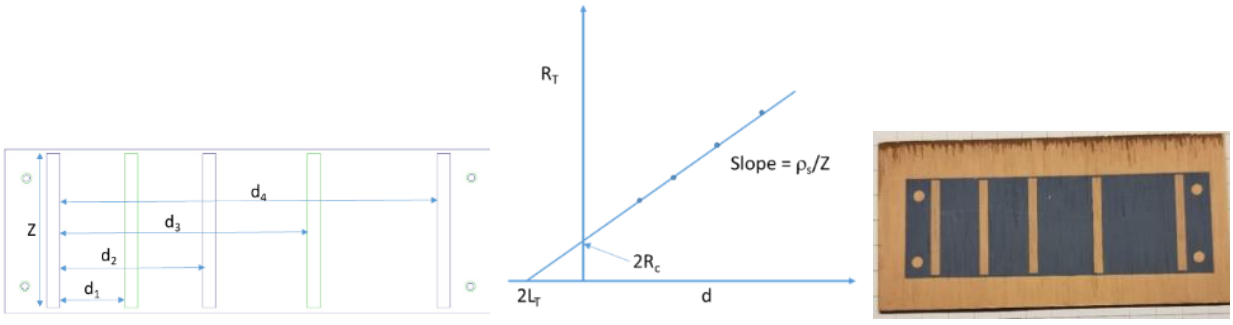

Figure 52 Linear Transfer Length Method

In practice, current spreading made it difficult to achieve straight lines with the data and calculate parameters from the line. Additionally, it required a different set of contacts to be made when the sample size changed. Because of this, it was dropped from consideration.

cTLM

Circular transfer length method (cTLM), also called circular transmission line method, is a variant on the transfer length method (TLM) where concentric ring contacts are used to determine contact resistance [108].

Theory

A simple cTLM structure (Figure 53) such as investigated by [109] the resistance between the contacts can be shown to use the equation [107]

Equation 1

$$R = \frac{R_{sh}}{2\pi}\left[\frac{L_T}{r_1}\frac{I_0(r_1/L_T)}{I_1(r_1/L_T)} + \frac{L_T}{r_1+d}\frac{K_0(r_1/L_T)}{K_1(r_1/L_T)} + \ln\left(1+\frac{d}{r_1}\right)\right]$$

where I and K are modified Bessel functions of the first order, R_{sh} is the sheet resistance, L_T is the transfer length, r_1 is the radius of the inner electrode, and d is the gap size. If $r_1 >> 4L_T$ the ratios I_0/I_1 and K_0/K_1 go toward unity and the equation becomes

Equation 2

$$R = \frac{R_{sh}}{2\pi}\left[\frac{L_T}{r_1} + \frac{L_T}{r_1+d} + \ln(1 + \frac{d}{r_1})\right]$$

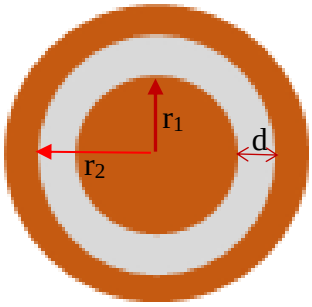

Figure 53 Annular cTLM layout

If $r_1 >> d$, then equation 2 can be rewritten as

Equation 3

$$R = \frac{R_{sh}}{2\pi r_1}[d + 2L_T]c$$

Where c is a correction factor

Equation 4

$$c = \frac{r_1}{d}\ln(1 + \frac{d}{r_1})$$

In practical terms $r_1 > 4d$ is sufficient and the final probe design used this to determine the radii of the inner and outer electrodes. These constraints enable the data plots of resistance vs gap size to be linearized and then electrical parameters can be extracted as in linear TLM.

Design Iterations

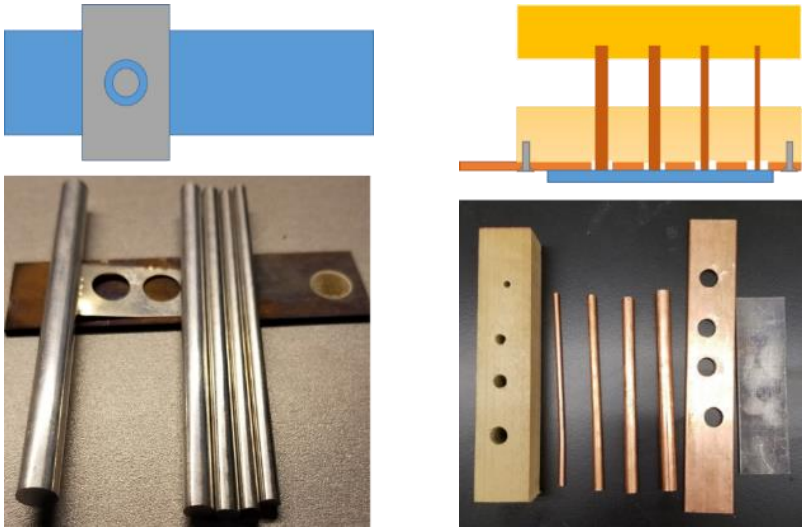

a. *b.*

Figure 54 cTLM probe design 1

Initial design consisted of sheet metal with holes drilled to specified size and multiple sizes of aluminum rods for the center electrode (Figure 54a). Next iteration used copper rods for better conductivity coupled with wood gaskets and a copper bar for the outer electrode (Figure 54b). Maintaining good electrical contact was difficult but did show possibility of the methodology.

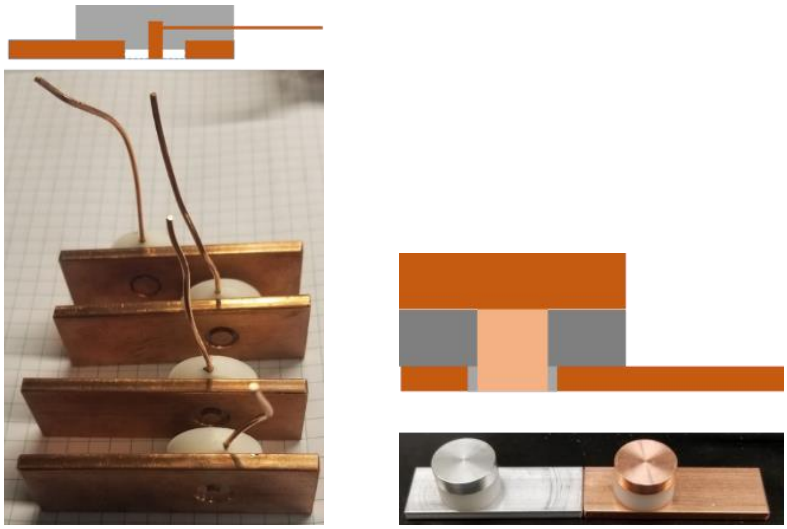

a. *b.*

Figure 55 cTLM probe design 2

The next effort was designed to allow the probe to be inserted into the 81706B apparatus to apply pressure to both the center electrode and the outer electrode bar (Figure 55). The first effort utilized a copper post embedded in a polymer cap with a wire soldered to the post for making electrical contact (Figure 55a). The second replaced the wire by making the copper post pass through the polymer and electrical contact was via the top electrode of the 81706B apparatus (Figure 55b). Both relied on some compression of the polymer to allow the slightly recessed post to contact with the substrate. This made controlling the amount of recess critical to achieving electrical contact and produced a large differential between the pressure on the post and the pressure on the bar. The design showed an improvement in data quality vs. the original design, but improvements in the pressure uniformity between the post and bar were necessary.

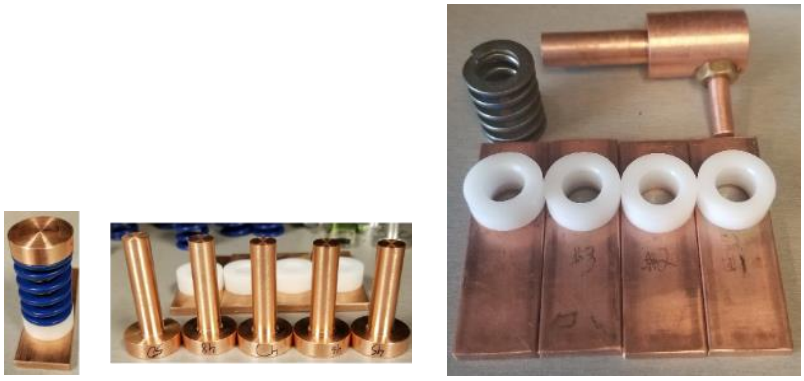

a. *b.*

Figure 56 cTLM probe design 3

The third design utilized a spring to transmit force to the bar electrode while the post was directly pressed by the 81706B apparatus Figure 56). The length of the post determined the pressure ratio between the bar and the post (Figure 56a). Best results were obtained when pressure on bar and post were both ~200 psi when the nominal force on the scale was 185-200 lbs. To minimize the number of electrical connections an integrated post was manufactured (Figure 56b).

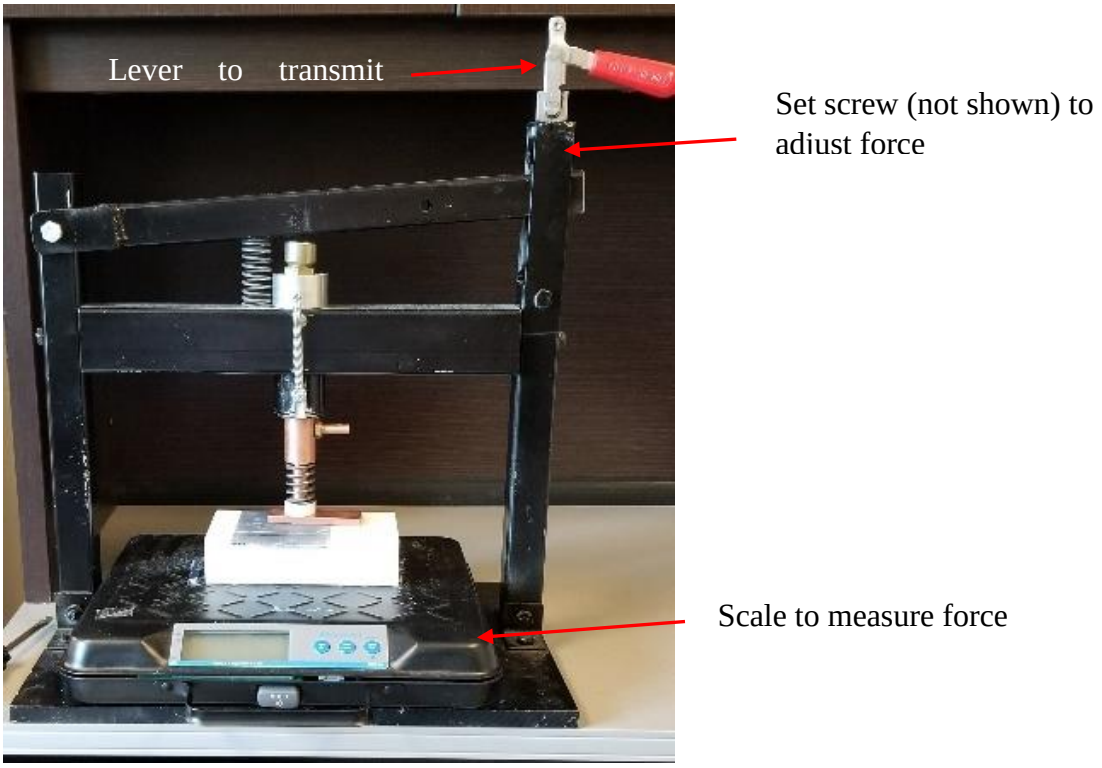

a.

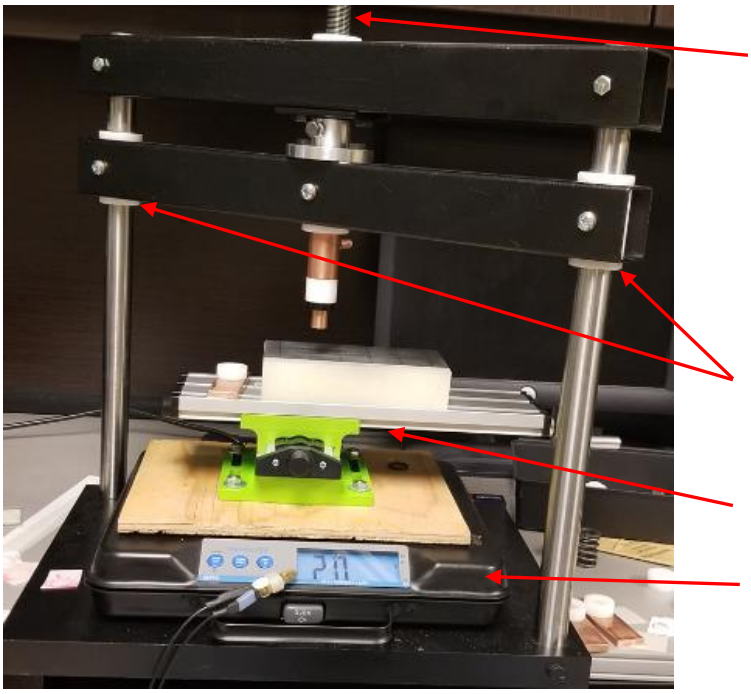

b.

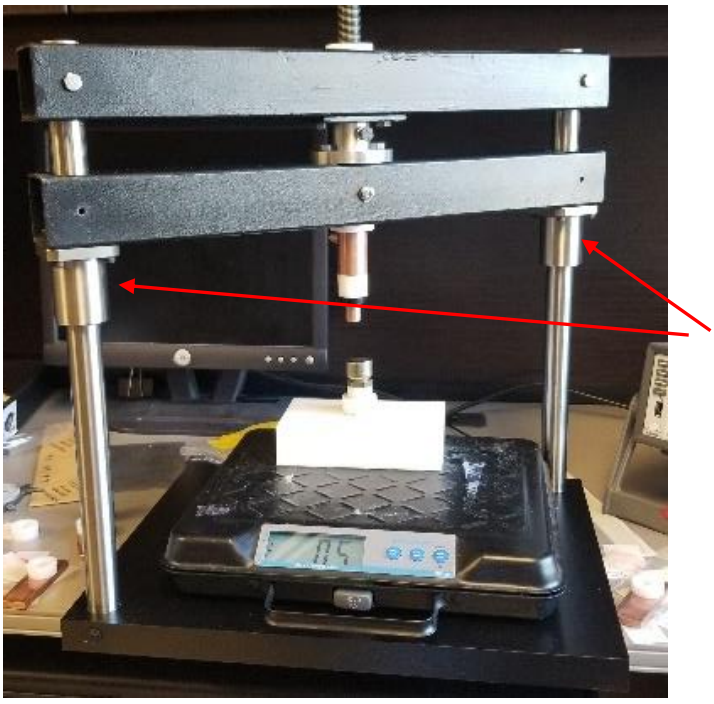

c.

Figure 57 Design Changes to 81706B Apparatus

Design changes were made to the pressure inducement apparatus as well (Figure 57). The original apparatus (Figure 57a) used coupled levers and springs to transmit force. It was prone to pressure

changes during measurements so a new apparatus utilizing a screw mechanism was developed (Figure 57b). Originally this device used simple sleeves to slide up and down the guideposts but there were often height differences between the sleeves resulting in non-uniform pressure across the probe. The sleeves were replaced with linear bearings to minimize the pressure gradient (Figure 57).

Finally, Fujifilm pressure sensitive paper was used to determine the pressure uniformity of the bar and the post. This led to re-machining the posts and bars to maximize the planarity of each. Use of the Fujifilm paper also enabled samples to be leveled before measurement to assure uniform pressure and electrical contact of the probes.

Probe Material Selection

Three copper alloys (Cu101, Cu110, and Cu182) and two aluminum alloys (Al6061 and Al6063-T5). Copper alloys were preferred because of higher conductivity and generally more consistent results, except for the Cu110 alloy.

Table 19 gives the alloy conductivity and comments on suitability as a probe material.

Table 19 Alloy Suitability as Probe Material

Alloy	**Conductivity (Siemens/m)**	**Suitability**
Cu101	5.8e7	Generally gave lowest contact resistance, easily damaged by substrate, left considerable residue on substrate limiting repeat measurements
Cu110	5.6e7	Generally did not yield data, reason unknown
Cu182	4.6e7	Contact resistance somewhat higher than Cu101, no residue on substrate, no damage to probe, generally yielded more data than Cu101
Al6061	2.5e7	Generally did not yield data
Al6063-T5	3.1e7	Measured contact resistance was significantly higher than Cu101 or Cu182, generally yielded less data than Cu101 or Cu182

For best results with the copper alloys, it was necessary to etch them periodically to remove tarnish. Probes were immersed in white vinegar for 10 min, rinsed with deionized water, and air dried before use. Aluminum would have been preferable for this reason, but readily available alloys had insufficient conductivity. The Cu182 alloy was selected as the material for the final probe design.

Known Issues

- Copper-based probes must be etched periodically to remove tarnish and enable good electrical contact with the substrates.
- Locations where data did not form a line with $r^2 \geq 0.80$
    - Improvements made

        - Re-machining probes for planarity
        - Re-machining probes so that pressure differential between inner and outer electrodes was minimized
        - Monitoring pressure gradients with Fujifilm paper and leveling
        - Adjust process to increase pressure slowly
- The occurrence of data where a line is formed with a negative y-intercept which is a non-physical result. Two possible reasons:
    - The resistances as measured are systemically low thus shifting the entire line downward
    - There is a systemic resistance proportional to the gap size that increases the slope of the line.
    - The first seems more likely. A mismatch in pressure, where the center electrode is significantly higher than the outer electrode, could push metal up into the gap and reduce the effective resistance measured.
- Flexing of the Delrin® polymer inserts allowing the inner electrode to shift off center.
    - This would lower the resistance measured and could play a role in the negative intercept issue.
- Issues with the original apparatus
    - Pressure changed significantly during measurement
    - Samples often shifted at the end of a measurement when pressure was released
    - Inadvertent shifting of samples when outer electrodes were changed

Results

Coated Panels

Freshly coated panels were obtained from Dipsol and tested first with the standard 81706B methodology then using the cTLM methodology (Table 20).

Table 20 Comparison on Freshly Coated Panels

Panel	**r^2**	**R_c (mΩ)**	**L_T (cm)**	**R_{sh} (Ω/ϒ)**	**ρ_c (mΩ cm^2)**	**cTLM (mΩ)**	**81706B (mΩ)**
ST ZN CoF 0hr	0.959 ± 0.044	1.26 ± 0.21	0.0063 ± 0.0063	1.08 ± 0.94	5.33 ± 0.89	0.83 ± 0.14 17%	54 ± 25 46%
ST ZN TCP 0hr	0.94 ± 0.05	1.14 ± 0.75	0.028 ± 0.034	0.30 ± 0.16	4.8 ± 3.2	0.75 ± 0.49 65%	53 ± 16 30%
ST EN ZN CoF nobake 0hr	0.959 ± 0.061	8.5 ± 7.9	0.026 ± 0.019	1.7 ± 1.1	36 ± 33	5.6 ± 5.2 93%	51 ± 26 51%
ST EN ZN CoF bake 0hr	0.943 ± 0.097	1.29 ± 0.33	0.00453 ± 0.00068	1.23 ± 0.49	5.5 ± 1.4	0.84 ± 0.22 26%	25.4 ± 9.3 37%
ST EN ZN TCP nobake 0hr	0.968 ± 0.031	1.20 ± 0.53	0.0109 ± 0.0051	0.55 ± 0.19	5.1 ± 2.2	0.79 ± 0.35 44%	66 ± 25 38%
ST EN ZN TCP Bake 0hr	0.949 ±0.055	2.90 ± 0.54	0.0168 ± 0.0093	0.81 ± 0.58	12.3 ± 2.3	1.90 ± 0.35 18%	42 ± 21 50%

Corroded Panels

Panels were scanned and ImageJ was used to estimate the corrosion coverage of the panels (Figure 58). Contact resistance was measured by cTLM and was compared to previous results from the standard 81706B method. All samples had been subject to 336 hrs of salt spray exposure according to the B117 standard. Note that when salt spray exposure exceeded 336 hrs cTLM measurements of contact resistance could not be made.

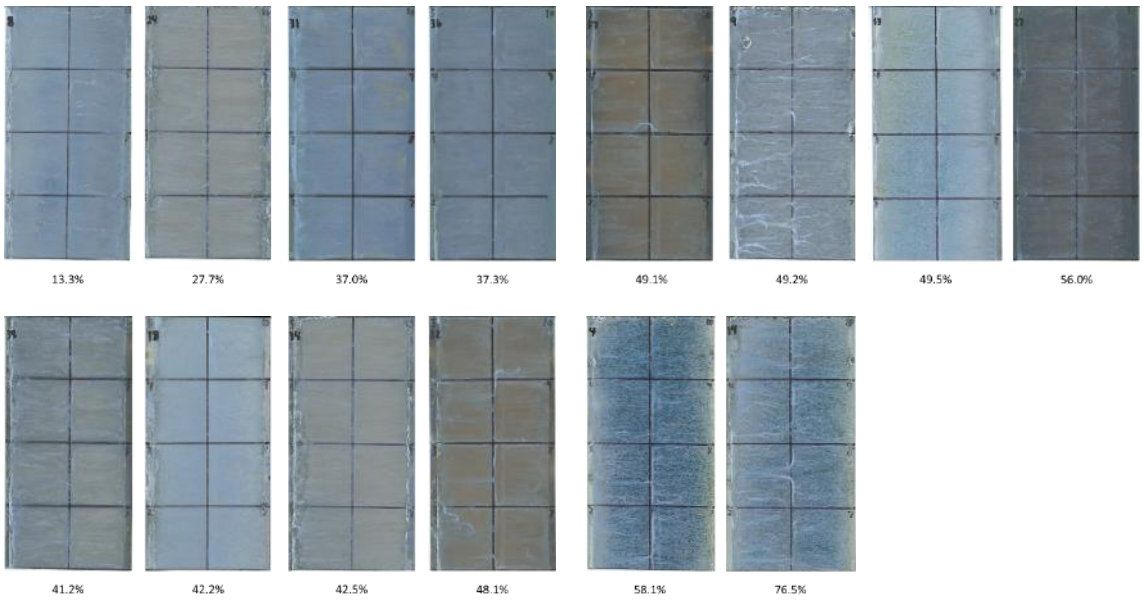

Figure 58 Corroded Panels and Corrosion Coverage

In Table 21 a comparison is made of results using cTLM vs. the standard methodology.

Table 21 cTLM Compared to 81706B on Corroded Panels

Panel	**r^2**	**cTLM (mΩ)**	**81706B (mΩ)**
#4 336 hrs	0.993	72.87225	*187.39*
#8 336 hrs	0.835-0.917	48 ± 27	*150.54*
#9 336 hrs	0.976-0.996	61± 64	*198.25*
#13 336 hrs	0.988-0.990	44± 18	*93.4*
#14 336 hrs	0.855-0.994	82.0 ± 4.5	*228.95*
#18 336 hrs	0.810-0.984	52 ± 46	*270.8*
#24 336 hrs	0.925-0.979	46 ± 16	*150.61*
#27 336 hrs	0.947-1	2.1 ± 1.1	*44.24*
#31 336 hrs	0.825-0.991	8 ± 11	*70.95*
#32 336 hrs	0.939-0.955	39 ± 56	*196.23*
#34 336hrs	0.904-0.999	45 ± 23	*201.9*
#36 336 hrs	0.967	11.04871	*40.06*
#37 336 hrs	0.903-0.960	2.8 ± 2.3	*102.96*
#39 336 hrs	0.810-0.999	2.18 ± 0.68	*85.06*

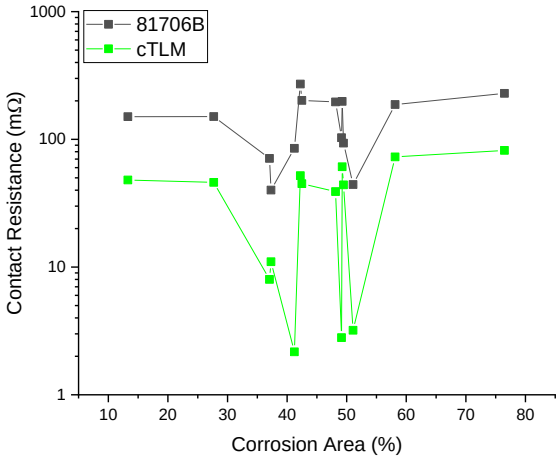

Figure 59 Contact Resistance vs Corrosion Area

In Figure 59 a similar relationship of contact resistance to corrosion area is seen with both the standard 81706B methodology and cTLM. The contact resistance is stable in the 10-20% range, drops when corrosion coverage is 30-40% and 50-55%, and is stable again at 60-80%. In general, the cTLM values are ~1/3 of the values measured using the 81706B methodology.

Developing a Standard

A major issue in contact resistance measurement is there is no method and materials to use as a standard for evaluating contact resistance measurements. A standard material would be useful in providing a reproducible surface to validate a contact resistance methodology. Processing the surface to achieve uniform results across the area would also be useful: currently it is difficult to determine if variability seen is due to the measurement methodology or non-uniformity of the surface.

Toward this end some work was performed using 1008 steel panels. Three panels were manually polished using 320 grit silicon carbide paper, rinsed in deionized water, and air dried. Measured results are shown in Table 22.

Table 22 Repeatability of Measurements on 1008 Steel Panels

R_C (mΩ)	**L_T (cm)**	**R_{SH} (Ω/ϒ)**	**ρ_C (mΩ cm2)**	**81706B equiv (mΩ)**
0.178 ± 0.017 (9.6%)	0.0128 ± 0.0029 (23%)	0.0773 ± 0.0047 (6.1%)	0.753 ± 0.070 (9.3%)	0.117 ± 0.012 (10%)

Results are encouraging, measured parameters, except transfer length L_T have standard errors of 10% or less. Note that these panels were corroded in multiple spots before polishing and that polishing did not fully remove all evidence of corrosion. Better results could likely be obtained by using panels made of stainless steel or aluminum.

A standard methodology is more difficult, but some work has been done in the direction by using multiple source-measure units (SMU) in a modified van der Pauw method to measure contact resistance of arbitrary samples [110]. This methodology used a Keithley 4200-SCS Parameter

Analyzer with 4 SMU cards and PSPICE simulation to estimate errors caused by geometrical factors. The methodology enables measurement of the contact resistance of all four contacts plus determining the linearity and rectifying properties of the contacts. This methodology could be used to validate the accuracy of simpler alternate contact resistance methods, albeit at a high cost in equipment ($20k-$50k+ on used market).

Conclusions and Implications for Future Research/Implementation

Coating Development

Divalent cobalt in TCPs significantly improves corrosion resistance on γ-ZnNi coated steel and aluminum alloys. While some variability remains in the test data, cobalt-containing passivations typically withstand 3 or more weeks of ASTM B117 salt spray exposure while remaining electrically conductive. Initially it seemed that the underlying substrate (steel vs. aluminum) could have an effect on corrosion performance, it was later revealed that the primary influencing component was the level of Cr(VI) content in the passivation. Since the amount of Cr(VI) content was positively correlated with the corrosion performance and divalent cobalt facilitated Cr(VI) production during salt spray exposure, it is clear that a TCP containing cobalt would perform better simply by increasing the Cr(VI) content. However, the specimens with the highest Cr(VI) content did not always perform as well and some cobalt-free TCP specimens, such as the ones on the initial SAE 1008 steel panels, did perform well. These results indicate that Cr(VI) content alone is not a sufficient predictor of improved corrosion performance.

The heat treatments showed contradictory results on Cr(VI) content between the two passivations, both increasing and decreasing the amounts in the different passivations. The replicatable change in OCP between heat-treated and non-heat-treated passivations clearly indicates that the passivation has been altered by the heat treatments. However, both passivations exhibited similar OCPs after heat treatment despite having largely different amounts of Cr(VI) and no consistent differences in Cr species detected by XPS. This suggests that the heat treatments have caused a relevant change in the bulk of the passivation with little effect on the surface, caused physical changes that dominate the OCP response despite chemical differences, or had a variety of changes that by coincidence leave both passivations at the same OCP after heat treatment. The third option is highly unlikely and thus disregarded but the bulk could be studied through depth profiling of the passivation before and after heat treatment while the second has already been observed indirectly in the present research through comparison of the physical features on the first steel and aluminum samples.

While physical changes such as crack size, crack density, passivation thickness, and passivation porosity were observed, they did not correlate well with corrosion performance. In the context of heat treatments causing morphological changes to the passivations, processing parameters being different between the two passivations, and Cr(VI) content being measured separately from passivation physical features, it is clear that corrosion performance should be a function of both Cr(VI) content and physical aspects of the passivation. This combined examination of the data gathered offers insight into what is happening during corrosive exposure of the TCPs to create a model for how the TCPs protect their underlying substrate. Since the corrosion starts at localized areas and typically grows outward, it is clear that some local aspect of the coating, such as a crack, flaw, or uncovered area in a crevice, results in failure at certain points but not others. When TCPs

contain cobalt and Cr(VI) content is high, Cr(VI) can leach into the corrosive aqueous solution and deposit at these sites to form a mixture of the corrosion products, zinc carbonate hydroxide hydrate ($Zn_4CO_3(OH)_6 \bullet H_2O$) and zinc chloride hydroxide hydrate ($Zn_5(OH)_8Cl_2 \bullet H_2O$), with the Cr(III) oxide or hydroxide reduced from the Cr(VI) species. This mixture is very similar to the passivation that consists of amorphous Cr(III) oxides/hydroxides, zinc oxides/hydroxides, and small amounts of Co(II) oxides/hydroxides but has a greater molar volume from the additional carbonate, chlorine, and water present. Eventually, this mixture would grow to a thickness where it prevents the Cr(VI) from reaching the active corroding metal allowing the corrosion product to blister the nearby passivation and grow unchecked.

The EN layer on steel did not have a measurable effect on corrosion performance which helped to confirm that it was factors other than the underlying substrate that contributed to the performance differences originally observed between the steel and aluminum substrate specimens. This observation helps support the idea that the mechanism of corrosion and corrosion protection for TCP coated specimens is surface focused and depends only upon the passive film and its immediate underlying substrate (γ-ZnNi coating). While the presence of divalent cobalt in the passive films aids corrosion performance through interaction with Cr(VI), the fact that the cobalt-free TCP on the initial steel specimens withstood ASTM B117 salt spray for 1000 hours with minimal corrosion acts as a proof of concept that a superior and conductive cobalt-free TCP could be produced if the relevant physical, chemical, and processing parameters were optimized.

Identifying divalent cobalt and its relation to Cr(VI) as important to corrosion performance of TCPs was important but a few aspects of the system still remain unclear. Future work should thus focus on experiments that identify these key aspects and determine their effect on corrosion performance to create a model that can predict the time until failure of a TCP based on measurable aspects of the film. A focus on tight control of the processing and optimization of the processing parameters to produce physically and chemically consistent TCPs would help minimize the variability observed in the prior studies. Research questions that could be answered with such well controlled specimens include:

- Can cracks in the passive films be prevented by processing changes? (wetting of surface, temperature, pH, high humidity drying, etc.)
- Can an increase/decrease in γ-ZnNi surface area affect corrosion performance?
- Could other divalent dopants such as Ni(II), Mn(II), or Mg(II) behave similarly to cobalt in TCPs?
- Could corrosion performance be maintained by tetravalent dopants vs. divalent dopants without affecting conductivity?

This research did not focus much on processing changes affecting the deposition of the TCPs even though it is likely that observed cracks are a result of the passivating process. Since localized corrosion was observed in almost all cases of passivation failure, it is expected that a passive layer with no flaws would perform better than one with flaws. This is also why wetting of the chemical deposition bath solution should be investigated since there was inconclusive evidence that the deep cracks and crevices in the γ-ZnNi coating were protected by a passive layer. It is possible that some level of exposed substrate surface is necessary to facilitate reduction of Cr(VI) to Cr(III), or that Cr(VI) protection correlates with exposed passivation surface area, both of which could be

revealed by systematically examining changes to the deposition bath parameters and γ-ZnNi electroplating parameters.

This research did not conclusively identify how the divalent cobalt interacted with the Cr(VI) to improve corrosion performance which could warrant more research of its own but does leave open the possibility that similar effects can be achieved by using other catalytic divalent dopants such as Ni(II), Mn(II), and Mg(II). In a similar vein, the early test specimens had their contact resistance measured which were found to be electrically conductive as required for the intended use as passivations on electrical connectors. The present research did not examine whether the passivation was a p-type or n-type conductor which opens the possibility for tetravalent dopants to replace cobalt, but the corrosion performance impact would have to be measured. Since there is interest in making TCPs without cobalt, searching for alternatives to take the role of cobalt would be a worthwhile endeavor for future experiments.

Alternative Contact Resistance Methodology

A known contact resistance measurement method (cTLM) has been used to measure contact resistance on bare, coated, and corroded metal panels with results comparable to the standard 81706B methodology and generating more information than the standard method. The cTLM method also has potential for better repeatability than the standard method. Additional work performed also showed the potential to develop flexible probes that could be used on curved substrates such as connectors. Other work performed demonstrated the possibility to develop standard substrates for validating methodologies.

Flexible Probes

One of the stretch goals of the project was developing an alternative that could be used on curved substrates such as directly on connectors. A limited amount of testing was done to determine the viability of using cTLM on curved substrates.

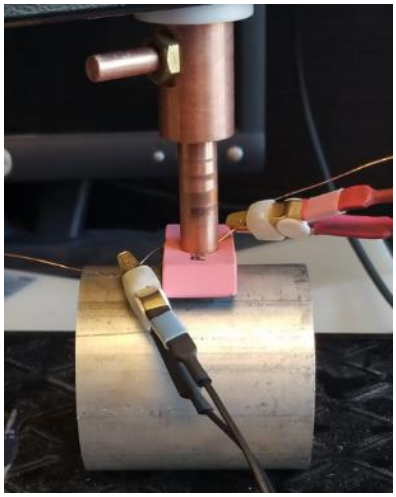

Issues

- Inner electrode is off center
- Inner and outer electrodes shift when probe is flexed so that gap width is not consistent
- Silicone glue used leaves residue on substrate and electrodes

Figure 60 Flexible Probe

Despite the issues the flexible probe (Figure 60) was used to measure contact resistivity on the aluminum cylinder of ~6 mΩ cm^2 which is equivalent to a contact resistance of ~0.9 mΩ using an

81706B apparatus. This is comparable to the values typically measured on flat aluminum panels using either the standard cTLM probe or 81706B.

Modifications of the design should be possible to mitigate the known issues and develop a probe routinely capable of measurements on curved substrates.

Literature Cited

[1] J. E. Bringas, Handbook of Comparative World Steel Standards, 5th ed., vol. Handbook of Comparative World Steel Standards, J. E. Bringas, Ed., West Conshohocken, PA 19428-2959: ASTM International, 2016.

[2] J. E. Bringas, Carbon and Alloy Steels for General Use, Handbook of Comparative World Steel Standards, %th ed., J. E. Bringas, Ed., West Conshohocken, PA: ASTM Inteernational, 2016.

[3] Alloy and Temper Designation Systems for Aluminum and Aluminum Alloys. Properties and Selection: Nonferrous Alloys and Special-Purpose Materials, vol. 2, ASM International, 1190.

[4] A. Brenner and G. E. Riddel, "Nickel plating on steel by chemical reduction," *Journal of Research of the National Bureau of Standards,* pp. 31-34, 1946.

[5] M. Schlesinger and M. Paunovic, Eds., Electroless Deposition of Nickel, Hoboken: John Wiley & Sons, Incorporated, 2014, pp. 447-458.

[6] R. C. Agarwala and V. Agarwala, "Electroless alloy/composite coatings: A review," *Sadhana,* vol. 28, no. 3, pp. 475-493, 2003.

[7] F. C. Campbell, Ed., Metal Fabrication: Understanding the Basics, ASM International, 2013.

[8] K. R. Sriraman, H. W. Strauss, S. Brahimi and et al, "Tribological behavior of electrodeposited Zn, Zn-Ni, Cd and Cd-Ti coatings on low carbon steel substrates," *Tribology International,* pp. 107-120, 2012.

[9] "ASTMB117-19 Standard Practice for Operating Salt Spray (Fog) Apparatus," American Society for Testing and Materials, 2019.

[10] B. Veeraraghavan, H. Kim, B. Haran and B. Popov, "Comparison of Mechanical Corrosion, and Hydrogen Permeation Properties of Electroless Ni-Zn-P Alloys with Electrolytic Zn-Ni and Cd Coatings," *Corrosion,* vol. 59, no. 11, 2003.

[11] "Cadmium and Cadmium Commpounds," 2011.

[12] J. R. Edwards and W. C. Prozialeck, "Cadmium, diabetes and chronic kidney disease," *Toxicology and Applied Pharmacology*, pp. 289-293, 1 Aug 2009.

[13] L. Järup, "Cadmium overload and toxicity," *Nephrology, dialysis, transplantation,* vol. 17, no. 2, pp. 35-39, 2002.

[14] "Medical Evaluation of Renal Effects of Cadmium Exposures," 2013.

[15] "Auatic Life Ambient Water Quality Criteria-Cadmium 2026," EPA, 2016.

[16] "Lead (Pb) Toxicity: What Are U.S. Standard for Lead Levels?," CDC, 2021.

[17] "Directive 2000/53/EC of the European Parliament and of the Council of 18 September 2000 on end-of-life vehicles," Queen's Printer of Acts of Parliament;nd.

[18] M. Palaniappa, M. Jayalakshmi and K. Balasubramanian, "Effect of Zincation/Sonication on Electroplated Gold Deposited on Aluminum Substrate," *Journal of Materials Engineering and Performance,* pp. 1028-1035, 2011.

[19] "The Tin Plating Process: A Step-By-Step Guide-Sharretts Plating," Sharretts Plating Company, 2015.

[20] "Metal Plating (Cadmium, Tin, Zinc, Nickel, Silver, Copper, & Others)," n.d..

[21] K. Whitlaw, A. Egli and M. Toben, "Preventing whiskers in electrodeposited tin for semiconductor lead frame applications," *Circuit World*, pp. 20-24, 2004.

[22] "実日野, 賢吾平松, 典秀西田, 実平松, 仁士川崎. 硫酸浴からのZn-Co合金めっきの組成と耐食性.," *表面技術*, pp. 873-877, 1993.

[23] J. Mahieu, K. De Wit, B. De Cooman and A. De Boeck, "The properties of electrodeposited Zn-Co coatings," *Journal of Mateerials Engineering and Performance*, pp. 561-570, 1999.

[24] "Zinc Electroplating".

[25] R. Mason, M. Neidbalson, M. Klingenberg, P. Khabra and C. Handsy, "Update on alternatives for cadmium coatings on military electrical connectors," *Metal Finishing*, pp. 12-20, 2010.

[26] R. Ramanauskas, P. Quintana, L. Maldonado, R. Pomes and M. Pech-Canul, "Corrosion resistance and microstructure of electrodeposited Zn and Zn alloy coatings," *Surface and Coatings Technology*, pp. 16-21, 1997.

[27] H. Hu, Y. Zhu, Z. Tu and W. Liu, "High Anticorrosion Nan Zn-Fe Coatings by Pulse Electrodepositing," *Advanced Materials Research*, pp. 2209-2215, 2011.

[28] S. Dubent, M. Mertens and M. Saurat, "Electrodeposition, characterization and corrosion behaviour of tin-20wt.% zinc coatings electroplated from a non-cyanide alkaline bath," *Materials Chemistry and Physics,* pp. 371-380, 2010.

[29] D. Shilfer, R. Conrad and A. Sheetz, "Environmental Evaluation of a Cadmium Replacement Coating for Use in a Marine Environment," 2003.

[30] S. Rajagopalan, "Characterization of Electrodeposited Zn-Ni Alloy Coatings As A Replacement For Electrodeposited Zn and Cd Coatings," Montreal, Quebec, Canada, 2012.

[31] H. Okamoto, "Ni-Zn (nickel-zinc)," JPE, 2003.

[32] Bruet-Hotellaz, J. Monino, A. Rousset, Marolleau and E. Chauveau, "Structure of zinc-nickel alloy electrodeposits," *journal of Materials Science,* vol. 34, no. 4, pp. 881-886, 1999.

[33] K. Moonjae, J. Du-hwan, C. Soo Hyoun, K. Hyun Tae, P. Jon-Tae and P. Jong Myung, "Characterization of the influence of Ni content on the corosion resistance of electrodeposited Zn-Ni alloy coatings," *Surface and Coatings Technology,* pp. 163-170, 2016.

[34] W. Tian, F. Xie, X. Wu and Z. Yang, "Study on corrosion resistance of electroplating zinc-nickel alloy coatings," *Surface and Interface Analysis,* pp. 251-254, 2009.

[35] O. Girciene , L. Gudavieiute, R. Juskenas and R. Ramanauskas, "Corrosion resistance of phosphated Zn-Ni alloy electrodeposits," *Surface and Coatings Technology,* pp. 3072-3077, 2009.

[36] A. Alfantazi and U. Erb, "Corrosion Properties of Pulse-Plated Zinc-Nickel Alloy Coatings," *Corrosion,* pp. 880-888, 1996.

[37] D. Siitari, M. Sagiyama and T. Hara, "Corrosion of Ni-Zn electrodeposited alloy," pp. 959-966, 1983.

[38] C. Muller, M. Sarret and E. Garcia, "Heat-Treatment on Black-Passivated Zn-Ni Alloys," *Journal of the Electrochemical Society,* 2003.

[39] C. Muller, M. Sarret and E. Garcia, "Heat treatment effect on the corrosion behavior of black passivated ZnNi alloys," *Corrosion Science,* pp. 307-321, 2005.

[40] R. Fratesi and G. Roventi, "Corrosion resistance of Zn-Ni alloy coatings in industrial production," *Surface and Coatings Technology,* pp. 158-164, 1996.

[41] M. Oki, T. Oki and E. Charles, "Chromate and Chromate-Phosphate Conveersion Coatings on Aluminium," *Arab J Sci Eng,* pp. 59-64, 2012.

[42] G. Wilcox, "Replacing Chromates for the Passivation of Zinc Surfaces," *Transactions of the IMF*, pp. B13-B15, 2003.

[43] G. Ilevbare, J. Scully, J. Yuan and R. Kelly, "Inhibition of Pitting Corrosion on Aluminum Alloy 2024-T3: Effect of Soluble Chromate Additions vs Chromate Conversion Coating," *Corrosion*, pp. 227-242, 2000.

[44] T. Bellezze, G. Roventi and R. Fratesi, "Electrochemical study on the corrosion resistance of Cr III-based conversion layers on zinc coatings," *Surface and Coatings Technology*, pp. 221-230, 2002.

[45] G. Lu, E. Ada and G. Zangari, "Investigations of the effect of chromate conversion coatings on the corrosion resistance of Ni-based alloys," *Electrochimica Acta*, pp. 1461-1473, 2004.

[46] W. Zhu, W. Li, S. Mu, N. Fu and Z. Liao, "Comparative study on Ti/Zr/V and chromate conversion treated aluminum alloys: Anti-corrosion performance and epoxy coating adhesion properties," *Applied Surface Science*, pp. 157-168, 2017.

[47] M. Kendig, A. Davenport and H. Isaacs, "The mechanism of corrosion inhibition by chromate conversion coatings from x-ray absorption near edge spectroscopy," *Corrosion Science*, pp. 41-49, 1993.

[48] "Toxicological review of hexavalent chromium," EPA, 1998.

[49] "Chromium (VI) Compounds," in *Aresenic, Metals, Fibres, and Dusts*, vol. 100C n.d., IARC.

[50] A. Magalhaes, I. Margarit and O. Mattos, "Molybdate conversion coatings on zinc surfaces," *Journal of Electroanalytical Chemistry*, pp. 433-440, 2004.

[51] D. Cowieson and A. Scholefield, "Passivation of tin-zinc alloy coated steel," in *Transactions of the IMF*, 1985.

[52] L. Ll, W. Bw and S. Gm, "Characterization and Performance of a Zr/Ti Pretreatment Conversion Coating on AA2024-T3," *Journal of the Electrochemical Society*, pp. C279-C284, 2015.

[53] J. Costa, R. Dei Agnoli and J. Ferreira, "Corrosion behavior of a conversion coating based on zirconium and colorants on galvanized steel by electrodeposition," *Tecnologia em Metalurgia Materiais e Mineração*, pp. 167-175, June 2015.

[54] Y. Guo and G. Frankel, "Active Corrosion Inhibition of AA2024-T3 by Trivalent Chrome Process Treatment," *Corossion*, vol. 68, no. 4, 2012.

[55] D. Johnson, "Zinc and Cadmium Passivating Bath". UNITED STATES Patent 2559878, 1951.

[56] H. Sheu, H. Lee, S. Jian, C. Hsu and C. Lee, "Investigation on the corrosion resistance of trivalent chromium conversion passivate on electroplated Zn-Ni alloy," *Surface and Coatings Technology,* pp. 241-248, 2016.

[57] J.-T. Qi, T. Hashimoto, J. Walton, X. Zhou, P. Skeldon and G. Thompson, "Trivalent chromium conversion coating formation on aluminium," *Surface and Coatings Technology,* pp. 317-329, 2015.

[58] A. Gardner and J. Scharf, "High Performance Alternative to Hexavalent Chromium Passivation of Plated Zinc and Zinc Alloys," SAE International, Warrendale, PA, 2001.

[59] C. Boin, "Black passivation films without hexavelnt chromium on top of electroplated layers of zinc and zinc alloys," SAE International, Warrendale, PA, 2007.

[60] S. Hesamedini, G. Ecke and A. Bund, "Structure and formation of trivalent chromium conversion coatings containing cobalt on zinc plated steel," *Journal of the Electrochemical Society,* pp. 657-669, 2018.

[61] W. Hesamedini and A. Bund, "Trivalent chromium conversion coatings," *Journal of Coating Technology,* pp. 623-641, 2019.

[62] J. Da Fonte, "Trivalent chromium passivate solution and process". UNITED STATES Patent 4359345, 1982.

[63] B. Ramezanzadeh and M. Attar, "Effects of Co(II) and Ni(II) on the Surface Morphology and Anticorrosion Performance of the Steel Samples Pretreated by Cr(III) Conversion Coating," *Corrosion,* vol. 68, no. 1, 2012.

[64] B. Ramezanzadeh, M. Attar and M. Farzan, "Corrosion performance of a hot-dip galvanized steel treated by different kinds of conversion coatings," *Surface and Coatings Technology,* pp. 874-884, 2010.

[65] K. Cho, V. Shankar Rao and H. Kwon, "Microstructure and electrochemical characterization of trivalent chromium based conversion coating on zinc," *Electrochimica Acta,* pp. 4449-4456, 2007.

[66] D. Preikschat P., D. Janesn R. and D. Hulser P., "Chormate-free conversion layer and process for producing the same". UNITED STATES Patent 6287704, 2001.

[67] "Formation of Trivalent Chromium Passivation Layers. n.d.".

[68] A. Iyer, W. Willis, S. Fruch and et al., "Characterization of NAVAIR Trivalent Chromium Pocess (TCP) coatings and solutions," *Plating and Surface Finishing,* vol. 97, no. 4, pp. 32-41, 2010.

[69] C. Matzdorf, M. Kane and J. Green, "Corrosion resistant coatings for aluminum and aluminum alloys". UNITED STATES Patent 6375726, 2002.

[70] H. Kawaguchi, O. Funatsumaru, H. Sugawara and et al., "Development of Trivalent Chromium Passivation for Zn Plating with High Corrosion Resistance after Heating," *SAE International Journal of Materials and Manufacturing,* vol. 9, no. 3, pp. 833-838, 2016.

[71] C. Tomachuk, C. Elsner, A. Di Sarli and O. Ferraz, "Morphology and Corrosion Resistance of Cr(III)-based conversion treatments for electrogalvanized steel," *Journal of Coatings Technology and Research,* vol. 7, no. 4, 2010.

[72] H. Bhatt, "Trivalent Chromium Conversion Coating for Corrosion Protection of Aluminum Surface," in *2009 DOD Corrosion Conference*, 2009.

[73] N. Zaki, "Trivalent chrome conversion coating for zinc and zinc alloys," *Metal Finishing,* vol. 105, no. 10, pp. 425-435, 2007.

[74] L. Grasso, A. Fantoli, M. Ienco and et al., "Corrosion resistance of Cr (III) based conversion layer on zinc coatings in comparison with a traditional Cr (VI) based passivation treatment," *la metallurgia italiana,* pp. 31-39, 2006.

[75] N.-T. Wen, C.-S. Lin, C.-Y. Bai and M.-D. Ger, "Structures and characteristics of Cr(III)-based conversion coatings on electrogalvanized steels," *Surface and Coatings Technology*, pp. 317-323, 2008.

[76] R. Berger, U. Bexell, T. Mikael Grehk and S.-E. Hornstrom, "A comparative study of the corrosion protective properties of chromium and chromium free passivation methods," *Surface and Coatings Technology*, vol. 202, no. 2, pp. 391-397, 2007.

[77] A. Di Sarli, J. Culcasi, C. Tomachuk, C. Elsner, J. Ferreira-Jr and I. Costa, "A conversion layer based on trivalent chromium and cobalt for the corrosion protection of electrogalvanized steel," *Surface and Coatings Technology,* pp. 426-436, 2014.

[78] L. Li and G. Swain, "Effects of Aging Temperature and TIme on the Corrosion Protection Provided by Trivalent Chromium Process Coatings on AA2024-T3," *ACS Applied Material Interfaces,* pp. 7923-7930, 2013.

[79] S. Hesamedini and A. Bund, "Formation of Cr(VI) in cobalt containing Cr(III)-based treatment solution," *Surface and Coatings Technology,* pp. 444-449, 2018.

[80] E. McCafferty, "Getting Started on the Basics," in *Introduction to Corrosion Science*, Springer-Verlag, 2010, pp. 13-21.

[81] E. McCafferty, "Getting Started on the Basics," in *Introduction to Corrosion Science*, New York, Springer-Verlag, 2010, pp. 25-27.

[82] E. McCafferty, "Thermodynamics of Corrosion: Electrochemical Cells and Galvanic Corrosion," in *Introduction to Corrosion Science*, New York, Springer-Verlag, 2010, pp. 73-89.

[83] F. LaQue, Marine Corrosion: Causes and Prevention, New York: Wiley, 1975, p. Chapter 6.

[84] B. Popov, Corrosion Engineering, Elsevier, 2015, pp. Chapter 5 166-169.

[85] J. Qi, B. Zhang, Z. Wang, Y. Li, P. Skeldon and G. Thompson, "Effect of an Fe(II)-modified trivalent chromium conversion process on Cr(VI) formation during coating of AA 2024 alloy," *Electrochemistry Communications,* vol. 92, pp. 1-4, 2018.

[86] C. Tomachuk, C. Elsneer and A. Di Sarli, "Electrochemical characterization of chromate free conversion coatings on electrogalvanized steel," *Materials Research,* vol. 17, no. 1, pp. 61-68, 2013.

[87] J. Qi and G. Thompson, "Comparative studies of thin film growth on aluminium by AFM, TEM and GDOES characterizatioin," *Applised Surface Science,* pp. 109-120, 2016.

[88] J. Qi, T. Hashimoto, J. Walton, X. Zhou, P. Skeldon and G. Thompson, "Fomation of a Trivalent Chromium Conversion Coating on AA2024-T351 Alloy," *Journal of the Electrochemical Society,* vol. 163, no. 2, pp. C25-C35, 2016.

[89] J. Qi, T. Hashimoto, G. Thompson and J. Carr, "Influence of Water Immersion Post-Treatment Parameters on Trivalent Chromium Conversion Coatings Formed on AA2024-T351 Alloy," *Journal of the Electrochemical Society,* vol. 163, no. 5, pp. C131-C138, 2016.

[90] S. Dardona and M. Jaworowski, "In situ spectroscopic ellipsometry studies of trivalent chromium coating on aluminum," *Applied Physics Letters,* vol. 97, no. 18, 2010.

[91] L. Li, G. Swain, A. Howell, D. Woodbury and G. Swain, "The Formation, Structure, Electrochemical Properties and Stability of Trivalent Chrome Process (TCP) Coatings on AA2024," *Journal of the Electrochemical Society,* vol. 158, no. 9, p. C274, 2011.

[92] C. Munson and G. Swain, "Structure and chemical composition of different variants of a commercial trivalent chromium process (TCP) coating on aluminum alloy 7075-T6," *Surface and Coatings Technology*, pp. 150-162, 2017.

[93] A. Wiryawan, R. Retnowati, R. Burhan and Syekhfani, "Method of Analysis for Determination of the Chromium (Cr) Species in Water Samples by Spectrophotometry with Diphenylcarbazide," *Journal of Environmental Engineering & Sustainable Technology,* vol. 5, no. 1, pp. 37-46, 2018.

[94] Z. Marczenko and M. Balcerzak, "Chromium," in *Analytical Spectroscopy Libray*, vol. 10, Elsevier, 2000, pp. 159-166.

[95] B. Popov, "Chapter 5," in *Corrosion Engineering*, Elsevier, 2015, pp. 201-202.

[96] B. Popov, "Chapter 5," in *Corrosion Engineering*, Elsevier, 2015, pp. 207-213.

[97] S. Esmailzadeh, M. Aliofkhazraei and H. Sarlak, "Interpretation of Cyclic Potentiodynamic Polarization Test Results fo rStudy of Corrosion Behavior of Metals: A Review," *Protection of Metals and Physical Chemistry of Surfaces,* vol. 54, no. 5, pp. 976-989, 2018.

[98] M. Orazem and B. Tribollet, "The Krameers-Kronig Relations," in *Electrochemical Impedance Spectroscopy,* John Wiley & Sons, Ltd, 2008, pp. 427-445.

[99] "MIL-DTL-81706B Chemical Conversion Materials For Coating Aluminum and Aluminum Alloys," 2004.

[100] E. Committee, "Test Methods for Determining Average Grain Size," ASTM International, n.d..

[101] M. Biesinger, B. Payne, L. Gosvenor, W. Lau, A. Gerson and R. Smart, "Resolving surface chemical states in XPS analysis of first row tranisition metals, oxides and hydroxides: Cr, Mn, Fe, Co and Ni," *Applied Surface Science,* pp. 2717-2730, 2011.

[102] P. Pokorny, P. Tej and P. Szelag, "Chromate conversion coatings and their current application," *Metalurgija,* vol. 55, pp. 253-256, 2016.

[103] K. Foster, J. Claypool, W. Fahrenholtz, M. O'Keefe, T. Nahlawi and F. Almodovar, *ACS Applied Material Interfaces,* vol. 13, pp. 4535-4544, 2021.

[104] Wikipedia, "Four-Terminal Sensing," [Online]. Available: https://en.wikipedia.org/wiki/Four-terminal_sensing.

[105] B. J. Lanterman, A. A. Riet, N. S. Gates, J. D. Flygare, A. D. Cutler, J. E. Vogel, D. R. Wheeler and B. A. Mazzeo, "Micro-Four-Line Probe to Measure Electronic Conductvity and Contact Resistance of Thin-Film Battery Electrodes," *Journal of the Electrochemical Society,* pp. A2145-A2151, 2015.

[106] J. D. Flygare, A. A. Riet, B. A. Mazzeo and D. R. Wheeler, "Mathematical Model of Four-Line Probe to Determine Conductive Properties of Thin-Film Battery Electrodes," *Journal of the Electrochemical Society,* pp. A2136-A2144, 2015.

[107] D. K. Schroder, Semiconductor Material and Device Characterization 3rd Ed, John Wiley & Sons, Inc., 2006.

[108] G. K. Reeves, "Specific Contact Resistance Using A Circular Transmission Line Model," *Solid-State Electronics Vol 23,* pp. 487-490, 1980.

[109] G. S. Marlow and M. B. Das, "The Effects of Contact Size and Non-Zero Metal Resistance on the Determination of Specific Contact Resistance," *Solid State Electronics, Vol 25, No. 2,* pp. 91-94, 1982.

[110] G. Gonzalez-Diaz, D. Pastor, E. Garcia-Hemme, D. Montero, R. Garcia-Hernansanz, J. Olea, A. del Prado, E. San Andres and I. Martil, "A Robust Method to Determine the

Contact Resistance Using the Van der Pauw Set Up," *Measurement, Vol 98,* pp. 151-158, 2017.

Appendices

Supporting Data

The Boeing Company, St Louis, Mo. 20-00242

Informal Tech Memo

Development and Evaluation of Non-Chromate LHE ZnNi Passivation's for DOD Electrical Connectors

Issue Date: 12/20/2022

Prepared By:

Sam Furfaro

Sam Furfaro
Electrical Engineer
Electrical Laboratories

Approved By:

David Zika
Technical Lead Engineer
Electrical Laboratories

Approved By:

Linda Halgash
Group Manager
Physical Sciences

DISTRIBUTION STATEMENT: - Distribution is authorized to the Department of Defense and DOD contractors only to protect information in management reviews, records, or contract performance evaluation, or other advisory documents evaluating programs of contractors, and to protect technical or operational data (determined on 8 March 2012).

Warning – This document contains technical data whose export is restricted by the Arms Export Control Act (Title 22, U.S.C. Sect 2751 et seq.) or Executive Order 12470. Violations of this export laws are subject to severe criminal pen-

List of Scientific/Technical Publications

APPLIED MATERIALS & INTERFACES

www.acsami.org Research Article

Characterization of Cobalt-Containing and Cobalt-free Trivalent Chromium Passivation Layers on γ-ZnNi-Coated Al6061-T6 Substrates

Kevin Foster,* James Claypool, William G. Fahrenholtz, Matthew O'Keefe, Tarek Nahlawi, and Felix Almodovar

Cite This: ACS Appl. Mater. Interfaces 2021, 13, 4535−4544 Read Online

ACCESS | Metrics & More | Article Recommendations

ABSTRACT: The corrosion performance and electrical contact resistance were investigated for a trivalent chromium passivation layer and a cobalt-free version of that same passivation layer on γ-ZnNi-coated Al 6061-T6. Both passivation layers had a similar surface morphology, were amorphous, had similar thicknesses, and contained pores within the passivation layer. The cobalt-containing passivation layer initially had an exchange current density of 9.5 × 10^{-4} A/cm^2 and a polarization resistance of 290 Ω/cm^2. The cobalt-free passivation layer initially had an exchange current density of 10.6 × 10^{-4} A/cm^2 and a polarization resistance of 116 Ω/cm^2. After 500 h of exposure to neutral salt spray, the cobalt-containing passivation layer showed no visible corrosion and had an exchange current density of 2.9 × 10^{-4} A/cm^2 and a polarization resistance of 136 Ω/cm^2. The cobalt-free passivation layer showed uniform corrosion and had an exchange current density of 5.2 × 10^{-4} A/cm^2 and a polarization resistance of 80 Ω/cm^2. After 500 h of exposure to neutral salt spray on specimens which were scribes down to the Al substrate, the cobalt-free passivation layers were uniformly corroded, but scribed specimens with the cobalt-containing passivation layers were only partially corroded. Both the cobalt-containing and cobalt-free passivation layers were found to be viable alternatives to hexavalent chromium as per the requirements of cobalt-containing MIL-DTL-81706 offering protection comparable to hexavalent chromium and cobalt-free offering less. The presence of cobalt in the TCP layer was found to improve corrosion performance and suggested that an intermediate species such as cobalt is beneficial to the oxidation of Cr(III) to Cr(VI).

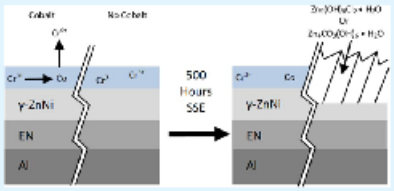

KEYWORDS: *TCP, trivalent chromium passivation, corrosion protection, Al6061-T6, hexavalent chrome, contact resistance, MIL-DTL-38999, MIL-DTL-81706, cobalt*

INTRODUCTION

Cadmium coatings have long been used to protect various metals from corrosion.[1,2] The carcinogenic,[3−5] teratogenic,[6] toxicological,[7−9] and environmental[10] effects related to the use of cadmium led to a search for alternative coatings that were less toxic. Many alternatives were investigated and found to be viable replacements, including γ-ZnNi coatings.[11−13] ZnNi coatings protect the underlying metal in a manner similar to galvanization by acting as a sacrificial anode. While ZnNi coatings alone offer some corrosion resistance, these coatings are often passivated to increase the functional lifespan of the coated components.

Hexavalent chromium is an anticorrosion passivation layer that can be used to protect sacrificial coatings due to its active corrosion inhibition mechanism that allows protection of damaged areas of the passivation layer or flaws in the passivation layer after deposition.[14−16] While hexavalent chromium is an excellent passivation layer, it is also a human carcinogen[17,18] and toxicological[19,20] environmental contaminant. These negative health effects prompted regulatory agencies in the United States and European Union to limit usage and industrial exposure to hexavalent chromium resulting in a need for alternative passivation layers.[21,22] One potential alternative passivation layer is based on trivalent chromium.

Investigations into trivalent chromium passivation (TCP) layers have shown excellent anticorrosion performance on

Received: November 9, 2020
Accepted: January 4, 2021
Published: January 14, 2021

https://dx.doi.org/10.1021/acsami.0c20015
ACS Appl. Mater. Interfaces 2021, 13, 4535−4544

Thin Solid Films 735 (2021) 138894

Contents lists available at ScienceDirect

Thin Solid Films

journal homepage: www.elsevier.com/locate/tsf

Characterization of cobalt containing and cobalt-free trivalent chromium passivations on γ-ZnNi coated steel substrates

Kevin Foster [a,*], James Claypool [a], William G. Fahrenholtz [a], Matthew O'Keefe [a], Tarek Nahlawi [b], Felix Almodovar [b]

[a] Missouri University of Science & Technology, 401 W. 16th St., 101 Straumanis-James Hall, Rolla, MO, 65409, United States
[b] Dipsol of America, 34005 Schoolcraft Rd., Livonia, MI, 48150, United States

ARTICLE INFO

Keywords:
Trivalent chromium passivation
Zinc-nickel coating
Corrosion
Steel
Transmission electron microscopy
Cobalt

ABSTRACT

The corrosion performance was studied for standard trivalent chromium passivations and cobalt-free trivalent chromium passivations on steel substrates. The steel substrates were either polished or unpolished and coated with γ-phase ZnNi prior to passivation. For unpolished substrates, cobalt-free specimens had 50 ± 8 cracks/mm, a thickness of 69 ± 4 nm, and notable porosity compared to cobalt-containing passivations which had no cracks, a thickness of 40 ± 5 nm, and no porosity. For polished substrates, cobalt-free passivations had 50 ± 3 cracks/mm, a thickness of 38 ± 2 nm, and notable porosity compared to cobalt-containing passivations with 16 ± 2 cracks/mm, thickness of 48 ± 2 nm, and no porosity. After 1000 hours of salt-spray exposure, cobalt-free passivations had visible white rust on 4% of the surface area while cobalt-containing passivations had 22% of the surface area covered by white rust. The thickness of both passivations increased on both polished and unpolished specimens after salt spray exposure. Electrochemical testing showed that the cobalt-free passivation had the least change before and after salt spray exposure. The difference in corrosion performance was attributed to the greater porosity in the cobalt-free passivations influencing the amount of corrosion inhibiting species present.

1. Introduction

Electroplated cadmium has been used to protect materials such as steel or aluminum from corrosion for decades [1,2]. Unfortunately, cadmium is carcinogenic, which has led to regulations that limit cadmium exposure and necessitated alternative plating technologies [3–7]. Electroplated zinc and zinc alloys are potential replacements for cadmium-based platings and are widely used in the steel and automotive industries [8–11]. One zinc alloy that is a viable alternative to Cd is the γ-phase of ZnNi [11–16].

Similar to galvanization, ZnNi coatings act as a sacrificial anode to cathodically protect the underlying substrate through galvanic coupling. To slow the corrosion and extend the lifetime, passivations can be employed in addition to the sacrificial coatings. One of the most effective passivations is based on hexavalent chromium, which can exhibit active corrosion inhibition that protects portions of the exposed surface where the passivation has been damaged or removed [17–19]. Unfortunately, hexavalent chromium is also carcinogenic and regulations have been passed to limit usage in the United States and the European Union [20,21]. These regulations necessitated development of alternative passivation technologies.

Trivalent chromium passivations (TCPs) have been demonstrated as viable alternatives to hexavalent chromium. The Cr(III) species that are predominant in TCPs are formed naturally as part of the corrosion response of hexavalent chromium coatings as described by Equations 1-3 [22] and consisting of metal dissolution, hydrogen evolution, and subsequent reduction of Cr(VI) from locally increased pH. While TCPs may or may not exhibit active corrosion protection [23], the performance of TCPs exceeds the corrosion protection of hexavalent chromium coatings in some cases such as the impedance work provided by Di Sarli et al.,[24] the corrosion work by Foster et al.[25], and the comparisons between Cr(VI) and Cr(III) made by Zaki [26]. Additions of cobalt have been shown to improve the corrosion performance of TCPs during salt spray testing [27,28]; however, regulations in the European Union limiting cobalt exposure have led to the development of TCP deposition processes that do not use cobalt.

* Corresponding author at: 401 W. 16th St., 101 Straumanis-James Hall, Rolla, MO, 65409, United States
E-mail addresses: klfmkd@mst.edu (K. Foster), jbcgyf@mst.edu (J. Claypool), billf@mst.edu (W.G. Fahrenholtz), mjokeefe@mst.edu (M. O'Keefe), tnahlawi@dipsolamerica.com (T. Nahlawi), falmodovar@dipsolamerica.com (F. Almodovar).

https://doi.org/10.1016/j.tsf.2021.138894
Received 21 January 2021; Received in revised form 12 August 2021; Accepted 13 August 2021
Available online 18 August 2021